Aus dem Institut für Zell- und Neurobiologie der Medizinischen Fakultät
Charité – Universitätsmedizin Berlin

DISSERTATION

Transcriptional regulation of cerebellar neuron specification

Transkriptionelle Regulation der Spezifikation von
Kleinhirnneuronen

zur Erlangung des akademischen Grades
Doctor of Philosophy (MD/PhD)

vorgelegt der Medizinischen Fakultät
Charité – Universitätsmedizin Berlin

von

Aleksandra Rusanova

Table of contents

1. Abstract

The cerebellum regulates motor coordination and is involved in non-motor functions, such cognition and social behavior. The cerebellum is composed by excitatory and inhibitory neurons, originating from Ptf1a expressing ventricular zone and the Atoh1 expressing rhombic lip, respectively. During my studies, I focused on the development ventricular zone derivatives, Purkinje cells and inhibitory interneurons, which are generated between embryonic day 11 to birth in mice. However, the molecular mechanisms controlling the specification of these two distinct neuronal populations remain to be identified. In this thesis, I will present data that identify the transcription factor Olig3 as a major regulator in the development of early born cerebellar neurons. In the rhombic lip, Olig3 regulates cell proliferation, whereas in the ventricular zone this factor secures the specification of Purkinje cells, by suppressing a differentiation program characteristic of inhibitory interneurons. Furthermore, I will show the transcription factors Olig2 and Neurod6 regulate also distinct aspects of cerebellar GABAergic neuron development. Olig2 has a complementary function to Olig3, but it has more limited function, whereas Neurod6 is key in specification of inhibitory interneurons. Taking together, these data demonstrate key players in the transcriptional regulation that regulates cerebellar development. Most of the results presented in this dissertation have been recently published in eLife (2021, 10:e64684)

Abstrakt

Das Kleinhirn reguliert die motorische Koordination von Wirbeltieren und ist darüber hinaus bei Funktionen wie Kognition und Sozialverhalten beteiligt. Es besteht aus erregenden und hemmenden Neuronen, die in der Ptf1a-exprimierenden ventrikulären Zone und den Atoh1-exprimierenden Rautenlippen gebildet werden. Während meines Studiums konzentrierte ich mich auf die Entwicklung von Derivaten der ventrikulären Zone: Purkinje-Zellen und hemmende Interneurone, die bei Mäusen zwischen dem embryonalen Tag 11 bis zur Geburt erzeugt werden. Die molekularen Mechanismen, die die Spezifikation dieser zwei unterschiedlichen neuronalen Populationen steuern, sind jedoch noch nicht aufgeklärt. In dieser Arbeit werde ich Daten präsentieren, die den Transkriptionsfaktor Olig3 als wichtigen Regulator bei der Entwicklung von frühstadlichen Kleinhirnneuronen identifizieren. Im Bereich der Rautenlippen regelt Olig3 die Zellproliferation, wohingegen in der ventrikulären Zone dieser Faktor die Spezifikation der Purkinje-Zellen sicherstellt, indem eine Charakteristik im

Differenzierungsprogramm inhibitorischer Interneurone unterdrückt wird. Darüber hinaus zeige ich, dass die Transkriptionsfaktoren Olig2 sowie Neurod6 auch verschiedene Aspekte der GABAergen Neuronenentwicklung im Kleinhirn regulieren. Der Faktor Olig2 hat eine komplementäre, jedoch eingeschränkte, Funktion gegenüber Olig3, während Neurod6 bei der Spezifizierung von inhibitorischen Interneuronen eine Schlüsselrolle spielt. Zusammengenommen identifizieren diese Daten molekulare Schlüsselakteure in der Transkriptionsregulation, welche die Entwicklung des Kleinhirns steuert. Die meisten der in dieser Dissertation präsentierten Ergebnisse wurden kürzlich in Fachjournal eLife (2021, 10:e64684) veröffentlicht.

2.1 Introduction

The cerebellum (latin for „little brain") is a structure in the central nervous system of vertebrates that locates in the fossa posterior of the cranium and belongs to the hindbrain. It seems at a first glance very familiar and it classically defined as the major center for motor coordination. Despite its relatively small size, when comparing to the cerebrum, the human cerebellum represents about 78% of the area of the cerebral cortex (3). Furthermore, the cerebellum is densely populated by neurons and contains more than half of the total amount of neurons of the central nervous system (4). These facts, together with its extensive afferent connections with other brain regions appear to suggest that the cerebellum integrates a large variety of neurological functions, which are not only restricted to the classical understanding of motor control.

Cerebellar functions can be group into different categories. The first group of functions are directly involved in motor coordination (5, 6). As such, the cerebellum mediates movement initiation and termination, the coordination and ability to perform smooth movements during gating or keeping body position (5). The cerebellum receives indirectly information from cerebral cortex about movement intentions and it directly connected with spinal cord and vestibular nerves (7-9). These cortico-cerebellar and cerebello-spinal circuits allow the brain to integrate relevant information about position and movements of the head and body, respectively (9, 10). The cerebellum also controls both simple single-joint and complex multi-joint movements (6, 11, 12). For instance, flexion of an arm or leg are simple single-joint movement and it involves one joint. Point to an object, pick up an object, or throw a ball requiring the participation of several joints and therefore called complex multi-joint movements. Cerebellar lesions impaired the correct coordination of muscular tension and relaxation, which cause hypometric ("undershooting") and hypermetric ("overshooting") movements (13, 14). This means for example, the commission of uncoordinated movements of a large amplitude than necessary by attempting to touch an object with the index finger. Oppositely, by hypometric movements, the individual can`t reach the point, due to insufficient range of motion. These clinical presentations are defined as dysdiadochokinesia (15, 16). Similarly, a number of cerebellar lesions might result in adiadochokinesia, that is the complete inability to perform fast alternating movements (16). An important cerebellar motor function is to controls grip forces, that is application of right physical power, depending on the weight, type and shape of the object. Such for example, to lift up the piece of paper and dumbbell requires applying of different muscle force in hands and arms. Thus, cerebellar lesions

result in hypometric and hypermetric movements, the loss of directional determination, dysfunction of the speed and the rhythm muscular contraction and relaxation patterns, which are noticeable by an unstable gaiting, static coordination, and overall motoric disorders (17). Clinically, the collection of all the above mentioned symptoms are frequently described as cerebellar ataxia (18). More recently, the cerebellum also has been shown to play important function in various other nonmotoric behaviors, which included cognition, learning, speech, memory, and even emotional states (19-22). Furthermore, the cerebellum actively regulates social behaviors, for example in the recognition of emotions displayed by other individuals and providing an appropriate feedback (20, 22, 23). The implication of the cerebellum in the aforementioned behaviors supported by clinical cases and it is observable in neurological diseases, such as autism spectrum disorders, attention deficits and hyperactivity disorders, among many others (24-26).

Cerebellar dysfunction can occur by congenital or acquired conditions. First, I would like to describe a few congenital genetic diseases and malformations affecting cerebellar development, and subsequently I will describe some common neurological and neuropsychiatric diseases affecting cerebellar function.

Congenital cerebellar diseases

Dandy-Walker malformation and cerebellar hypoplasia are the most common cerebellar malformations affecting cerebellar development. They are characterized by cerebellar underdevelopment and hydrocephalus (that is an accumulation of the liquid in the brain`s cavities). These abnormalities are recognizable by ultrasonic explorations at fetal stages and result from largely unknown genetic reasons. In a few cases, congenital cerebellar malformations can be highly specific and affect particular cerebellar neurons populations, oftentimes exclusively the Purkinje cell population (27). Congenital non-progressive ataxia is another frequent cerebellar malformation caused by not yet understood mutations linked to the X chromosome affecting predominantly male children (28). Autosomal recessive ataxia like Friedreich's ataxia is the most common ataxia and caused by mutation in chromosome 9 in *FXN* gene expressing frataxin protein (29, 30). The disease manifested at childhood and the clinical picture is due to the organs where this protein expressed. In cerebellum frataxin expressed in dentate nucleus, which clinically reflects in ataxia, also in skeletal muscles, heart, cerebral cortex and other organs, what determined pathology causing by disease (31, 32). Maternal inherited

mitochondrial ataxia caused by mutation in *POLG* gene in 17 chromosome (33). The enzyme polymerase γ is synthetized from the *POLG* gene, which function is replication of the mitochondrial DNA(34). The clinical picture in patient with this ataxia characterizedby cerebellar and/or sensory ataxia, speech and intellectual disability, seizures, lesions in peripheral nervous system and organs can be affected (33, 34).

Acquired cerebellar diseases

Cerebellar dysfunction is associated with various neuro-degenerative and developmental psychiatric diseases, such as autism spectrum, schizophrenia, attention deficits, hyperactivity disorders, dyslexia and depression (21, 26, 35, 36). For example, clinical investigation in patients diagnosed with autism spectrum disorders shows significant changes in the gross anatomy of the cerebellum, and these changes is also observed in mice models of autism disorder (24, 25, 35). In such cases, the cerebellum is underdeveloped (hypoplastic), it loses grey matter volume that is characterized by a pronounced decrease of functional connectivity of both input and output connections (26). Another clinical example can be found in patients with attention-deficit/hyperactivity disorders, collectively characterized by hyperactivity, impulsivity, inability to keep attention, who presents with significant posterior vermis reduction and decreased in cerebellar volume (26, 35, 37). Interestingly, the severity in the cerebellar vermix reduction correlates with the severity of the attention-deficit/hyperactivity diseases (26). Furthermore, decreased activity of the cerebellum, detected by neuroimaging, is commonly seen in patients with schizophrenia (21, 38). In this regard, several studies also indicated the selectively loss of specific cell populations in the cerebellum, such as the reduction of Purkinje cells in the vermis (21, 39).

Taking together, the etiology and pathological mechanism of many cerebellar diseases, mentioned above, are deeply rooted in the earliest stages of our life, or in other words during embryonic development. Despite the large amount of knowledge accumulated over the last three decades on cerebellar development, many details are still missing and the precise molecular mechanism controlling the specific development of the carious GABAergic and glutamatergic neuron cerebellar populations remains fragmentary known. In the following part of my introduction, I would like to describe the cellular organization of the cerebellum and subsequently the known mechanisms acting in cerebellar development.

Cerebellar cytoarchitecture

The cerebellar surface is covered by a folded cerebellar cortex that contains most of the cerebellar neuron populations, under which a region of abundant white matter contains a tiny collection of neurons that form the cerebellar efferent nuclei system (see figure 1 and below). The cerebellar cortex is laminated and 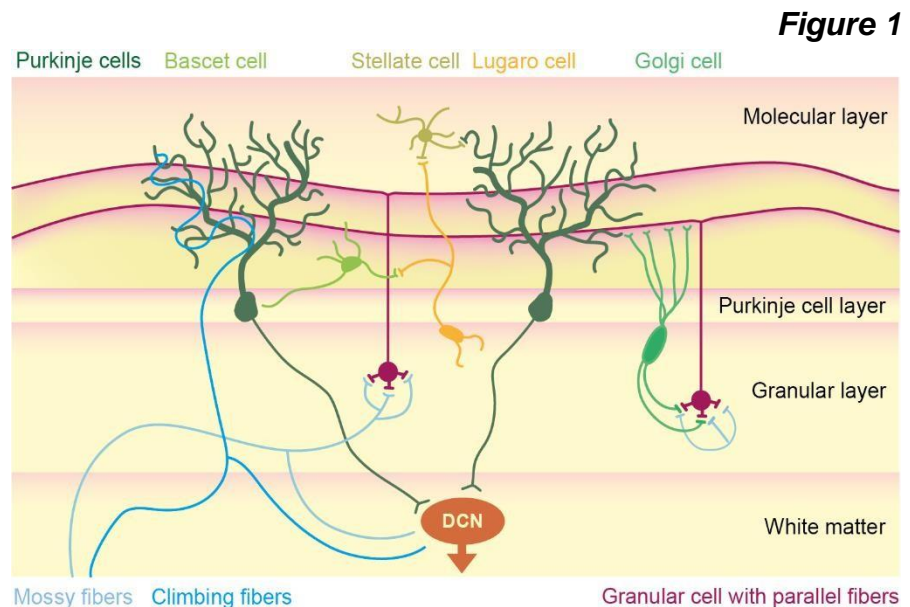presents with three distinct layers a) the most superficial lamina is called the molecular layer and contains medium size GABAergic interneurons (Basket and Stellate cells), b) the intermediate lamina is called the Purkinje cell layer and contains a monolayer of GABAergic Purkinje cells, c) the deepest lamina is called the granular layer and

Figure 1

Figure 1: Cerebellar cellular composition.

Schematic representation of the main cell groups of the cerebellum. Incoming signals pass to the cerebellum along mossy fibers and climbing fibers, all outgoing information goes out through DCN – deep cerebellar nucleus neurons. On the top indicated the GABAergic neuronal populations. This is original schema.

contains small size glutamatergic granular cells. Three small additional populations can be found in the granular layer: Golgi cells (inhibitory), Lugaro cells (inhibitory) and unipolar brush cells (excitatory). As described above, within the cerebellar white matter there exists a collection of cerebellar efferent neurons called deep cerebellar nuclei neurons or merely deep cerebellar neurons (40). In a minimalistic manner, granular cells receive input from the brainstem and spinal cord via mossy fiber neurons, whereas the Purkinje cells receive information from the brainstem via climbing fiber neurons (see figure 1 and more details below).

- The molecular cell layer

The outer-most layer contains two main types of the GABAergic inhibitory interneurons, the stellate cells and the basket cells. They both form synapses with Purkinje cell dendrites and tightly regulate their activity. The stellate cell occupy a very superficial part in the molecular layer and form synapses with distal dendrites of Purkinje cells, whereas

the basket cells locate deeper and closer to proximal dendrites of Purkinje cells, where they form the synapses (41). In addition to this neuronal population, the molecular layer also contains axons and dendrites of the granular and Purkinje cells, respectively.

- The Purkinje cell layer

The Purkinje cell layer contains a monolayer of large GABAergic cells, the Purkinje cells, which give rise to the name of this cortical layer. The Purkinje cell populations is key in cerebellar functioning. The Purkinje cells are inhibitory neurons, which receive excitatory input from the granular cells located in the granular layer. Furthermore, the Purkinje cell dendritic trees receive excitatory input from the brainstem via climbing fibers, which input afferents from the inferior olivary nucleus. The inferior olivary nucleus is a group of projecting interneurons located on the ventral medulla oblongata. These axons wrap around the Purkinje cell dendritic tree, thereby forming the strongest synaptic connection in whole nervous system (42). The inferior olive/Purkinje cell pathway plays an important role in synaptic plasticity and provides the neuronal substrate for motor learning and integrative correction of motor errors, and it is also implicated in reward-learning (43-45). The output information of Purkinje cells will be relay to the deep cerebellar nuclei neurons (see below).

- The granular cell layer

This layer represents the innermost lamina of the cerebellar cortex. It contains four distinct neuronal cells: the Granule cells, the Unipolar brush cells, the Golgi cells and the Lugaro neurons.

Granule cells. These cells are the largest cerebellar cell population, which provides so massive numbers of neurons in the cerebellum as a total (46). Granule cells use glutamate as neurotransmitter and provide excitatory drive to target neurons. Granule cells are the smallest neurons in our brains, they usually are multipolar and have 3-5 dendrites which form a glomerular structure, called the dendritic claw (47). This dendritic claw receives the information from mossy fibers, these are axons that provide the main input to cerebellum from other parts of the brain. The electrical activity within the dendritic claw is locally modulated by Golgi cells (described below). Each granular cell connects with about 4 mossy fiber axons, and each mossy fiber can synapse up to 30 different granular cells (48). Granular cells send axons through the layer of Purkinje cells to molecular layer, there the axon bifurcates and lying parallel to pia surface of the

cerebellum, this bifurcated granular cell axon calls parallel fibers. The parallel fibers can connect with several thousand of dendrite simultaneously (49).

Golgi cells. These neurons a scatter within the granular layer and intermingle with the granular cells. They are GABAergic in nature and regulate the local information within a dendritic claw (50-52). Golgi cells receive direct input information from mossy fibers but also from granular cell axon collaterals. They act as regulators of excitation of granular cells, and limit hence whole incoming excitation in cerebellum.

Lugaro cells. These neurons are GABAergic and have characteristic spindle-shaped bodies. They represent relative small cell population within the granular layer, but they project long dendrites that reach the Purkinje cell layer, where they receive synaptic input from the Purkinje cells as well as from basket and stellate interneurons (53, 54)(55). *Lugaro* cells have the specific function of inhibiting Golgi cells.

- Deep cerebellar nuclei

Within the cerebellar white matter, there is a collection of excitatory projection neurons intermingle with inhibitory neurons collectively known as deep cerebellar nuclei neurons. There are three distinct deep cerebellar nuclei called: fastigial (medial), interpositus (intermediate) and dentate (lateral). The excitatory projection neurons located in the deep cerebellar nuclei represent the unique cerebellar efferent system (56). Deep cerebellar neurons receive and excitatory drive from incoming mossy fibers and an inhibitory drive from Purkinje cells.

In the next section of my introduction, I would like to summarize the main events that regulate cerebellar development.

Cerebellar development

The cerebellum develops from the dorsal part of rhombomere 1 immediately after the closure of neuronal tube and the formation of the primary vesicles of the central nervous system: the prosencephalon, mesencephalon, rhombencephalon (57). The developing rhombencephalon can be further subdivided into the myelencephalon that gives rise to the medulla oblongata and the metencephalon that originates the cerebellum. The part of the metencephalon called cerebellar anlage gives rise to the cerebellum. In mice, this is first seen at embryonic day (E) 9.5 (58). The cerebellar neurons emerge from two distinct progenitor regions: the ventricular zone and the rhombic lip (Figure 2D). The ventricular zone is the part of the alar plate which also form the upper boundary for fourth ventricle.

From the ventricular zone all cerebellar GABAergic inhibitory neurons emerge, whereas from the rhombic lip all excitatory cerebellar neurons originate (59). Recent data, however, shows that there is one exception to this rule, and that is a relatively small Glycinergic inhibitory neuron population that will reside in the nucleus fastigial, which has an origin in the rhombic lip (59, 60). The rhombic lip and the ventricular zone contain all cerebellar neuronal progenitors, that is cells with mitotic activity that have the capacity to proliferate but also to differentiate in particular neuronal types. Interestingly, birth dating experiments have shown that each cerebellar neuron type develops in a precise temporal window (Figure 2A-C). For example, the Purkinje cells, which originate from ventricular zone, develop from E11.5 to E13.5 in mice, whereas inhibitory interneurons (basket, stellate, Golgi and Lugaro cells) develop from E14.5 until the first days of postnatal life (61). The generation of the different cerebellar neuron types, in their characteristic temporal order, requires a precise molecular control. Transcription factors are the major regulators of neuron cell specification, and the transition from progenitor state to a differentiated postmitotic stage. Transcription factors can directly or indirectly bind to DNA and regulate gene expression. For development and specification of cerebellar neurons, two transcription factors have been associated with the specification of all GABAergic and glutamatergic cerebellar neurons (Figure 2D). These factors are the Pancreas specific transcription factor 1 subunit alpha (Ptf1a, expressed in ventricular zone progenitors) and Atonal homolog 1 transcription factor (Atoh1, expressed I rhombic lip progenitor cells) (62-64). Despite the fact that mutation of Ptf1a and Atoh1 severely disrupts the development of GABAergic and glutamatergic cerebellar neurons, we still do not know, how the distinct neuron cell types from the rhombic and the ventricular zone become subspecified. In other words, which molecular mechanisms in a progenitor zone such as the ventricular zone allow for the timely specification Purkinje cells versus the specification of GABAergic inhibitory interneurons.

In my PhD, I focused on defining the molecular control of GABAergic neuron development from the ventricular zone and teamed up with Mr. Elijah Lowestein (my co-author) who focused on development of excitatory cerebellar neurons from the rhombic lip. Together, we have recently published our research as co-first authors in eLife (16.02.2021). Below I will present the results obtained during my studies that are of my own and clearly point out when the data was generated by my co-author. Dr. Hernandez-Miranda supervised my thesis and research.
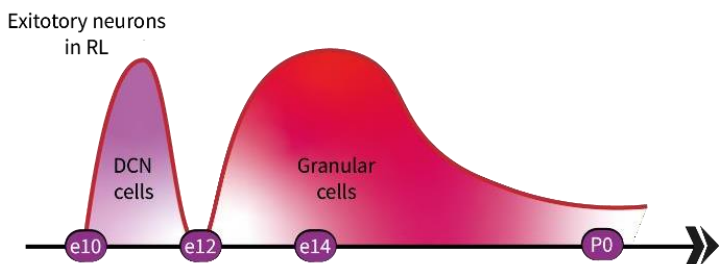
Figure 2

A

| Type of the neuron	Generation time	Generation place	Final position	Postmitotic transcription factor	Type of neurotransmitter	Excitatory or Inhibitory
Purkinje cells	E11.5–E13.5	Ventricular zone	Purkinje cells layer (cerebellar cortex)	Foxp2	GABA	Inhibitory
Inhibitory Interneurons: 1.Bascet cells and Stellate cells	E13.5- P5 (peak P0)	Ventricular zone	Molecular layer (cerebellar cortex)	Pax2	GABA	Inhibitory
2.Lugaro cells	E13.5–postnatal		Granular layer(cerebellar cortex)			
3.Golji cells	E13.5–postnatal (peak E14–E16		Granular layer(cerebellar cortex)			
Granular cells	E10.5-E15.5, at E13.5-E14.5 EGL is forming	Rhombic lip	Granular layer (cerebellar cortex)	Pax6	Glutamine	Excitatory
Deep cerebellar nucleus (DCN)	E10.5–E12.5	Rhombic lip	In cerebellar white matter under, cerebellar cortex	Tbr1 -Fastigii, Brn2 Interpositus and Dentatus DCN cells	Glutamine	Excitatory
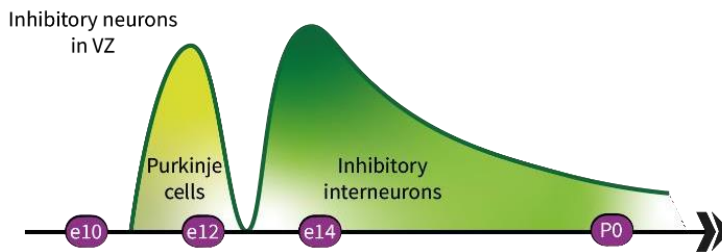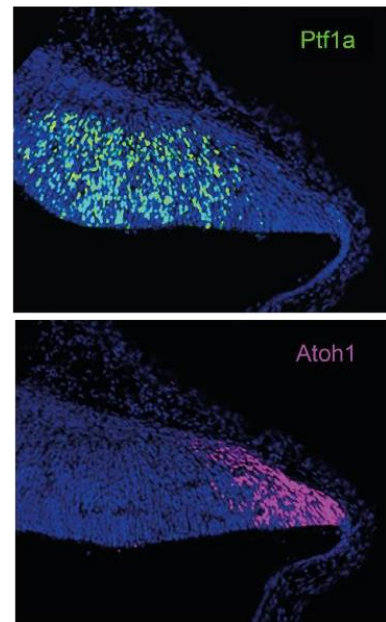
Figure 2: Development of cerebellar cells and cerebellar progenitor zones.
(**A**) In the table is summarized the information about the major cerebellar neurons populations (**B, C**) The graphical representation of neuron generation in the rhombic lip (RL) and ventricular zone (VZ) between E10.5 and P0 (**D**)The sagittal sections of the cerebellum stained against Ptf1a (green) and Atoh1 (red), and DAPI (blue) at E12.5. Pictures by D adapted from the published article (1), others are original.

2.2 Materials and methods

Animals

All animal experimentation was performed according to the guidance and policies of the Charité Universitätsmedizin Berlin, Germany; the Max-Delbrück-Center for Molecular Medicine Berlin, Germany; and the Institute of Neuroscience, Lobachevski University of Nizhny Novgorod, Russian Federation (1).

For the *in-utero* electroporation, wildtype mice were used. For lineage tracing experiments and mutant analysis, the following mouse strains were used: Olig3creERT2 (65), Olig3GFP (66), MaptnLacZ, Rosa26lsl-tdT(67), and Olig2cre (68).All mice strains had a mixed genetic background(1).

The animal experiments were performed by myself, my supervisor Dr. Hernandez-Miranda, Elijah D. Lowenstein.

Histology and cell quantifications

The protocols used for tissue preparation, immunohistochemistry, imaging and analysis had been previously described (69). In short, brain tissue was fixed in 4% paraformaldehyde (PFA) diluted in phosphate buffered saline (PBS) for 3 hours at 4 °C (1). The PFA was prepared from the paraformaldehyde powder, cooked and filtered. After fixation in the 4% PFA in PBS, the tissue was washed in PBS solution and placed in sucrose diluted in PBS. First, the tissue was incubated in 15% sucrose/PBS solution for 2 hours and later transferred to 30% sucrose/PBS solution for additional 10-12 hours (overnight). After that, the tissue embedded in the plastic molds filled with Tissue-Tek OCT (Sakura Finetek), frozen in dry ice and store at -80°C until required. Before sectioning, the tissue was incubated at -20°C at least 30 min.

To section the tissue, I used the thickness 20 µm or 40 µm, the temperature in the cryostat chamber was -16/-17 °C, the cryostat table temperature -18/-19 °C. After sectioning, the tissue was well dried or frozen until immunohistochemistry (IHC) has been performed.

To perform IHC the sections were washed in PBS and transferred to PBS-based blocking solution (0.1% Triton X-100 and goat serum 5%) and incubated at room temperature for 1 hour. Then, the primary antibodies of interest were dissolved in the blocking solution and applied to the slides with subsequent incubation overnight at room temperature. Next day, the slides were washed in PBS from primary antibody and a solution with secondary

antibody was applied and incubated at room temperature for 2-4 hours, depends on the thickness of the sections. The full list of primary and secondary antibodies, which were used during my work on the project is indicated in the Table from section "Material and methods" in the article (1).

For BrdU labeling pregnant dams were injected with BrdU (Sigma, 16 mg/ml) dissolved in PBS. The tissue was collected in 45 minutes. The subsequent analysis was performed on non-successive sections with the thickness 20-µm, non-blind, the sections were collected along sagittal cerebellar axis. For analysis, 6-10 sections pro animal were used. Whole-mount embryos at E12.5 were analyzed for β-gal using X-gal (0.6 mg/ml; Merck Millipore, B4252) in saline solution which contained potassium ferrocyanide 4 mM, NP-40 0.02% and MgCl2 2mM as described in protocol (70). To measure the volume of the cerebellar area, whole cerebellum was sliced with the same thickness of slices (each slice is 20 µm) and Nissl-stained. For each cerebellar sample were about 32-35 sections collected. Cerebellar area was measured from each section using ImageJ software and the total volume of the cerebellum were quantified by using the Cavalieri's method (71).

For imaging, we used a Zeiss LSM 700 confocal and photographs obtained from this microscope were assembled using the ZEN2012 software. In addition, several photographs were obtained using the spinning disk confocal microscope Zeiss. Lastly, we also used the Leica SPL confocal microscope and the generated images were assembled using Image J and the „stitching" plug in. During my doctoral study I performed all imaging on the Zeiss spinning disk confocal microscope and Leica SPL confocal microscope.

In utero electroporation

Whereas *in utero* electroporation with cortical targets is well established technic in our institute, the electroporation aimed to target hindbrain was never performed. Targeting the hindbrain using *in utero* electroporation is difficult and only two laboratories in the world were capable to carry such technique. During my PhD time, I set out to establish this technique in our group and I am very proud for succeeding in its implementation in our group. This powerful method is now allowing us to perform loss-of-function and gain-of-function experiments for the study of cerebellar and hindbrain development *in vivo.* In simple words, we can now introduce exogenous plasmids into the cerebellum or hindbrain of living embryos to turn on or turn off the expression of particular gene of interest. This

technique is minimally invasive and electroporated embryos can continue their normal development, they can be born and they can reach a normal adult age.

The general principles for *in utero* electroporation, which were the bases for my experiments had been described elsewhere (72). For my research article, I wanted to induce overexpression of two transcription factors in the cerebellar ventricular zone, the factors of interests were Olig3 and Pax2. For this, I clone the coding sequence of Olig3 (NM_053008.3) and Pax2 (NM_011037.5) into an empty pCAG-empty-IRES-GFP (1). To do this, I cloned the sequences of the genes of interest using the NEB-builder system, according to the manufacturer's instructions. Then, the generated plasmids wereverified by Sanger sequencing. When the plasmids were ready, I prepared working solutions, which contained DNA (plasmids) with total concentration 0.5 mg ml - 1 and FastGreen (1:10 from the volume). Fast green is used to visualize the injected volumes withinthe ventricular system of the embryos to be electroporated.

For control experiments, I used only the empty plasmid (pCAG-Empty-IRES-GFP) at a concentration of 0.5 mg ml−1; for the Olig3 overexpression experiment, pCAG-Olig3-IRES-GFP was used at a concentration of 0.5 mg ml−1; and for the Pax2 overexpression experiment, pCAG-Pax2-IRES-GFP was also used at a concentration of 0.5 mg ml−1. The working solution containing DNA-plasmid and Fast Green was injected with a glass micropipette into the fourth ventricle of the embryos from outside the uterus. The embryo's head was hold with forceps-type electrodes (NEPA GENE), and five to six electric pulses (50 ms of 37 V) were delivered at intervals of 950 ms with a square electroporator (Nepa Gene, CUY21)(1).

I would like to mention two critical points for successful electroporation. First – the access to the fourth ventricle. I faced either high embryo mortality or high survival rate with complete absence of traces of electroporation. That depends on place of injection and depths. A deep puncture, access to the fourth ventricle from the lateral sides, center, or caudal side, causes lethality of the embryos. By insufficient deep puncture, electroporation will be absent. A very bright color and a change in the position of the liquid is a sign of under-targeting of the fourth ventricle, that means that the injection was not deep enough. The best position, which I found was to inject the rostral fourth ventricle, at the border between hindbrain and midbrain. The good sign to recognize a successful electroporation was to observe a pale and confined drop in the fourth ventricle and the mesencephalic aqueduct. A second important detail to succeed in targeting the developing cerebellum is the electrode position. The best way to place the electrodes is

shown in the panel A of the figure 5 of my research article (eLife 10: e64684, 2021). In short, the negative electrode must be placed below the injection site and the positive

electrode in the frontal lobe. To summarize, I have implemented in our group a powerful method that allows for the overexpression of exogenous DNA materials *in vivo*, and this technique can also be used for the creation of disease models.

Brain clearing, lightsheet microscopy and analysis

The procedure of brain clearing is described in literature and was performed using the CUBIC protocol (73). To prepare tissue, the brains were isolated and fixed in 4% PFA overnight at 4°C, and after washed in PBS. Then, the Reagent-1 (25% urea, 25% Quadrol, 15% Triton X-100, 35% dH2O) was applied to remove the lipids, and the tissue was incubated at 37° C for 4 days at 4°C (1). Next, brains were washed in PBS overnight and the Reagent-2 (25% urea, 50% sucrose, 10% triethanolamine, 15% dH2O) was applied for 3 days at 37°C to match the refractive index (1). Cleared brains then were imaged using a Zeiss Lightsheet Z.1 microscope. The 3D-reconstructions, videos and photos was made using the arivis Vision4D software. My co-first author Mr. Elijah D. Lowenstein performed these experiments.
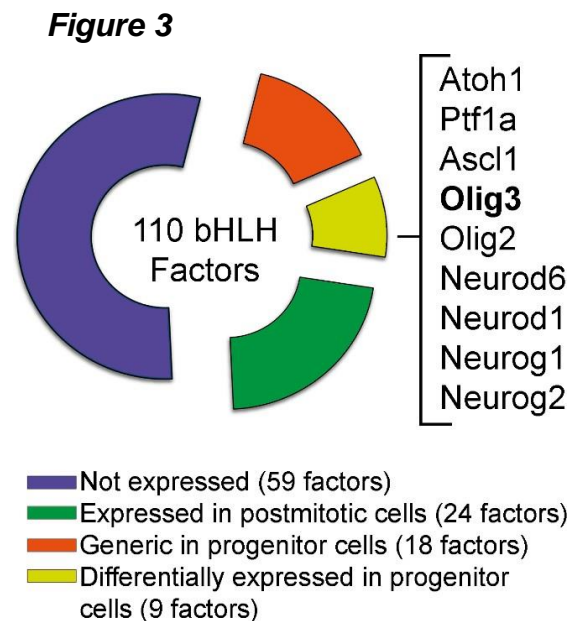
Statistics

All data is plotted using columns scatter plot charts with the calculated values for mean and standard deviations. For statistical analyses and plotting of the data, we used the software Graph Pad Prism 8. To perform pair comparison of normally distributed data we used the two-tailed t test, and for multiple comparisons we used one-way ANOVA analysis followed by Tukey's post hoc test. In our study, no randomization nor blinding methods were used. The sample size was not statistically pre-determined. In bar charts,the number of points indicates the number of analyzed samples (n).

2.3 Results

The first step in current work was to identify specific basic helix–loop–helix (bHLH) transcription factors acting in the specification of the different derivatives from the ventricular zone and the rhombic lip. We focused on these factors as they are well known to be essential for progenitor cell differentiation and key in neuronal specification (74-78). Around 130 such transcription factors are present in humans, whereas 110 transcription factors are expressed in mice and humans (75, 79). First we analyzed the spatial-temporal expression patterns of the 110 bHLH shared genes through the development of the cerebellum in mice, using publicly available data from the Allen Developing Mouse Brain Atlas (https://developingmouse.brain-map.org)(2). Only 51 bHLH transcription factors were expressed in the developing cerebellum, so the number of candidates was reduced by more than half (Figure3, 4). Among these 51 genes, we found 27 transcription factors expressed in the progenitor regions of the ventricular zone and the rhombic lip, whereas the

Figure 3

Atoh1
Ptf1a
Ascl1
Olig3
Olig2
Neurod6
Neurod1
Neurog1
Neurog2

110 bHLH Factors

■ Not expressed (59 factors)
■ Expressed in postmitotic cells (24 factors)
■ Generic in progenitor cells (18 factors)
■ Differentially expressed in progenitor cells (9 factors)

Figure3: The screening of the transcription factors (1).

The diagram illustrating the screening of the expression of 110 bHLH transcription factors during cerebellar development (1). The diagram is adapted from (1).

remaining transcription factors were expressed by postmitotic neurons outside the ventricular zone and the rhombic lip (Figure 4). Next, we looked in detail the expression of the 27 genes expressed in the cerebellar progenitor regions and found that only 9 of such genes had a temporal differential expression in the rhombic lip and ventricular zone, whilst the other genes appear to be generically expressed by all progenitor cells. For example, rhombic lip progenitors express Atoh1 and Olig3 between E11.5 and E13.5, whereas these progenitors express Atoh1 and Neurod1 between E14.5 and birth. Similarly, ventricular zone progenitors express Ptf1a, Olig3, Olig2 and Ascl1 between E11.5 and E13.5, while Ptf1a Neurod6, Neurog1 and Neurog2 between E14.5 and birth. For my PhD project, I focused on ventricular zone progenitors and their derivatives: the GABAergic neurons, whereas my co-first author Mr. Elijah D. Lowenstein focused on rhombic lip progenitors and their derivative neuron populations.

Figure 4

A

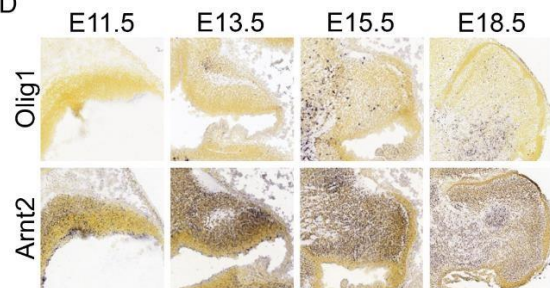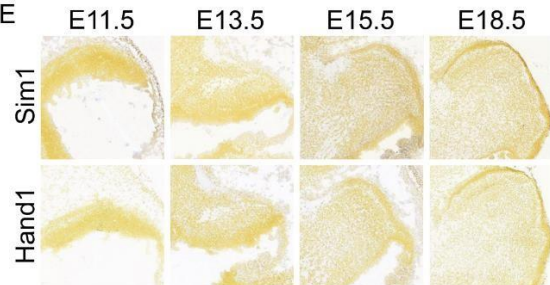| bHLH factors expressed in cerebellar progenitor niches: Rhombic lip (RL), Ventricular zone (VZ) and/or external granule cell layer (EGL)					
Gene Name	Expressed in progenitors?	Developmental stage: embryonic (E) day			
		E11.5	E13.5	E15.5	E17.5/E18.5
Ascl1	Yes	VZ	VZ	Weak in VZ	Not expressed
Atoh1	Yes	RL	RL & EGL	RL & EGL	RL & EGL
Hes1	Yes	Not expressed	RL & VZ	Not expressed	Not expressed
Hes5	Yes	RL & VZ	RL & VZ	RL & VZ	Postmitotic cells
Hes6	Yes	RL & VZ	RL, VZ & EGL	EGL	No data
Hes7	Yes	RL & VZ	Weak in RL, VZ	Weak in RL, VZ	Not expressed
Hey1	Yes	Not expressed	Not expressed	EGL	EGL
Hif1a	Yes	RL & VZ	Weak in RL, VZ	Not expressed	Not expressed
Id1	Yes	RL & VZ	In blood vessels	In blood vessels	In blood vessels
Id3	Yes	RL & VZ	RL, VZ & EGL	RL, VZ & EGL	EGL
Max	Yes	Weak in RL & VZ	Not expressed	Not expressed	Not expressed
Mxd3	Yes	RL & VZ	RL, VZ & EGL	EGL	EGL
Mxi1	Yes	Weak in RL & VZ	RL, VZ & EGL	RL, VZ & EGL	Weak in EGL
Mycl	Yes	RL & VZ	RL, VZ & EGL	EGL	EGL
Mycn	Yes	Strong in RL & VZ	Not expressed	Not expressed	Not expressed
Neurod1	Yes	Not expressed	Not expressed	Strong in EGL	Strong in EGL
Neurod6	Yes	Not expressed	Weak in VZ	VZ	Broad expression
Neurog1	Yes	Not expressed	VZ	Not expressed	Not expressed
Neurog2	Yes	Not expressed	Weak in VZ	Strong in VZ	Not expressed
Olig2	Yes	Weak in VZ	Strong in VZ	Postmitotic cells	Postmitotic cells
Olig3	Yes	RL & weak in VZ	RL & VZ	Not expressed	Not expressed
Ptf1a	Yes	Strong in VZ	Strong in VZ	Weak in VZ	Not expressed
Srebf1	Yes	Not expressed	RL, VZ & EGL	Weak in EGL	Not expressed
Srebf2	Yes	Weak in RL & VZ	RL & VZ	Postmitotic cells	Postmitotic cells
Tcf12	Yes	RL & VZ	RL, VZ & EGL	RL, VZ & EGL	RL, VZ & EGL
Tcf3	Yes	RL & VZ	RL, VZ & EGL	RL, VZ & EGL	RL, VZ & EGL
Tcf4	Yes	RL & VZ	RL, VZ & EGL	RL, VZ & EGL	RL, VZ & EGL

B
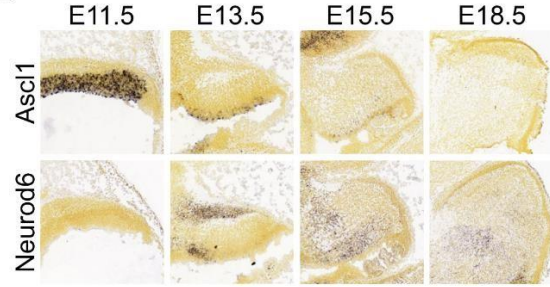
C
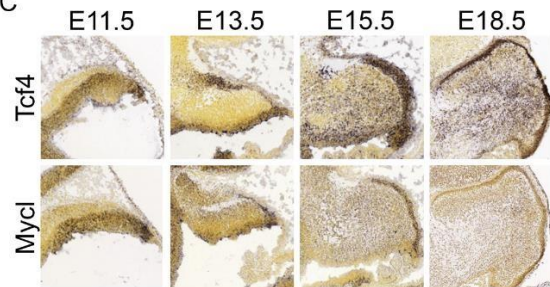
D

E

F

bHLH factors expressed in postmitotic	bHLH factors not expressed in the cerebellum during development
Gene name:	Gene name:
Arntl, Arnt2, Bhlhe22, Clock, Epas1, Id2, id4, Mlx, Mnt, Mxd1, Mxd4, Myc, Ncoa1, Ncoa2, Neurod2, Neurog3, Nhlh1, Nhlh2, Npas3, Npas4, Olig1, Scx, Sim2, Usf1 & Usf2	Ahr, Ahrr, Arnt, Arntl2, Ascl2, Ascl3, Ascl4, Ascl5, Atoh7, Atoh8, Bhlha15, Bhlha9, Bhlhb9, Bhlhe23, Bhlhe40, Bhlhe41, Ferd3l, Figla, Hand1, Hand2, Helt, Hes2, Hes3, Hes4, Hey2, Heyl, Hif3a, Lyl1, Mesp1, Mesp2, Mitf, Mlxip, Mlxipl, Msc, Myf5, Myf6, Myod1, Myog, Ncoa3, Neurod4, Npas1, Npas2, Sim1, Sohlh1, Sohlh2, Tal1, Tal2, Tcf15, Tcf21, Tcf23, Tcf24, Tcfl5, Tfap4, Tfe3, Tfeb, Tfec, Twist1 & Twist2

Figure 4: Screening of bHLH factors during cerebellar development (1).

(**A**, **F**) bHLH transcription factors grouped in the tables by being expressed or not expressed during cerebellar development in mice. (**B-E**) The spatial-temporal expression pattern of 110 bHLH transcription factors was analyzed, using data from the Allen Developing Mouse Brain Atlas (2). (**B**)Transcription factors differentially expressed in the cerebellar progenitor regions, (**C**) transcription factors generally expressed in the cerebellar progenitor cells, (**D**) transcription factors expressed in postmitotic cells, (**E**) transcription factors not expressed during cerebellar development (1, 2). All pictures are adapted from (1).
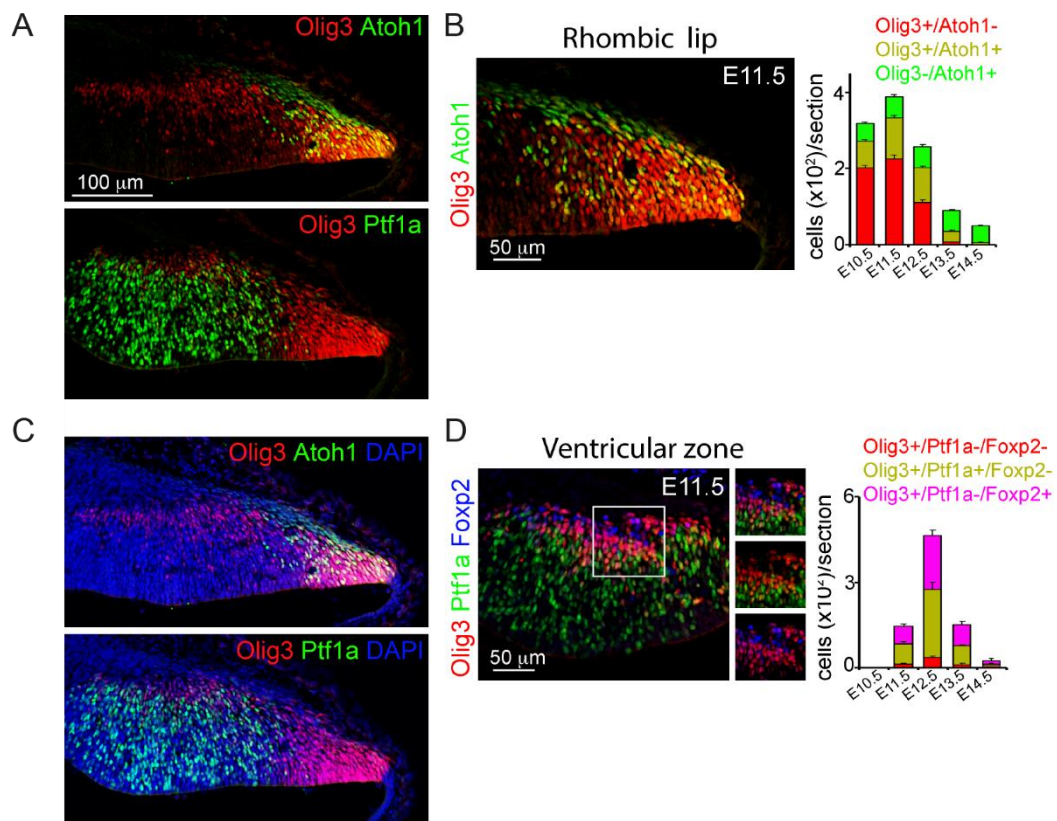
Figure 5
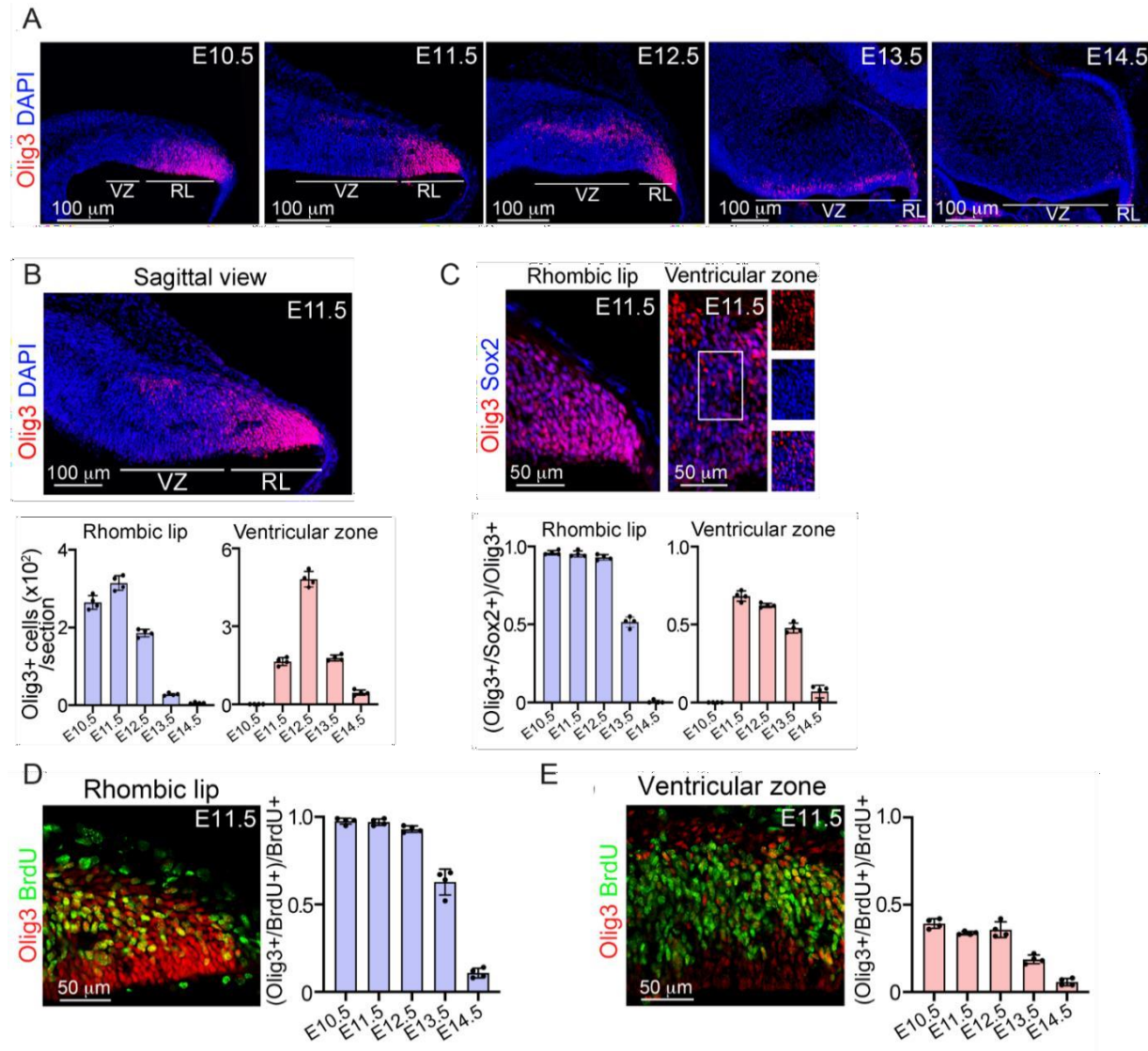
Figure 5: Olig3 expression during cerebellar development (1).

(A) The expression of Olig3 (red) in VZ and RL during developmental stages E10.5-E14.5. The expression of Atoh1 and Ptf1a indicating VZ and RL respectively. (**B**) Top, the cerebellar section stained against Olig3 (red) and DAPI (blue) at E11.5. Bottom, quantification of the Olig3+ positive cells from E10.5-E14.5 in the RL and VZ (1). (**C**) Top, the enlarged view of the VZ and RL stained against Olig3 (red) and Sox2 (blue) at E11.5 (1). Bottom, the quantification of the proportion of Olig3+ cells co-expressing Sox2 at E10.5-E14.5 (1). (**D**) Proliferative BrdU+ (green) cells co-expressing Olig3 (red) in the rhombic lip (**left**) and ventricular zone (**right**) between E10.5 and E14.5 with quantifications(1). All pictures are adapted from (1).

From the above-described analysis, the transcription factor Olig3 caught our attention (Figure 5), as it had never been implicated in cerebellar development, although it is known to play important functions in neuronal specification of dorsally emerging hindbrain known

to play important functions in neuronal specification of dorsally emerging hindbrain and spinal cord neurons (65, 66, 80, 81). As describe above Olig3 expressed in both the rhombic lip and ventricular zone at between E11.5-E13.5. Here, derivatives emerging from the ventricular zone (i.e. Purkinje cells, born E11.5-13.5) and from the rhombic lip (i.e. deep cerebellar neurons, born E11.5- E13.5). We next characterized the expression in detail using immunofluorescence. In the ventricular zone, Olig3+ cells appear at E11.5, their numbers achieve the maximum at E12.5 and became barely observed at E14.5 (1) (Figure 5A-E). To analyze, whether Olig3 positive cells are progenitors or postmitotic neurons, we performed IHC with a marker for progenitors – Sox2 and performed BrdU+ experiment, where all proliferating cells all labeled. In the ventricular zone almost 60% of Olig3+ positive cells were also expressing Sox2 at E11.5 and E12.5, but this co-expression and also total number of Olig3+ positive cells decreased by E13.5 (1) (Figure 5C). Furthermore, around 30% of the BrdU+ co-expressed Olig3 in the ventricular zone (Figure 5E). Lastly, more than half of the Olig3+ positive cells in VZ were colocalized with Ptf1a, and 41% co-expressed the postmitotic cell marker for Purkinje cells - Foxp2 (1) (Figure 6D). This indicates that whereas most Olig3+ cells in the ventricular zone are progenitors, Olig3 is remains to be present during earlier stage, in early-born Purkinje cells (Olig3+/Ptf1a-/Foxp2+)(1). My co-author found that Olig3+ cells were abundant in the rhombic lip from E10.5 to E12.5, but their numbers declined by E13.5 and were rare by E14.5 (1) (Figure 5, 6B). Almost all (>98%) Olig3+ rhombic lip cells co-expressed the progenitor marker Sox2 between E10.5 and E12.5, but this co-localization, as well as the total number of Olig3+ cells, declined by E13.5 (1) (Figure 5C). In addition, most of the proliferative BrdU+ positive cells in the RL were also Olig3+ positive (1) (Figure 5D). Lastly, about third of Olig3+ positive cells in the RL colocalized with Atoh1 (1). Thus, all rhombic lip progenitors expressed Olig3, and a third of them co-express Atoh1. Next, my co-author carried out a long-term lineage-tracing experiment and light sheet microscopy to obtain a preliminary view of the global distribution of Olig3 derived cerebellar neurons. For this experiment, he used a tamoxifen-inducible Olig3creERT2/+ mouse line and the reporter Rosa26lsl-tdT. The cre-mediated recombination allows marking with the tdTomato fluorescent protein all cells with a history of Olig3 expression. He found that all cerebellar neurons as well as most Purkinje cells were marked with tdTomato (1) (Figure 7).
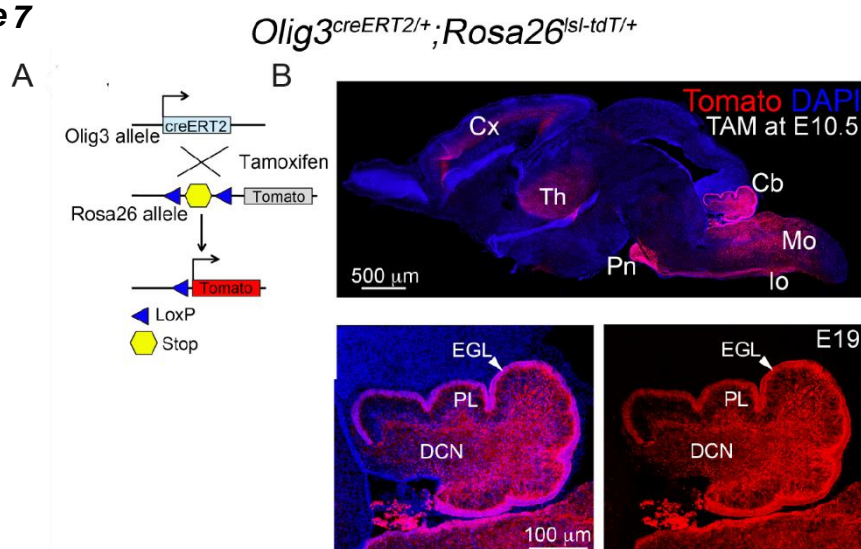
Figure 6

Figure 6: Characterization of Olig3 expression in the progenitors zones during cerebellar development (1).

(**A, C**) immunostaining against Olig3 (red) and Atoh1 (green) or Ptf1a (green) for identifications of RL and VZ respectively. (**B**) Left, immunostaining against Olig3 (red) and Atoh1 (green) at E11.5 with quantifications of the proportion of Olig3+ cells co-expressing Atoh1 at E10.5-E14.5 in RL (right) (1). (**D**) Left, immunostaining against Olig3 (red), Ptf1a (green), and the Purkinje cell marker Foxp2 (blue) at E11.5 with quantification of the proportion of Olig3+ cells co-expressing Ptf1a or Foxp2 at E10.5-E14.5 in VZ(1). All pictures are adapted from (1).

Figure 7

$Olig3^{creERT2/+};Rosa26^{lsl-tdT/+}$

Figure 7: Analysis of distribution of Olig3 derived cerebellar neurons by long-term lineage-tracing (1).

(**A**) Tamoxifen-dependent (TAM) cre recombinase driven by *Olig3* and the indicator allele Ai14 (*Olig3^{creERT2/+}; Rosa26lsl^{-tdT/+}* mice) labels cells with the history of Olig3. (**B**) Immunostaining against TdTomato (red) and DAPI (blue). All Olig3 derivatives marked with TdTomato, including thalamus region (Th), and its projections to the cortex (Cx) and, pontine nuclei (Pn), inferior olive (Io) and in the medulla oblongata (Mo)(1). Bottom, magnifications of the cerebellum. EGL -the external granule cell layer , Purkinje cell layer PL, and DCN neurons are labeled with tdTomato(1). All pictures are adapted from (1).

Next, we carried out a second long-term lineage-tracing experiment Olig3creERT2/+ mice and the MaptnLacZ reporter line. The cre-mediated recombination of the MaptnLacZ allows marking with nuclear beta galactosidase postmitotic neurons with a history of Olig3 expression. The immunofluorescence analysis showed that indeed most of deep cerebellar neurons, including the Tbr1+ fastigial neurons and the Brn2+ interposes and dentate neurons have a history of Olig3 expression (Figure 8E, H). In contrast, only a very few Pax2+ interneurons had a history of Olig3 expression (Figure 8G). Together, these data demonstrated that Olig3+ progenitor cells generate the earliest derivatives of the rhombic lip and the ventricular zone (1). Next, we assessed the developmental consequences of *Olig3* ablation in development of rhombic lip and ventricular zone derivatives. For this, we used *Olig3$^{-/-}$* mutant mice and analyzed their cerebella at birth (P0). Strikingly, the cerebellum of *Olig3$^{-/-}$* mutant mice was dramatically underdeveloped, as it had a strongly reduced size and lack of their characteristic foliation (Figure 9A-B). In particular, the volume of *Olig3$^{-/-}$* mutant cerebella was stronger reduced in the vermix area. Thus, ablation of Olig*3* results in severe hypoplasia (1). To further analyze the cerebellar cell composition in the *Olig3* mutant mice, we used immunofluorescence and label the different cell population. Regarding the rhombic lip, Elijah Lowenstein found a strong reduction of Tbr1+ and Brn2+ (DCN neurons), whereas I found a great reduction (over 52%) of Foxp2+ Purkinje cells and, surprisingly, an increase (over 70%) in Pax2+ inhibitory interneurons (1)(Figure 9E-F). To identify the onset of the phenotypes observed in *Olig3* mutant mice, we analyzed the cerebella of *Olig3$^{-/-}$* mutants at E13.5, a time point in which all Purkinje cells and deep cerebellar neurons are known to be specified. To this end, we used a Olig3^{GFP} knock-in mouse line that expresses GFP from the Olig3 locus (1). As controls we use *Olig3$^{GFP/+}$* heterozygous mice and mutants we used *Olig3$^{GFP/GFP}$* mice. Interestingly, I found not great changes in the number of Purkinje cells at this time point (Figure 10), nor in the number of Ptf1a+ progenitor cells or in the number of proliferative cells in the ventricular zone at earlier time points. This indicated that the reduction of Foxp2+ Purkinje cells observe in Olig3 mutant mice occur after their specification. In contrast, Elijah Lowenstein found a strong reduction in the number of Tbr1+ and Pax6+ progenitor cells that emerge from the rhombic lip already at E13.5 (Figure 11). Furthermore, Elijah Lowenstein observed a great reduction of Atoh1+ and BrdU+ rhombic lip progenitor cells at E11.5 and E12.5. We concluded that the function of Olig3 in the ventricular zone differs from its function in the rhombic lip, where Olig3 regulates progenitor cell proliferation (1).

Figure 8
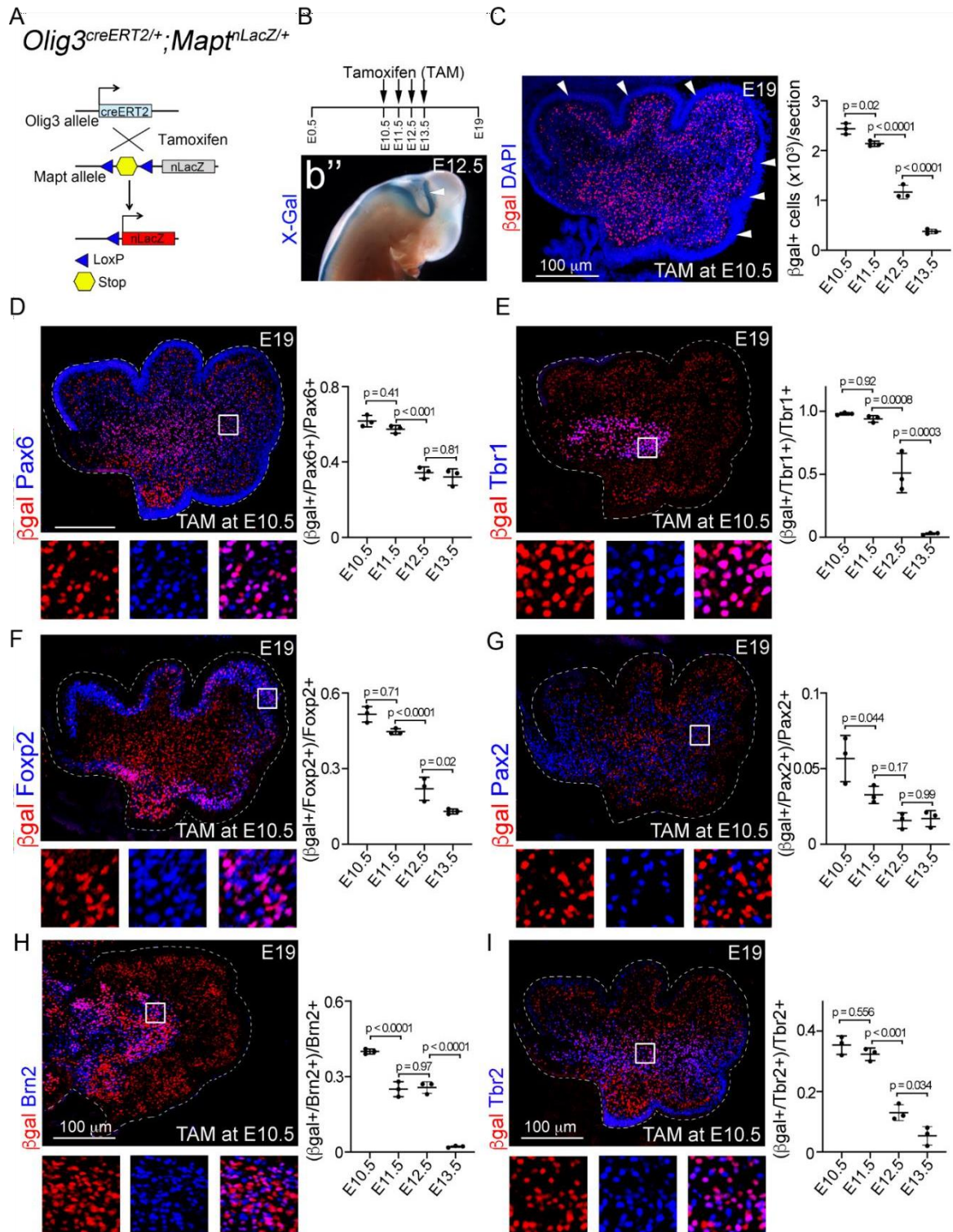
Figure 8: Long-term lineage-tracing of Olig3 derived cerebellar neurons (1).

(**A**) The labeling of the neurons derived from Olig3 by using the *Olig3creERT2* and the indicator allele Mapt-nuclear-LacZ (*Olig3creERT2/+;MaptnLacZ/+* mice) for all pictures on the panel. (**B**) Visualization cells with Olig3 history, the tamoxifen (TAM) was given to the mice on E10.5-E13.5 for one day and cerebellum was analyzed at E19. (**C**) The tamoxifen induced recombination was performed at E10.5, the section taken at E12.5. Arrowheads (white) indicate the βgal expression (red). (**D-I**)The cerebellar sections after recombination at E10.5, taken at E19.5 and immunostained against βgal and (**D**) Marker for EGL and granular cells Pax6 (blue), (**E**) marker for DCN neurons (Tbr1), (**F**) marker for Purkinje cells (Foxp2), (**G**) marker inhibitory interneurons (Pax2), (**H**) markers for dentatus/interpositus DCN neurons (Brn2) and (**I**) marker for unipolar brush cells(Tbr2), each picture has a panel with quantifications, namely the number of βgal+ positive /marker+ cells * 100 at E10.5-E13.5 (1). All pictures are adapted from (1).

22

Next, I analyzed Foxp2+ Purkinje cells and Pax2+ inhibitory interneurons in Olig3 mutant cerebella at E14.5, a time point in which inhibitory interneurons become specified. Strikingly, I observed that most Foxp2+ cells incorrectly co-expressed Pax2 (Figure 12A). Interestingly, the number of Foxp2+/Pax2+ cells decline over the time, and this decline coincided with the decrease of Purkinje (Foxp2+/Pax2-) cells and the increase in the number of inhibitory (Foxp2-/Pax2+) interneurons. Here, I hypothesized that Pax2 might suppress the expression of Foxp2 and thereby interfere with the differentiation program of Purkinje cells. To test this hypothesis, I overexpress Pax2 in the ventricular zone at E12.5, a time point in which Foxp2+ Purkinje cells are abundantly specified and no Pax2+ cell is observed in the cerebellum. This showed that no Pax2 electroporated cell co-express Foxp2, whereas over 70% of control electroporated cells did co-express Pax2. These experiments therefore demonstrated that Pax2 is capable to suppress Foxp2 expression (Figure 12). I next asked if Pax2 was sufficient to induce the differentiation program of inhibitory interneurons by suppressing Foxp2. To assess this, I electroporated Pax2 as describe above and stained electroporated cells with Parvalbumin, a known marker of inhibitory interneurons. This showed that more than 30% of the Pax2 electroporated cells co-expressed Pax2, whereas the control electroporated cells rarely do (Figure 13). Therefore, I concluded that Pax2 is capable to suppress Foxp2 and induce the differentiation program of inhibitory interneurons. Next, I asked if the function of Olig3 is to suppress Pax2 in the ventricular zone. To test this hypothesis, I electroporated Olig3 in the ventricular zone of wildtype embryos at E14, a time point in which Olig3 is absent and inhibitory interneurons initiate their differentiation. My results showed that indeed >70% of the Olig3 electroporated cells did not co-expressed Pax2, whereas most of the control electroporated cells did (Figure 14). Taking together, I concluded that Olig3 is essential to curtail the expression of Pax2 in the ventricular zone, and that this mechanism is central for the specification of Purkinje cells.
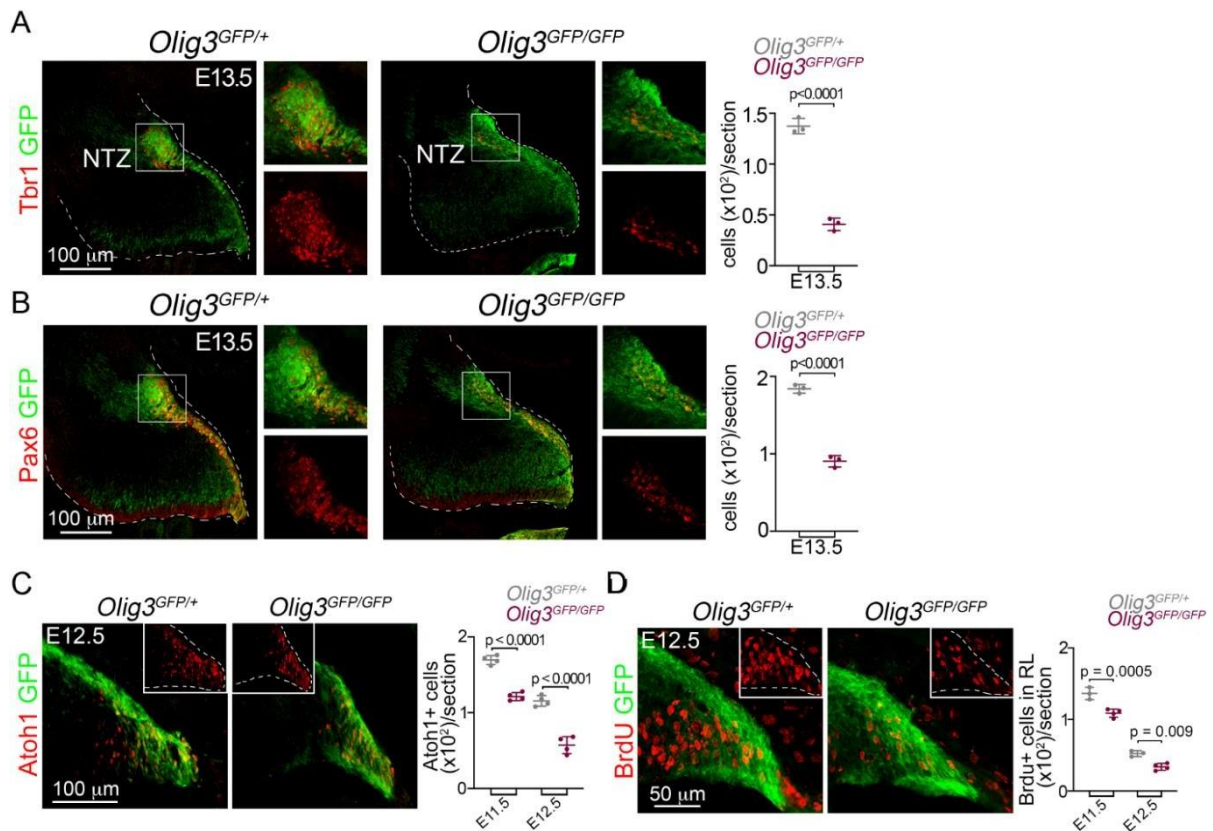
Figure 9
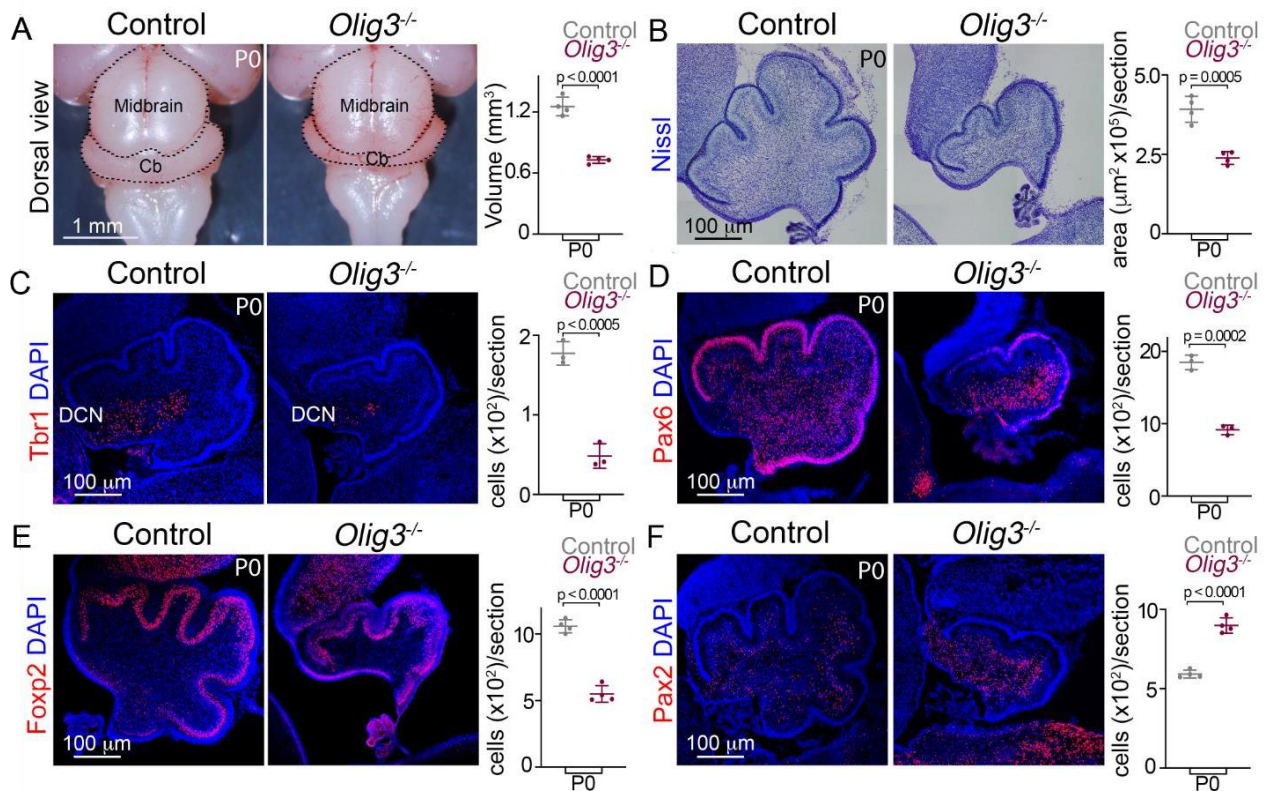
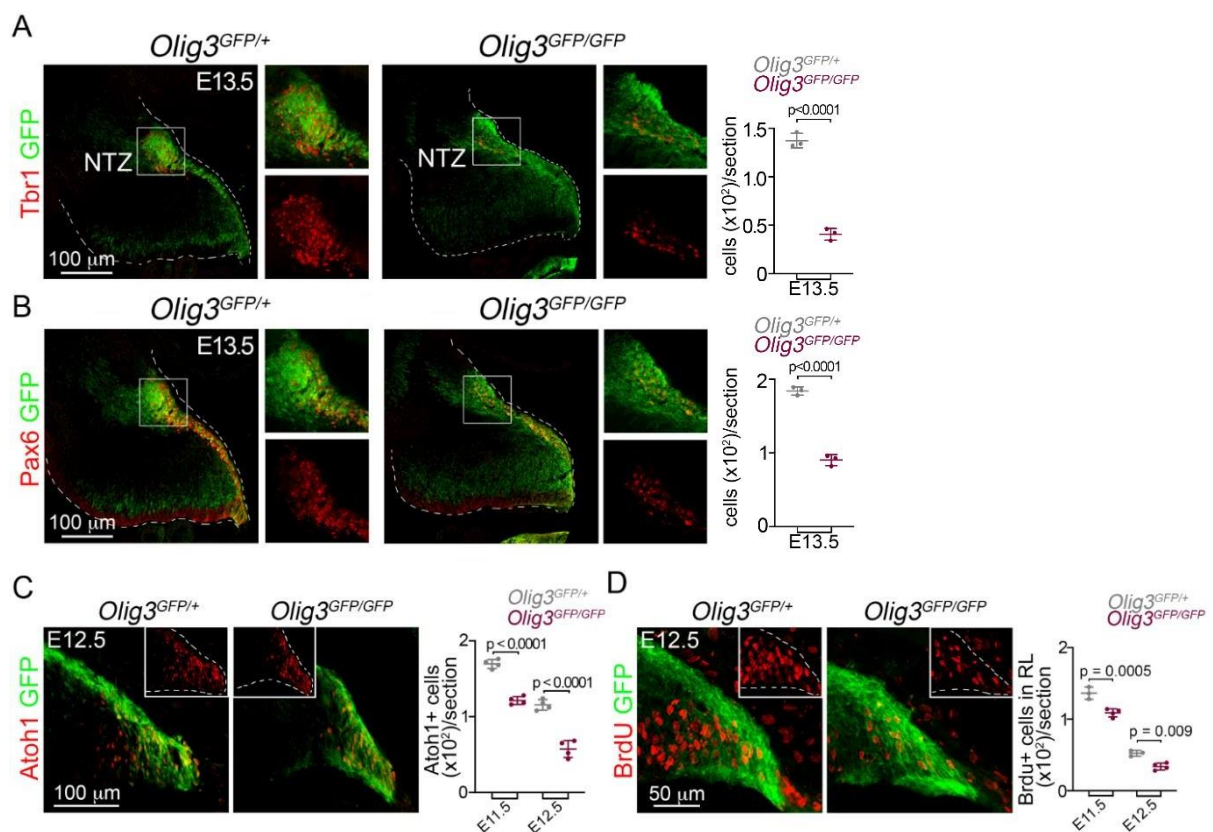**Figure 9: Characterization of Olig3 mutant mice with strong hypoplasia in phenotype (1).**

(**A**) The pictures of P0 cerebellum in control and Olig3-/- mutant and quantification of cerebellar volume in the mutant as compare to control (right). (**B**) Nissl staining on sagittal sections of newborn (P0) control and Olig3-/- mutant cerebellum, graphs shows the square of cerebellar area. (**C–F**) Immunostaining of the Olig3 mutant and control with marker in red (**C**) for DCN neurons (Tbr1), (**D**) for EGL and granule cells (Pax6), (**E**) for Purkinje cells (Foxp2), (**F**) for inhibitory interneurons (Pax2) and quantification. Cb - cerebellum; DCN - deep cerebellar nucleus(1). All pictures are adapted from (1).

Despite the fact that I found a great reduction (over 52%) of Foxp2+ Purkinje cells in the cerebellum of Olig3 mutant mice, many Purkinje cells were correctly specified. I therefore hypothesized that another factor might contribute to the specification of such cells. From our analysis of bHLH transcription factor during cerebellar development, we found that Ascl1 and Olig2 are also express during the specification of Purkinje cells (1). Whereas the mutation of Ascl1 in mice does not to alter the specification of Purkinje cells (82), the exact role of Olig2 in the generation of GABAergic derivatives is unclear (83, 84). To identify which function has the Olig2 during cerebellar neuron specification, the cerebellum of the Olig2 mutant was analyzed. We found a significant reduction in the number of Purkinje cell and a moderate increase in the number of inhibitory interneurons (Figure 15). Than we performed a long-term lineage-tracing experiment with Olig2cre and the MaptnLacZ allele (Olig2cre/+;MaptnLacZ/+) mice to clarify the role of Olig2 in the specification of the cerebellar GABAergic neurons.

Figure 10

Figure 11

25

Figure 10: Analysis of VZ progenitor cells in *Olig3* mutant embryos (1).

For all pictures, *Olig3* mutant (*Olig3GFP/GFP*) compared to control (*Olig3GFP/+*). (**A**) Characterization Foxp2+ Purkinje cells in control and *Olig3* mutant at E13.5 with magnification and (right) quantifications. (**B**) Characterization of Ptf1a+ ventricular zone cells in control and *Olig3* mutant at E12.5. Right, quantification of Ptf1a+ cells in control and mutant mice at E11.5 and E12.5. (**C**) Characterization of proliferative BrdU+ (red) in the ventricular zone control and *Olig3* mutant embryos at E12.5 with quantifications. All cerebellar sagittal sections were stained against GFP (green)(1). All pictures are adapted from (1).

Figure 11: Analysis of RL progenitor cells in *Olig3* mutant embryos (1).

For all pictures, *Olig3* mutant (*Olig3GFP/GFP*) compared to control (*Olig3GFP/+*). (**A, B**) Characterization Tbr1+ DCN neurons and Pax6+ EGL cells in control and *Olig3* mutant at E13.5 with magnification and (right), quantifications. NTZ is nuclear transitory zone. (**C**) Characterization of Atoh1+ rhombic lip cells in control and *Olig3* mutant at E12.5. Right, quantification of Ptf1a+ cells in control and mutant mice at E11.5 and E12.5. (**C**) Characterization of proliferative BrdU+ (red) in the rhombic lip control and *Olig3* mutant embryos at E12.5 with quantifications. (**E**) Characterization of Tunel+ apoptotic bodies (puncta, red) in control and *Olig3* mutant (*Olig3GFP/GFP*) mice at E12.5 with quantification Tunel+ apoptotic bodies in control and *Olig3* mutant mice at E11.5 and E12.5. All cerebellar sagittal sections were stained against GFP (green) (1). All pictures are adapted from (1).

Figure 12
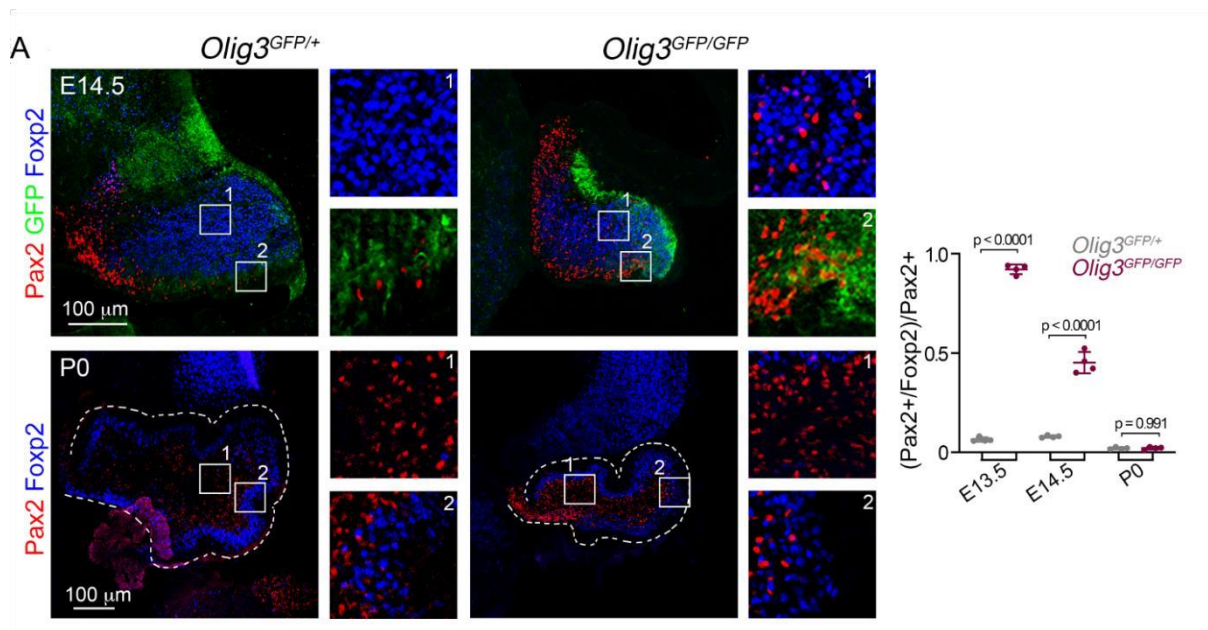
Figure 12: Misspecified Foxp2+/Pax2+ cells in *Olig3* mutant embryos (1).
(**A**) Analysis of Foxp2+ (blue) and Pax2+ (red) cells in control and *Olig3* mutant at E14.5 (top) and P0 (bottom) with two magnifications. GFP (green) shows expression originating from the *Olig3* locus, the expression can be seen at E14.5 but no longer by P0. Right, quantifications (the proportion of double positive Pax2+/Foxp2+ cells in Pax2+ cells). All pictures are adapted from (1).

Figure 13

A — Pax2 overexpression (E12.5-E14.5)

Merge | Pax2 | GFP | Foxp2

Control — 50 μm — 10 μm

Pax2 OE

Control
Pax2 OE

p<0.0001

(Foxp2+/GFP+)/GFP+

E14.5

B — Wildtype

E14.5

Parvalbumin Foxp2

100 μm

(Parvalbumin+/Foxp2+)/Parvalbumin+

E14.5

C — pCAG-GFP + pCAG-Empty-IRES-GFP

E14.5

Parvalbumin GFP

20 μm

pCAG-Pax2-IRES-GFP

Control
Pax2 OE

p < 0.0001

(Parvalbumin+/GFP+)/GFP+

E14.5
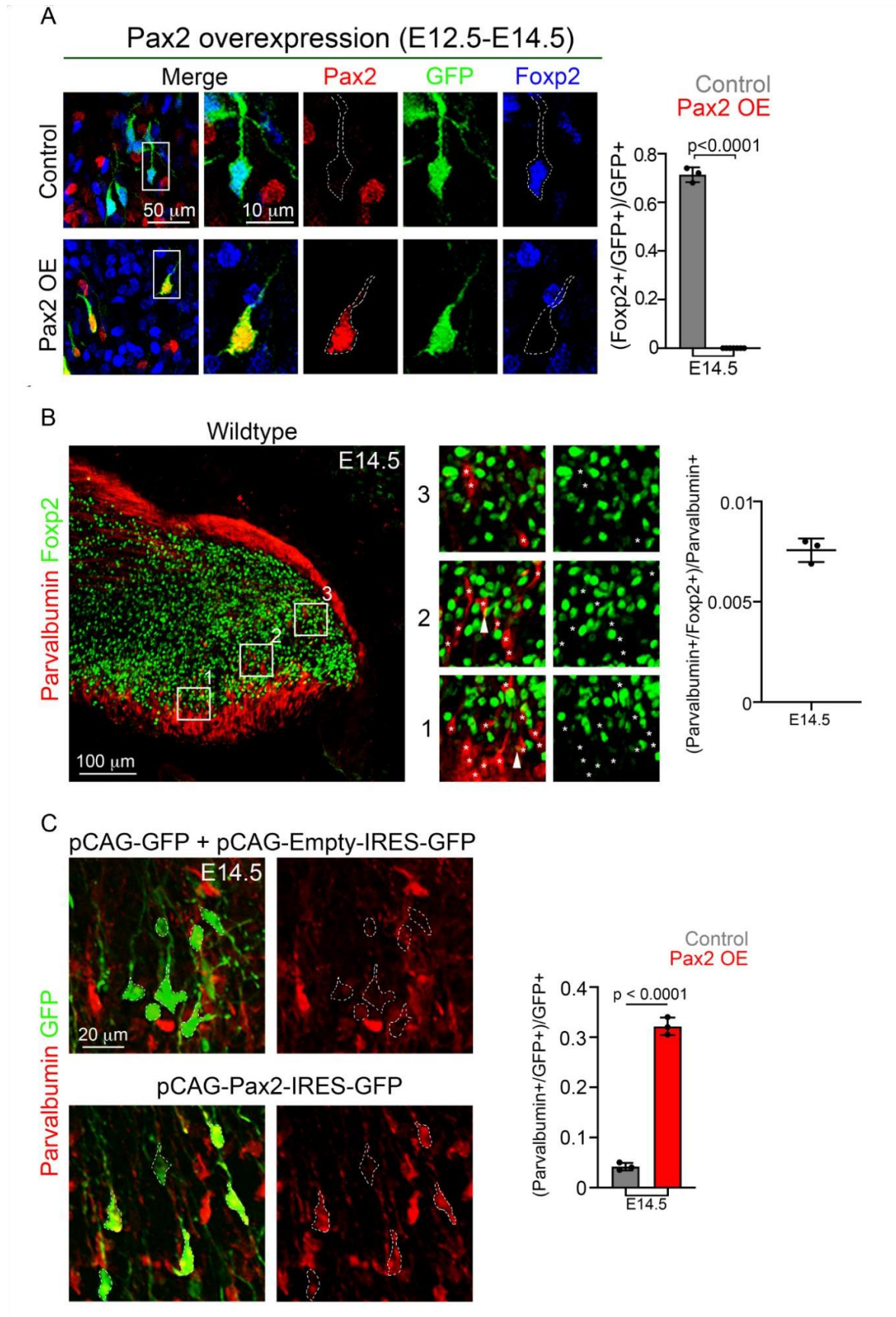
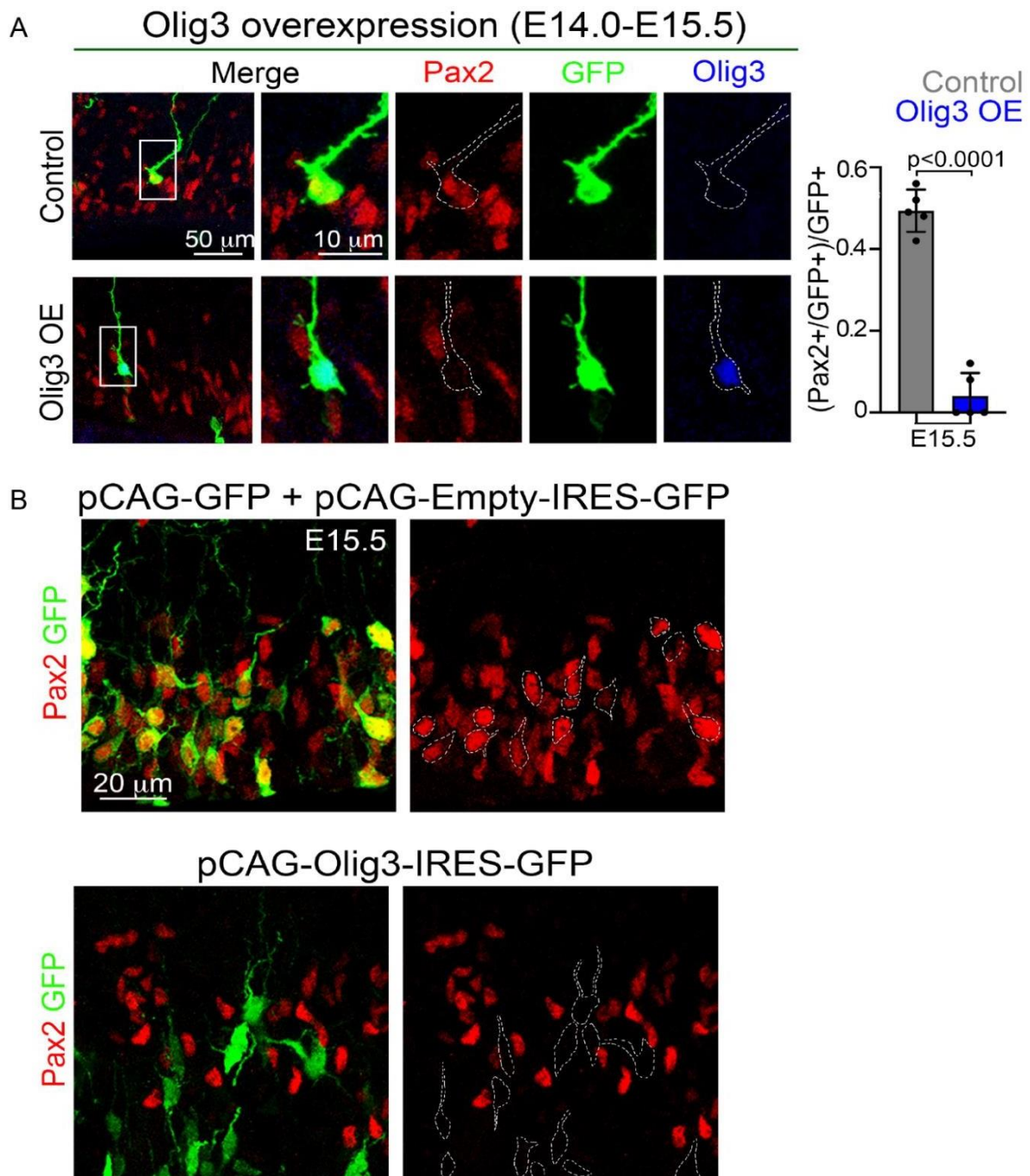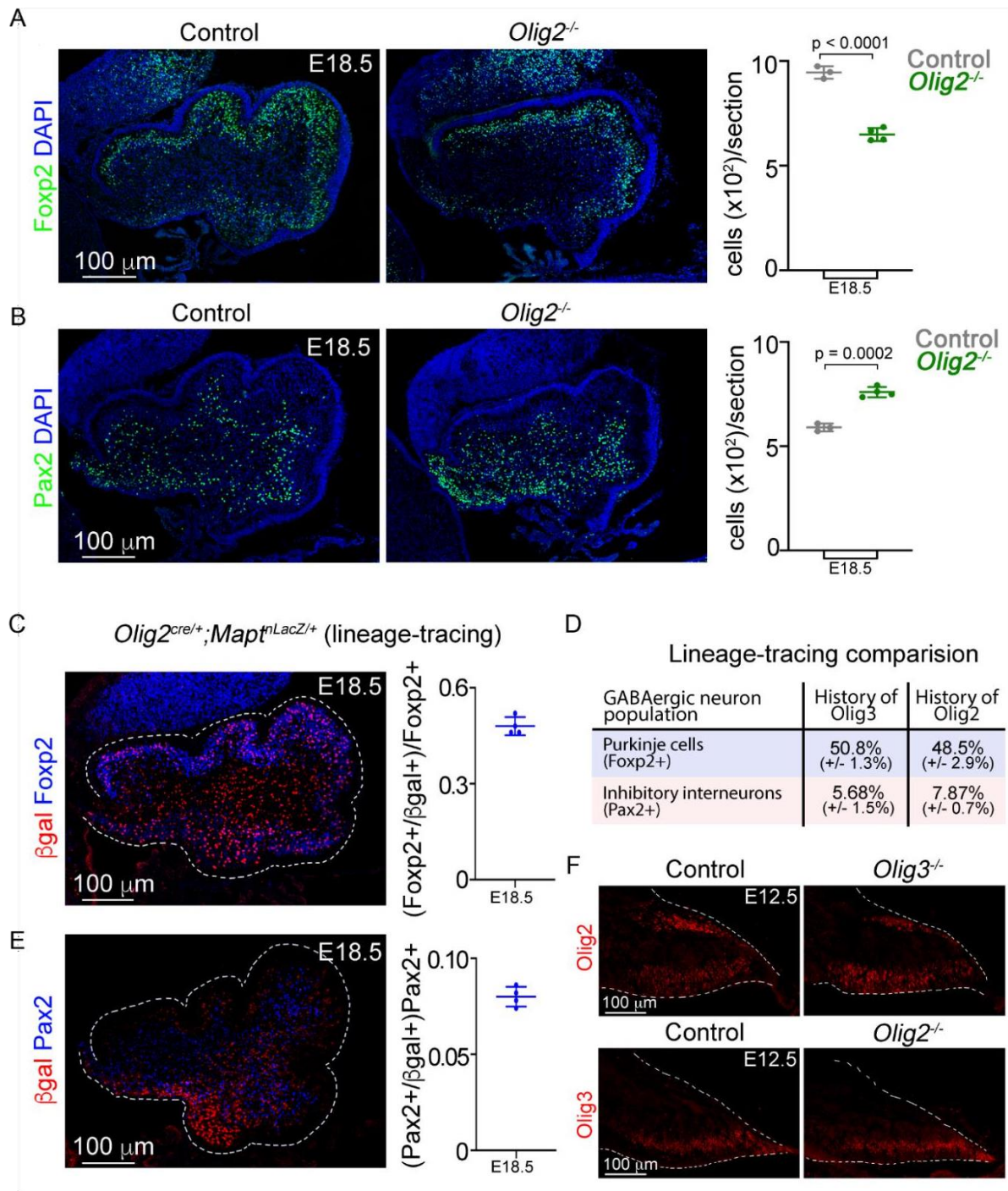**Figure 13: Pax2 is capable to suppress Foxp2 expression (1).**

(A) Wildtype mice electroporated at E12.5 with either empty pCAG-IRES-GFP as a control, or pCAG-PAx2-IRES-GFP or „Pax2-overexpression" plasmid. The electroporated cells in the cerebellum were analyzed at E14.5. Left, representative picture of analyzed electroporated cells in the cerebellum, stained against Pax2 (red), GFP (green), and Foxp2 (blue) with quantification of the proportion of GFP+ positive electroporated cells in control and Pax2-overexpression. (**B**) Immunohistochemistry staining against Parvalbumin (red) and Foxp2 (green) at E14.5 wildtype. Right, numbered pictures represents magnifications of the left pictures with co-immunostained Parvalbumin (red) and Foxp2 (green) or only Foxp2(green). The asterisks indicate the position of Parvalbumin+ positive cells. Right, quantification of the proportion of Parvalbumin+ positive cells co-expressing Foxp2 in the cerebellum of the wildtype mice at E14.5. (**C**) The representative pictures of electroporated at E12.5 cerebellar neurons. The electroporation was performed using empty control plasmid and Pax2-overexpression plasmid, the tissue was fixed at E14.5 and immunostained against Parvalbumin (red) and GFP (green). Right, quantification the proportion of cells co-expressing GFP and Parvalbumin in Pax2-overexpression and control (1). All pictures are adapted from (1).

This showed that around 50% Foxp2+ cells had a history of Olig2, only few of them originated from Olig2+ positive progenitors (Figure 15C). That let me to conclude, that Olig3 and Olig2 mutants shows partially analogical phenotype and probably have overlapping functions (summarized in Figure 15D). Next, I asked, how the absence of Olig3 would affect the expression of Olig2 in ventricular zone progenitors, and vice versa, if the ablation of Olig2 might affect the expression of Olig3. Mutation of Olig3 did not affect the expression of Olig2, and neither did mutation of Olig2, it did not change the expression of Olig3 in progenitor cells populations of the ventricular zone (Figure 15F). These results show that in ventricular zone the expression of Olig2 and Olig3 is autonomous and does not depend on other factor. Our next question was, if the absence of Olig2, similarly to Olig3, de-repress the Pax2 expression in the Purkinje cells. Indeed, we observed numerous Foxp2+/Pax2+ double-positive misspecified cells in Olig2 mutants at E13.5 (Figure 16A), but unlike Olig3 mutant embryos, these cells were only located in the rostral-most part of the ventricular zone (Figure 16A) (1). These data demonstrate that Olig2 might act as suppressor for Pax2, specifically for Purkinje cells generated in the rostral most part of the ventricular zone, while Olig3 has a broader function and it suppresses Pax2 in the most Purkinje cells in the entire ventricular zone region. I therefore conclude that Olig3 and Olig2 complementarily contribute to the correct specification of Purkinje cells by suppressing the expression of Pax2. Lastly, I tried to identify a transcription factor single out the specification of Pax2 inhibitory neurons. To this end, I looked at our list of bHLH transcription factor expressed in the ventricular zone at the time of interneurons specification, which is between E14.5 and birth. I found Neurod6 as a candidate gene, as its expression in the ventricular zone is absence between E11.5 and E13 but becomes activated from E14.5 and E16.6 (Figure 17A).

Figure 14

A Olig3 overexpression (E14.0-E15.5)

B pCAG-GFP + pCAG-Empty-IRES-GFP

pCAG-Olig3-IRES-GFP

Figure 14: Olig3 cell-autonomously suppress the expression of Pax2 in the ventricular zone (1).

(**A**) Wildtype mice electroporated at E12.5 with empty pCAG-IRES-GFP plasmid as a control, and pCAG-Olig3-IRES-GFP Olig3-overexpression plasmid. The electroporated cells in cerebellum were analyzed in 2 days at E14.5. Left, the representative picture of analyzed electroporated cells in the cerebellum, stained against Pax2 (red), GFP (green), and Foxp2 (blue). Right, magnifications and quantification of the proportion of GFP+ positive cells that co-express Foxp2 in Olig3-overexpression as compare to control. (**B**) Representative pictures of the cerebellar cells at E15.5 wildtype mice that were electroporated at E14.5 with either control or Olig3-overexpression constructs and stained against Pax2 (red) and GFP (green). Quantifications see at (**A**)(1). All pictures are adapted from (1).

Figure 15

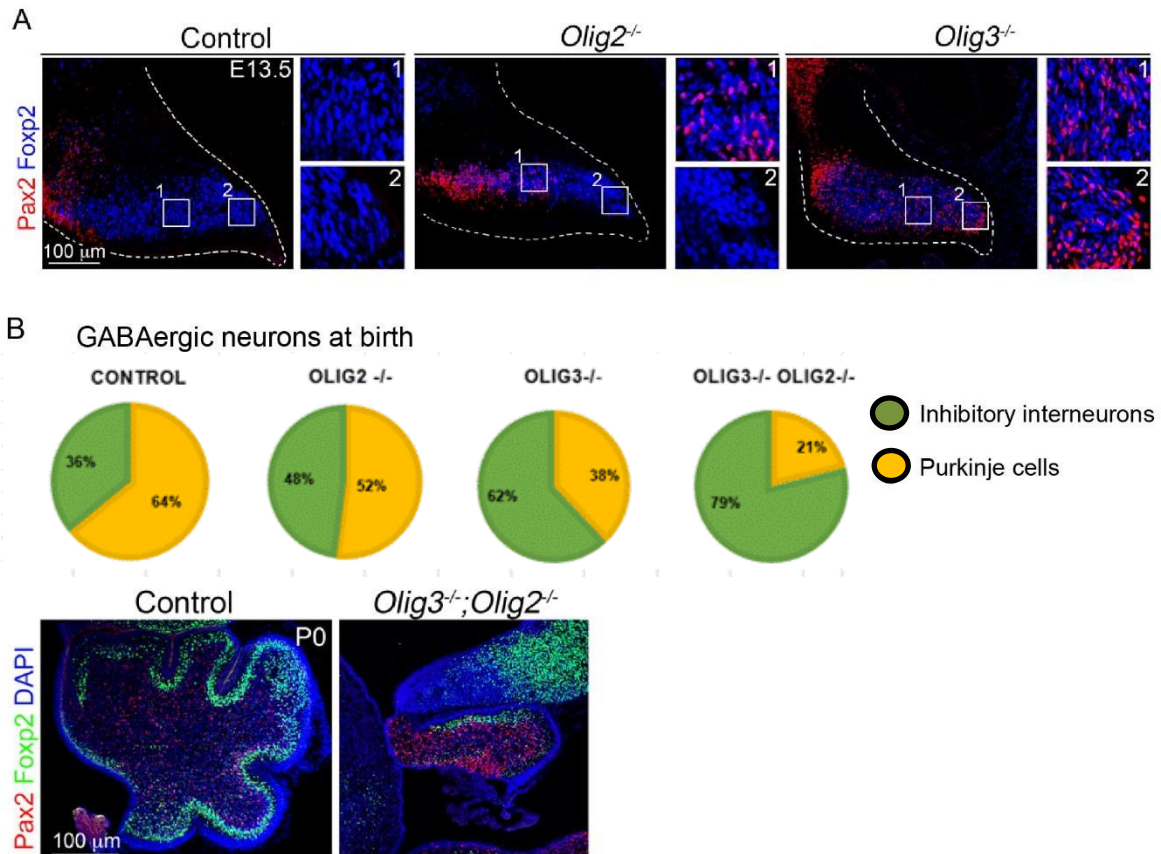**Figure 15: Analysis of GABAergic neurons in O*lig2* mutant mice (1).**
For all experiments on the panel was used *Olig2+/-* mice as a control and *Olig2-/-* mutant mice. In blue stained DAPI.
(**A**) Immunohistochemistry and quantifications of Foxp2+ positive (green) cells in control and *Olig2* mutant at E18.5. (**B**) Immunohistochemistry and quantifications of Pax2+ positive (green) cells in control and *Olig2* mutant at E18.5. (**C, E**) Analysis of inhibitory GABAergic neurons with a history of *Olig2* (βgal+) expression in cerebellum (red is βgal, blue is Pax2 /Foxp2) (**C**), and (**E**) inhibitory interneurons (Pax2). With quantification of double positive (βgal+/marker+) cells at E18.5. (**D**) Summary of the percentage of Pax2+ positive and Foxp2+ positive neurons with a history of Olig2 and Olig3. (**F**) Olig2 Expression in Olig3 mutant and control and Olig3 expression in Olig2 mutant and control(1). All pictures are adapted from (1).

Next, I analyzed the cerebella of Neurod6 mutant mice. Notably Neurod6 mutant mice, unlike Olig3 and Olig2 mutants that die at birth, are viable and fertile. Therefore, I analyzed the cerebellar of Neurod6 mice at two time points: postnatal day 2 and at two months of age. At postnatal day 2, not major changes were seen in Foxp2+ Purkinje cells, but more than 50% of Pax2+ inhibitory neurons were absent in *Neurod6* mutant mice. (Figure 17B). Comparing to control animals, I did not see any gross change in the morphology of Neurod6 mutant mice, but I did detect a great reduction of GABAergic interneurons in the molecular layer of Neurod6 mutant mice but not in the granular cell layer (Figure 17C). I conclude that Neurod6 is important for the specification of basket and stellate interneurons but not for the specification of Golgi or Lugaro cells.
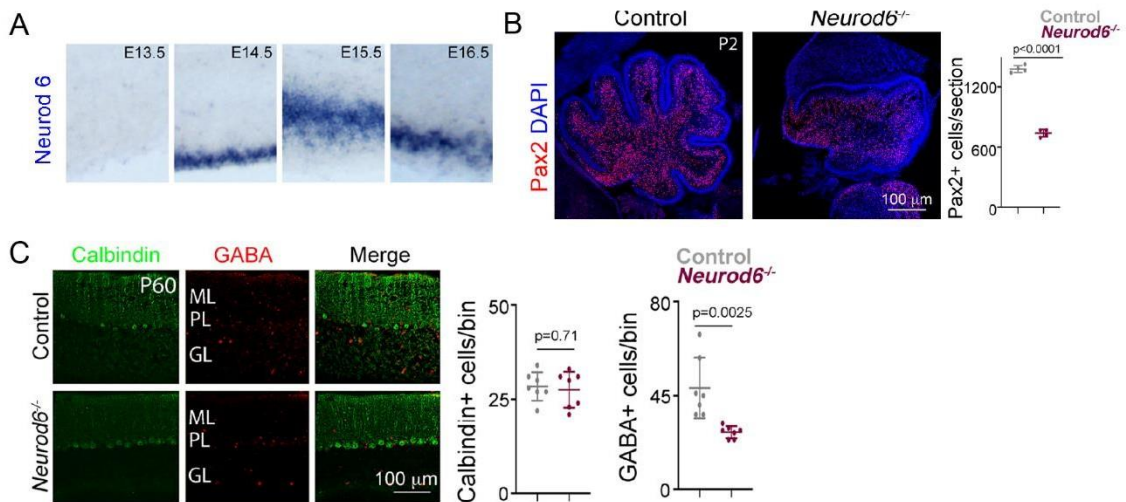
Figure 16

Figure 16: Analysis of GABAergic neurons in Olig2, Olig3 and Olig2/Olig3 mutant mice (1).
(**A**) Characterization of misspecified Foxp2+/Pax2+ cells at E13.5 in Olig2 and Olig3 mutants compare to control with magnifications(1). (**B**) Proportion of Inhibitory interneurons and Purkinje cells in control, Olig3 mutant, Olig2 mutant and Olig2/Olig3 double mutant. (**C**) Analysis of Pax2+(red) cells and Foxp2+(green) in Olig2/Olig3 double mutant and control mice at P0. The pictures A, C are adapted from (1) and diagrams by B are not published.

Figure 17

Figure 17: Analysis of GABAergic neurons in Neurod6 mutant mice.
For all experiments was used control (Neurod6+/-) and Neurod6 mutant (Neurod6-/-) mice. In blue stained DAPI. (**A**)The expression of Neurdo6 during cerebellar development. (**B**) Analysis of Pax2+ cells in Neurod6 mutant and control mice at P2 with quantification (**C**) Immunofluorescence characterization of cerebellar inhibitory interneurons with inhibitory neurons markers GABA+ (red) and Calbindin+ (green) in control and Neurod6--/- mutant mice at P60. Quantifications are on the right side. This figures and data are not published.

2.4 Discussion and summary

bHLH transcription factors act as main regulators in progenitor cell differentiation and neuronal cell type specification. In my doctoral project, I aimed to define the transcription factors and molecular mechanism essential for formation of different types of cerebellar GABAergic neurons. Cerebellum, unlike for example cortex, contains two adjacent germinal regions, ventricular zone and rhombic lip from which all GABAergic and glutamatergic neurons emerge, respectively. To search molecular mechanisms, I focused on the dynamic expression of bHLH transcription factor in the ventricular zone during cerebellar development. In doing so, I selected three factors that I demonstrated to be essential for Purkinje cells (Olig3 and Olig2) and inhibitory interneurons (Neurod6) specification. My co-author Elijah Lowenstein also showed that Olig3 is essential for deep cerebellar neuron specification. Together, we demonstrated that Olig3 is kernel in the specification of early neuronal derivatives emanating from both the ventricular zone and the rhombic lip.

My particular data show: i) that Olig3 and Olig2 are critical to curtail an inhibitory interneuron differentiation program in Purkinje cells, ii) that Olig3 does so by curtailing the expression of Pax2, iii) that Pax2 is an efficient suppressor of Foxp2 expression and the differentiation program of Purkinje cells, iv) that Pax2 alone is capable to induce the differentiation program of inhibitory interneurons, and v) the Neurod6 is an important player in the specification of basket and stellate inhibitory interneurons. The analysis of Olig3 and Olig2 mutant mice at birth showed a strong phenotype that is a hypoplastic cerebellum with few folia. Histological analysis of these mutant mice a revealed major alteration in Purkinje cell development and a "compensatory" increase in inhibitory neurons. Interestingly, preliminary data of double *Olig3/Olig2* mutant mice showed the almost complete absence of Foxp2+ Purkinje cells (Figure 16 B-C). This indicates that Olig3 and Olig2 specify complementary Purkinje cell populations. In *Neurod6* mutant mice, I observed the selective loss of GABAergic neurons that populate the molecular layer, which is basket and stellate cells, demonstrating that Neurod6 is essential for their development. However, no major changes were seen in GABAergic neurons that populate the granular layer, indicating that Golgi and Lugaro cells depend on other transcription factor for their specification. Based on our analysis of bHLH transcription factors expressed in the ventricular zone during the specification of inhibitory interneurons, I hypothesize that either Neurog1 or Neurog2 might be candidate genes for

the specification of Golgi and Lugaro cells. Future work is needed to assess this hypothesis.

Despite the fact my work and the work of my co-author has revealed the importance of Olig3, Olig2 and Neurod6 in the specification of distinct cerebellar neurons, the precise transcriptional regulation exerted by these factors remains to be elucidated. This information is relevant as to it can contribute to the prediction of disease-causing variants affecting cerebellar development and resulting in congenital ataxia. One way to elucidate such programs is to carry out chromatin immunoprecipitation assays using antibodies against Ptf1a, Olig3, Olig2 and Neurod6. Similarly, single cell sequencing could reveal the trajectories taken by different ventricular zone progenitors in the generation of, for example, Purkinje cells and the distinct types of inhibitory interneurons.

2.5 Description of own contribution

The published article "Olig3 regulates early cerebellar development" in eLife 10:e64684 (2021) has two co-first authors, myself and my colleague Elijah D Lowenstein. Here I would like to explain my role and position regarding this work, and to overview all my work, performed during my doctoral study. In modern science, it is became more and more common that many scientists join forces and work together on a project. It allows performing experiments in shorter time. The experiments thus can include highly specific technique, which give the opportunity to observe a complete picture of the analyzed phenomenon, especially in the field of fundamental neuroscience and molecular biology. This was the case of my research article and PhD project. Historically, my colleague Elijah Lowenstein initiated the project in the group of Dr. Hernandez-Miranda and carried out the initial lineage tracing experiments. I later joined the group of Dr. Hernandez-Miranda in 2019, and since that time, I started intense work on this project. Initially, the part regarding excitatory neurons was a sphere of interest of Elijah D Lowenstein; my interest was concentrated on GABAergic neurons. Therefore, we divided the work to achieve a complete picture of the mechanisms operating in the subspecification of cerebellar neurons. However, the identification a transcription factor Olig3 as a major determinant in the development of the earliest GABAergic and glutamatergic cerebellar neuron derivative from the ventricular zone and the rhombic lip signified the basis for writing a joint article. Such collaboration allowed us to combine highly specialized techniques that require many years of experience and knowledge. My colleague Elijah D Lowenstein performed completely the light sheet microscopy and brain clearing, with subsequent 3D reconstruction. This made our article much more complete. I performed the analysis of Olig2 and Neurod6 and performed *in vivo* electroporation *in utero*. I would like to acknowledge that my initial trials with *in utero* electroporation were done in collaboration with my colleague E. Epifanova. Setting up this complex and rare experimental procedure allowed us to demonstrate *in vivo* the ability of different transcription factors in the specification of distinct cerebellar neuron populations. Both Elijah D Lowenstein and I actively participated in the experimental part and in the preparation of our research article, with the guidance of our supervisor Dr. Hernandez-Miranda. By our initial agreement, and the decision of my supervisor, the contribution of Elijah D Lowenstein and my contribution was considered equal.

I decided to include in my thesis only this project, because of my personal special interest in this topic. However, it is not the only one project I performed during my PhD studies,

and it is not the only publication I obtained from my PhD work. During my five-years full time doctoral studies, I was mastered in most of laboratory techniques and became advanced in *in vivo* manipulations, surgeries, animal and behavior experiments, from which I obtained massive experience in scientific project management, as well as in presenting my own data. One of the first projects I participate was dedicated to ENU-mutagenesis, which we performed together with the institute of the neuroscience in Nizhniy Novgorod, Russia. The idea of the project was to identify a novel mutation by induced ENU-mutagenesis causing brain malformation. My results were published in the article *"Identification of Novel Mutations Controlling Cerebral Cortex Malformations Caused by ENU-Induced Mutagenesis in the Mouse"*(85), as well as my poster presentation with a poster "ENU-screening focused on mutations causing malformations of cortical development" on 11th FENS Forum of Neuroscience 7-11 July, 2018, Berlin, Germany. A second major project of my PhD studies focuses on kinases using *in situ* screening, with the aim to identify specific kinases regulating cortex-development and also, taking part in a big project aimed to explore the role of protein kinases in cortical neurons formation. With my data, I co-authored the article *"Polarity Acquisition in Cortical Neurons Is Driven by Synergistic Action of Sox9-Regulated Wwp1 and Wwp2 E3 Ubiquitin Ligases and Intronic miR-140"* in the Neuron (86). The third project, which I was performing during my PhD, dedicated to translational repressors. There, I first performed the screening of the translational repressors which potentially target Satb2, and focused on four translational repressors (Eif4Ebp1, Eif4Enif1, Samd4b and Pumilio2.), and I studied their role in the regulating the fate of SatB2+ neurons in cerebral cortex development. Part of my data (Pumilio2) included in the article available in pre-print version with a title: "Timed global reorganization of protein synthesis during neocortex neurogenesis at codon resolution*" (87)*. Remaining data will be a part of the subsequent article. Additionally, I was participating in many smaller collaboration-projects. Lastly, the special place in my doctoral study and my personal scientific passionate is the cerebellar project. I choose specifically this topic for my doctoral dissertation because it mostly reflects my scientific and medical interests. This topic let me fully to explore in myself as a scientist and allow me to summarize all my skills and knowledge in a research article, of which I feel very proud. This is not the end in my scientific path and I am currently continuing my work and expect to get fascinating data in the nearest future, already, as a postdoctoral fellow.

2.6 References

1.   Lowenstein ED, Rusanova A, Stelzer J, Hernaiz-Llorens M, Schroer AE, Epifanova E, Bladt F, Isik EG, Buchert S, Jia S, Tarabykin V, Hernandez-Miranda LR. Olig3 regulates early cerebellar development. Elife. 2021;10.

2.   Allen Developing Mouse Brain Atlas 2008.

3.   Sereno MI, Diedrichsen J, Tachrount M, Testa-Silva G, d'Arceuil H, De Zeeuw C. The human cerebellum has almost 80% of the surface area of the neocortex. Proceedings of the National Academy of Sciences. 2020;117(32):19538-43.

4.   Andersen BB, Korbo L, Pakkenberg B. A quantitative study of the human cerebellum with unbiased stereological techniques. Journal of Comparative Neurology. 1992;326(4):549-60.

5.   Manto M, Bower JM, Conforto AB, Delgado-García JM, da Guarda SNF, Gerwig M, Habas C, Hagura N, Ivry RB, Mariën P, Molinari M, Naito E, Nowak DA, Oulad Ben Taib N, Pelisson D, Tesche CD, Tilikete C, Timmann D. Consensus paper: roles of the cerebellum in motor control--the diversity of ideas on cerebellar involvement in movement. Cerebellum (London, England). 2012;11(2):457-87.

6.   Schweighofer N, Spoelstra J, Arbib MA, Kawato M. Role of the cerebellum in reaching movements in humans. II. A neural model of the intermediate cerebellum. Eur J Neurosci. 1998;10(1):95-105.

7.   Palesi F, De Rinaldis A, Castellazzi G, Calamante F, Muhlert N, Chard D, Tournier JD, Magenes G, D'Angelo E, Gandini Wheeler-Kingshott CAM. Contralateral cortico-ponto-cerebellar pathways reconstruction in humans in vivo: implications for reciprocal cerebro-cerebellar structural connectivity in motor and non-motor areas. Sci Rep. 2017;7(1):12841.

8.   Sengul G, Fu Y, Yu Y, Paxinos G. Spinal cord projections to the cerebellum in the mouse. Brain Struct Funct. 2015;220(5):2997-3009.

9.   Park SY, Yeo SS, Jang SH, Cho IH. Anatomical Location of the Vestibulocerebellar Tract in the Healthy Human Brain: A Diffusion Tensor Imaging Study. Brain Sci. 2021;11(2).

10.   Li N, Mrsic-Flogel TD. Cortico-cerebellar interactions during goal-directed behavior. Curr Opin Neurobiol. 2020;65:27-37.

11.   Hoogland TM, De Gruijl JR, Witter L, Canto CB, De Zeeuw CI. Role of Synchronous Activation of Cerebellar Purkinje Cell Ensembles in Multi-joint Movement Control. Curr Biol. 2015;25(9):1157-65.

12.   Zimmet AM, Cowan NJ, Bastian AJ. Patients with Cerebellar Ataxia Do Not Benefit from Limb Weights. Cerebellum (London, England). 2019;18(1):128-36.

13.   Bares M, Lungu OV, Husárová I, Gescheidt T. Predictive motor timing performance dissociates between early diseases of the cerebellum and Parkinson's disease. Cerebellum (London, England). 2010;9(1):124-35.

14.   Gilman S. The mechanism of cerebellar hypotonia. An experimental study in the monkey. Brain. 1969;92(3):621-38.

15.   Dichgans DHCDJ. Pathophysiology of cerebellar ataxia. Movement disorders. 1992;7(2).

16.   Dictionary FPM. Dysdiadochokinesia.(n.d.) 2012.

17.   Berardelli A, Hallett M, Rothwell JC, Agostino R, Manfredi M, Thompson PD, Marsden CD. Single-joint rapid arm movements in normal subjects and in patients with motor disorders. Brain. 1996;119 (Pt 2):661-74.

18.   Baier B, Stoeter P, Dieterich M. Anatomical correlates of ocular motor deficits in cerebellar lesions. Brain. 2009;132(8):2114-24.

19.   Habas C. Functional Connectivity of the Cognitive Cerebellum. Front Syst Neurosci. 2021;15:642225.

20.   Adamaszek M, Kirkby KC, D'Agata F, Olbrich S, Langner S, Steele C, Sehm B, Busse S, Kessler C, Hamm A. Neural correlates of impaired emotional face recognition in cerebellar lesions. Brain Research. 2015;1613:1-12.

21.   Mothersill O, Knee-Zaska C, Donohoe G. Emotion and Theory of Mind in Schizophrenia-Investigating the Role of the Cerebellum. Cerebellum (London, England). 2016;15(3):357-68.

22.   Adamaszek M, D'Agata F, Ferrucci R, Habas C, Keulen S, Kirkby KC, Leggio M, Mariën P, Molinari M, Moulton E, Orsi L, Van Overwalle F, Papadelis C, Priori A, Sacchetti B, Schutter DJ, Styliadis C, Verhoeven J. Consensus Paper: Cerebellum and Emotion. Cerebellum (London, England). 2017;16(2):552-76.

23.   Adamaszek M, D'Agata F, Kirkby KC, Trenner MU, Sehm B, Steele CJ, Berneiser J, Strecker K. Impairment of Emotional Facial Expression and Prosody Discrimination Due to Ischemic Cerebellar Lesions. The Cerebellum. 2014;13(3):338-45.

24.   Kelly E, Meng F, Fujita H, Morgado F, Kazemi Y, Rice LC, Ren C, Escamilla CO, Gibson JM, Sajadi S, Pendry RJ, Tan T, Ellegood J, Basson MA, Blakely RD, Dindot SV, Golzio C, Hahn MK, Katsanis N, Robins DM, Silverman JL, Singh KK, Wevrick R, Taylor MJ, Hammill C, Anagnostou E, Pfeiffer BE, Stoodley CJ, Lerch JP, du Lac S, Tsai PT. Regulation of autism-relevant behaviors by cerebellar-prefrontal cortical circuits. Nat Neurosci. 2020;23(9):1102-10.

25.   Bruchhage MMK, Bucci M-P, Becker EBE. Chapter 4 - Cerebellar involvement in autism and ADHD. In: Manto M, Huisman TAGM, editors. Handbook of Clinical Neurology. 155: Elsevier; 2018. p. 61-72.

26.   Stoodley CJ. The Cerebellum and Neurodevelopmental Disorders. Cerebellum (London, England). 2016;15(1):34-7.

27.   Aldinger KA, Timms AE, Thomson Z, Mirzaa GM, Bennett JT, Rosenberg AB, Roco CM, Hirano M, Abidi F, Haldipur P, Cheng CV, Collins S, Park K, Zeiger J, Overmann LM, Alkuraya FS, Biesecker LG, Braddock SR, Cathey S, Cho MT, Chung BHY, Everman DB, Zarate YA, Jones JR, Schwartz CE, Goldstein A, Hopkin RJ, Krantz ID, Ladda RL, Leppig KA, McGillivray BC, Sell S, Wusik K, Gleeson JG, Nickerson DA, Bamshad MJ, Gerrelli D, Lisgo SN, Seelig G, Ishak GE, Barkovich AJ, Curry CJ, Glass IA, Millen KJ, Doherty D, Dobyns WB. Redefining the Etiologic Landscape of Cerebellar Malformations. Am J Hum Genet. 2019;105(3):606-15.

28.   Zanni G, Bertini ES. X-linked disorders with cerebellar dysgenesis. Orphanet journal of rare diseases. 2011;6:24-.

29.   Williams CT, De Jesus O. Friedreich Ataxia. StatPearls. Treasure Island (FL): StatPearls Publishing

Copyright © 2021, StatPearls Publishing LLC.; 2021.

30.   Cook A, Giunti P. Friedreich's ataxia: clinical features, pathogenesis and management. British medical bulletin. 2017;124(1):19-30.

31.   Delatycki MB, Bidichandani SI. Friedreich ataxia- pathogenesis and implications for therapies. Neurobiology of Disease. 2019;132:104606.

32.   Campuzano V, Montermini L, Molto MD, Pianese L, Cossée M, Cavalcanti F, Monros E, Rodius F, Duclos F, Monticelli A. Friedreich's ataxia: autosomal recessive disease caused by an intronic GAA triplet repeat expansion. Science. 1996;271(5254):1423-7.

33.   Teive HA, Ashizawa T. Primary and secondary ataxias. Curr Opin Neurol. 2015;28(4):413-22.

34.   Rahman S, Copeland WC. POLG-related disorders and their neurological manifestations. Nat Rev Neurol. 2019;15(1):40-52.

35.   Stoodley CJ. Distinct regions of the cerebellum show gray matter decreases in autism, ADHD, and developmental dyslexia. Front Syst Neurosci. 2014;8:92.

36.   Minichino A, Bersani FS, Trabucchi G, Albano G, Primavera M, Delle Chiaie R, Biondi M. The role of cerebellum in unipolar and bipolar depression: a review of the main neurobiological findings. Riv Psichiatr. 2014;49(3):124-31.

37.   Health TNIoM. Attention-Deficit/Hyperactivity Disorder2019. Available from: https://www.nimh.nih.gov/health/topics/attention-deficit-hyperactivity-disorder-adhd/index.shtml.

38.   Crespo-Facorro B, Wiser AK, Andreasen NC, O'Leary DS, Watkins GL, Boles Ponto LL, Hichwa RD. Neural basis of novel and well-learned recognition memory in schizophrenia: a positron emission tomography study. Hum Brain Mapp. 2001;12(4):219-31.

39.   Okugawa G, Nobuhara K, Sugimoto T, Kinoshita T. Diffusion tensor imaging study of the middle cerebellar peduncles in patients with schizophrenia. Cerebellum (London, England). 2005;4(2):123-7.

40.   Goldowitz D, Hamre K. The cells and molecules that make a cerebellum. Trends Neurosci. 1998;21(9):375-82.

41.   Hirano T. Regulation and Interaction of Multiple Types of Synaptic Plasticity in a Purkinje Neuron and Their Contribution to Motor Learning. The Cerebellum. 2018;17(6):756-65.

42.   Streng ML, Popa LS, Ebner TJ. Complex Spike Wars: a New Hope. The Cerebellum. 2018;17(6):735-46.

43.   Larry N, Yarkoni M, Lixenberg A, Joshua M. Cerebellar climbing fibers encode expected reward size. Elife. 2019;8.

44.   Gilbert PFC, Thach WT. Purkinje cell activity during motor learning. Brain Research. 1977;128(2):309-28.

45.   Suvrathan A, Payne HL, Raymond JL. Timing Rules for Synaptic Plasticity Matched to Behavioral Function. Neuron. 2016;92(5):959-67.

46.   Iulianella A, Wingate RJ, Moens CB, Capaldo E. The generation of granule cells during the development and evolution of the cerebellum. Developmental Dynamics. 2019;248(7):506-13.

47.   EJ LRWKL. Ch. 7 Cerebellum The Synaptic Organization of the Brain. Oxford: Oxford Univ. Press; 2004.

48.   Larry Squire MDM, W. Thomas Thach. Fundamental Neuroscience, Chapter 32 Cerebellum

In: Larry Squire DB, Floyd E. Bloom, Sascha du Lac Anirvan Ghosh Nicholas C. Spitzer Larry R. Squire Darwin Berg Floyd Bloom Sascha du Lac Anirvan Ghosh Nicholas Spitzer, editor. Fundamental Neuroscience: Academic Press; 2013. p. 751-74.

49.   Mugnaini E. The length of cerebellar parallel fibers in chicken and rhesus monkey. Journal of Comparative Neurology. 1983;220(1):7-15.

50.   Duguid I, Branco T, Chadderton P, Arlt C, Powell K, Häusser M. Control of cerebellar granule cell output by sensory-evoked Golgi cell inhibition. Proceedings of the National Academy of Sciences. 2015;112(42):13099-104.

51.   Mapelli J, D'Angelo E. The Spatial Organization of Long-Term Synaptic Plasticity at the Input Stage of Cerebellum. The Journal of Neuroscience. 2007;27(6):1285-96.

52.   Kanichay RT, Silver RA. Synaptic and Cellular Properties of the Feedforward Inhibitory Circuit within the Input Layer of the Cerebellar Cortex. The Journal of Neuroscience. 2008;28(36):8955-67.

53.   Lainé J, Axelrad H. Extending the cerebellar Lugaro cell class. Neuroscience. 2002;115(2):363-74.

54.   Hirono M, Saitow F, Kudo M, Suzuki H, Yanagawa Y, Yamada M, Nagao S, Konishi S, Obata K. Cerebellar globular cells receive monoaminergic excitation and monosynaptic inhibition from Purkinje cells. PLoS One. 2012;7(1):e29663.

55.   Kalinichenko SG, Pushchin II. The modular architecture and neurochemical patterns in the cerebellar cortex. Journal of Chemical Neuroanatomy. 2018;92:16-24.

56.   D'Angelo E. Chapter 6 - Physiology of the cerebellum. In: Manto M, Huisman TAGM, editors. Handbook of Clinical Neurology. 154: Elsevier; 2018. p. 85-108.

57.   Martinez S, Andreu A, Mecklenburg N, Echevarria D. Cellular and molecular basis of cerebellar development. Frontiers in Neuroanatomy. 2013;7(18).

58.   Morales D, Hatten ME. Molecular markers of neuronal progenitors in the embryonic cerebellar anlage. J Neurosci. 2006;26(47):12226-36.

59.   Kebschull JM, Richman EB, Ringach N, Friedmann D, Albarran E, Kolluru SS, Jones RC, Allen WE, Wang Y, Cho SW, Zhou H, Ding JB, Chang HY, Deisseroth K, Quake SR, Luo L. Cerebellar nuclei evolved by repeatedly duplicating a conserved cell-type set. Science. 2020;370(6523):eabd5059.

60.   Bagnall MW, Zingg B, Sakatos A, Moghadam SH, Zeilhofer HU, Lac Sd. Glycinergic Projection Neurons of the Cerebellum. The Journal of Neuroscience. 2009;29(32):10104-10.

61.   Leto K, Arancillo M, Becker EBE, Buffo A, Chiang C, Ding B, Dobyns WB, Dusart I, Haldipur P, Hatten ME, Hoshino M, Joyner AL, Kano M, Kilpatrick DL, Koibuchi N, Marino S, Martinez S, Millen KJ, Millner TO, Miyata T, Parmigiani E, Schilling K, Sekerková G, Sillitoe RV, Sotelo C, Uesaka N, Wefers A, Wingate RJT, Hawkes R. Consensus Paper: Cerebellar Development. The Cerebellum. 2016;15(6):789-828.

62.   Hoshino M, Nakamura S, Mori K, Kawauchi T, Terao M, Nishimura YV, Fukuda A, Fuse T, Matsuo N, Sone M, Watanabe M, Bito H, Terashima T, Wright CV, Kawaguchi Y, Nakao K, Nabeshima Y. Ptf1a, a bHLH transcriptional gene, defines GABAergic neuronal fates in cerebellum. Neuron. 2005;47(2):201-13.

63.   Wang VY, Rose MF, Zoghbi HY. Math1 expression redefines the rhombic lip derivatives and reveals novel lineages within the brainstem and cerebellum. Neuron. 2005;48(1):31-43.

64.   Zordan P, Croci L, Hawkes R, Consalez GG. Comparative analysis of proneural gene expression in the embryonic cerebellum. Dev Dyn. 2008;237(6):1726-35.

65.   Storm R, Cholewa-Waclaw J, Reuter K, Bröhl D, Sieber M, Treier M, Müller T, Birchmeier C. The bHLH transcription factor Olig3 marks the dorsal neuroepithelium of the hindbrain and is essential for the development of brainstem nuclei. Development. 2009;136(2):295-305.

66.   Müller T, Anlag K, Wildner H, Britsch S, Treier M, Birchmeier C. The bHLH factor Olig3 coordinates the specification of dorsal neurons in the spinal cord. Genes Dev. 2005;19(6):733-43.

67.   Madisen L, Zwingman TA, Sunkin SM, Oh SW, Zariwala HA, Gu H, Ng LL, Palmiter RD, Hawrylycz MJ, Jones AR, Lein ES, Zeng H. A robust and high-throughput Cre reporting and characterization system for the whole mouse brain. Nat Neurosci. 2010;13(1):133-40.

68.   Dessaud E, Yang LL, Hill K, Cox B, Ulloa F, Ribeiro A, Mynett A, Novitch BG, Briscoe J. Interpretation of the sonic hedgehog morphogen gradient by a temporal adaptation mechanism. Nature. 2007;450(7170):717-20.

69.   Hernández-Miranda LR, Cariboni A, Faux C, Ruhrberg C, Cho JH, Cloutier JF, Eickholt BJ, Parnavelas JG, Andrews WD. Robo1 regulates semaphorin signaling to guide the migration of cortical interneurons through the ventral forebrain. J Neurosci. 2011;31(16):6174-87.

70.   Comai G, Tajbakhsh S. Molecular and cellular regulation of skeletal myogenesis. Curr Top Dev Biol. 2014;110:1-73.

71.   West MJ. Estimating volume in biological structures. Cold Spring Harb Protoc. 2012;2012(11):1129-39.

72.   Saito T, Nakatsuji N. Efficient gene transfer into the embryonic mouse brain using in vivo electroporation. Dev Biol. 2001;240(1):237-46.

73.   Susaki EA, Tainaka K, Perrin D, Yukinaga H, Kuno A, Ueda HR. Advanced CUBIC protocols for whole-brain and whole-body clearing and imaging. Nat Protoc. 2015;10(11):1709-27.

74.   Tutukova S, Tarabykin V, Hernandez-Miranda LR. The Role of Neurod Genes in Brain Development, Function, and Disease. Front Mol Neurosci. 2021;14:662774.

75.   Skinner MK, Rawls A, Wilson-Rawls J, Roalson EH. Basic helix-loop-helix transcription factor gene family phylogenetics and nomenclature. Differentiation. 2010;80(1):1-8.

76.   Bertrand N, Castro DS, Guillemot F. Proneural genes and the specification of neural cell types. Nat Rev Neurosci. 2002;3(7):517-30.

77.   Sommer L, Ma Q, Anderson DJ. neurogenins, a novel family of atonal-related bHLH transcription factors, are putative mammalian neuronal determination genes that reveal progenitor cell heterogeneity in the developing CNS and PNS. Mol Cell Neurosci. 1996;8(4):221-41.

78.   Dokucu ME, Zipursky SL, Cagan RL. Atonal, rough and the resolution of proneural clusters in the developing Drosophila retina. Development. 1996;122(12):4139-47.

79.   Dennis DJ, Han S, Schuurmans C. bHLH transcription factors in neural development, disease, and reprogramming. Brain Res. 2019;1705:48-65.

80.   Hernandez-Miranda LR, Ruffault PL, Bouvier JC, Murray AJ, Morin-Surun MP, Zampieri N, Cholewa-Waclaw JB, Ey E, Brunet JF, Champagnat J, Fortin G, Birchmeier C. Genetic identification of a hindbrain nucleus essential for innate vocalization. Proc Natl Acad Sci U S A. 2017;114(30):8095-100.

81.   Liu Z, Li H, Hu X, Yu L, Liu H, Han R, Colella R, Mower GD, Chen Y, Qiu M. Control of precerebellar neuron development by Olig3 bHLH transcription factor. J Neurosci. 2008;28(40):10124-33.

82.   Grimaldi P, Parras C, Guillemot F, Rossi F, Wassef M. Origins and control of the differentiation of inhibitory interneurons and glia in the cerebellum. Dev Biol. 2009;328(2):422-33.

83.   Ju J, Liu Q, Zhang Y, Liu Y, Jiang M, Zhang L, He X, Peng C, Zheng T, Lu QR, Li H. Olig2 regulates Purkinje cell generation in the early developing mouse cerebellum. Sci Rep. 2016;6:30711.

84.   Seto Y, Nakatani T, Masuyama N, Taya S, Kumai M, Minaki Y, Hamaguchi A, Inoue YU, Inoue T, Miyashita S, Fujiyama T, Yamada M, Chapman H, Campbell K, Magnuson MA, Wright CV, Kawaguchi Y, Ikenaka K, Takebayashi H, Ishiwata S, Ono Y, Hoshino M. Temporal identity transition from Purkinje cell progenitors to GABAergic interneuron progenitors in the cerebellum. Nat Commun. 2014;5:3337.

85.   E. V. Borisova EAE, S. A. Tutukova, I. I. Belousova, N. M. Zhidkova, A. M. Rusanova, V. A. Salina, E. A. Turovsky, M. V. Turovskaya, V. S. Tarabykin, A. A. Babaev Identification of Novel Mutations Controlling Cerebral Cortex Malformations Caused by ENU-Induced Mutagenesis in the Mouse. Соврем технол мед. 2018;3.

86.   Ambrozkiewicz MC, Schwark M, Kishimoto-Suga M, Borisova E, Hori K, Salazar-Lázaro A, Rusanova A, Altas B, Piepkorn L, Bessa P, Schaub T, Zhang X, Rabe T, Ripamonti S, Rosário M, Akiyama H, Jahn O, Kobayashi T, Hoshino M, Tarabykin V, Kawabe H. Polarity Acquisition in Cortical Neurons Is Driven by Synergistic Action of Sox9-Regulated Wwp1 and Wwp2 E3 Ubiquitin Ligases and Intronic miR-140. Neuron. 2018;100(5):1097-115.e15.

87.   Harnett D, Ambrozkiewicz MC, Zinnall U, Borisova E, Rusanova A, Dannenberg R, Imami K, Münster-Wandowski A, Fauler B, Mielke T, Selbach M, Landthaler M, Spahn CMT, Tarabykin V, Ohler U, Kraushar ML. Timed global reorganization of protein synthesis during neocortex neurogenesis at codon resolution. bioRxiv. 2021:2021.06.23.449626.

3. Statutory Declaration

Statutory Declaration

"I, Aleksandra Rusanova, by personally signing this document in lieu of an oath, hereby affirm that I prepared the submitted dissertation on the topic "Transcriptional regulation of cerebellar neuron specification/Transkriptionelle Regulation der Spezifikation von Kleinhirnneuronen", independently and withoutthe support of third parties, and that I used no other sources and aids than those stated.

All parts which are based on the publications or presentations of other authors, either in letter or in spirit, are specified as such in accordance with the citing guidelines. The sections on methodology (in particular regarding practical work, laboratory regulations, statistical processing) and results (in particular regarding figures, charts and tables) are exclusively my responsibility.

Furthermore, I declare that I have correctly marked all of the data, the analyses, and the conclusions generated from data obtained in collaboration with other persons, and that I have correctly marked my own contribution and the contributions of other persons (cf. declaration of contribution). I have correctly marked all texts or parts of texts that were generated in collaboration with other persons.

My contributions to any publications to this dissertation correspond to those stated in the below joint declaration made together with the supervisor. All publications created within the scope of the dissertation comply with the guidelines of the ICMJE (International Committee of Medical Journal Editors; www.icmje.org) on authorship. In addition, I declare that I shall comply with the regulations of Charité – Universitätsmedizin Berlin on ensuring good scientific practice.

I declare that I have not yet submitted this dissertation in identical or similar form to another Faculty.

The significance of this statutory declaration and the consequences of a false statutory declaration under criminal law (Sections 156, 161 of the German Criminal Code) are known to me."

Date 22.08.2021   Signature

4. Declaration of own contribution

Declaration of your own contribution to the top-journal publication for a PhD or MD/PhD degree

Aleksandra Rusanova contributed the following to the below listed publication:

Publication: Elijah D Lowenstein, Aleksandra Rusanova, Jonas Stelzer, Marc Hernaiz-Llorens, Adrian E Schroer, Ekaterina Epifanova, Francesca Bladt, Eser Göksu Isik, Sven Buchert, Shiqi Jia, Victor Tarabykin, Luis R Hernandez-Miranda, Olig3 regulates early cerebellar development, eLife , 2021

Contribution (please set out in detail):

Figure4 with 2 supplements:

The contribution of Miss Aleksandra Rusanova was as follows:
Main Figure: Panels A-E
Supplement figure 1: All panels
Supplement figure 2: All Panels
Technical contribution: Tissue preparation, cryosectioning, immunofluorescence, microscopy and cell quantifications.

Figure5 with 2 supplement figures:

The contribution of Miss Aleksandra Rusanova was as follows:
Main Figure: All panels
Supplement figure 1: All panels
Supplement figure 2: All Panels
Technical contribution: In utero electroporation, generation of overexpressing constructs, gene cloning, tissue preparation, cryosectioning, immunofluorescence, microscopy and cell quantifications.

Figure6 with 1 supplement:

The contribution of Miss Aleksandra Rusanova was as follows:
Main Figure: Panel E and F
Supplement figure 1: Panel A and B
Technical contribution: Tissue preparation, cryosectioning, immunofluorescence, microscopy and cell quantifications.

Signature of doctoral candidate (Miss Aleksandra Rusanova)

5. Journal Data Filtered By: **Selected JCR Year: 2019** Selected Editions: SCIE,SSCI Selected Categories: **"BIOLOGY"** Selected Category Scheme: WoS
Gesamtanzahl: 93 Journale

Rank	Full Journal Title	Total Cites	Journal Impact Factor	Eigenfactor Score
1	Physics of Life Reviews	1,627	14.789	0.003150
2	BIOLOGICAL REVIEWS	13,490	10.701	0.019440
3	CURRENT BIOLOGY	63,256	9.601	0.133170
4	BIOSCIENCE	19,069	8.282	0.014250
5	eLife	46,775	7.080	0.287130
6	PLOS BIOLOGY	31,650	7.076	0.060300
7	BMC BIOLOGY	6,440	6.765	0.018830
8	PHILOSOPHICAL TRANSACTIONS OF THE ROYAL SOCIETY B-BIOLOGICAL SCIENCES	46,796	5.680	0.063840
9	FASEB JOURNAL	43,126	4.966	0.043730
10	BIOELECTROCHEMISTRY	4,944	4.722	0.004950
11	PROCEEDINGS OF THE ROYAL SOCIETY B-BIOLOGICAL SCIENCES	55,054	4.637	0.075820
12	BIOESSAYS	10,189	4.627	0.016560
13	Science China-Life Sciences	3,248	4.611	0.006650
14	Current Opinion in Insect Science	2,247	4.565	0.008900
15	QUARTERLY REVIEW OF BIOLOGY	4,227	4.389	0.001130
16	Geobiology	2,390	4.385	0.004450
17	Communications Biology	1,326	4.165	0.004260
18	ASTROBIOLOGY	4,070	4.091	0.006180
19	Biology-Basel	1,424	3.796	0.003350
20	YALE JOURNAL OF BIOLOGY AND MEDICINE	2,230	3.549	0.003170
21	Interface Focus	2,218	3.514	0.005060
22	COMPUTERS IN BIOLOGY AND MEDICINE	6,737	3.434	0.010660
23	JOURNAL OF BIOLOGICAL RHYTHMS	3,258	3.122	0.003220
24	BIOLOGICAL RESEARCH	1,736	3.092	0.002210
25	JOURNAL OF EXPERIMENTAL BIOLOGY	34,195	3.014	0.032180
26	Life-Basel	1,260	2.991	0.004150
27	Biology Letters	10,299	2.869	0.017320
28	EXCLI Journal	1,622	2.837	0.002840
29	BIOCELL	346	2.821	0.000160
30	SAUDI JOURNAL OF BIOLOGICAL SCIENCES	3,994	2.802	0.005800
31	AEROBIOLOGIA	1,565	2.708	0.001250
32	RADIATION RESEARCH	8,707	2.657	0.005340
33	Life Science Alliance	310	2.622	0.001050

Rank	Full Journal Title	Total Cites	Journal Impact Factor	Eigenfactor Score
34	CHRONOBIOLOGY INTERNATIONAL	5,708	2.486	0.006600
35	Life Sciences in Space Research	456	2.453	0.001350
36	Advances in Experimental Medicine and Biology	21,809	2.450	0.035830
37	INTERNATIONAL JOURNAL OF RADIATION BIOLOGY	4,991	2.368	0.003460
38	JOURNAL OF THERMAL BIOLOGY	4,157	2.361	0.005170
39	JOURNAL OF THEORETICAL BIOLOGY	21,184	2.327	0.016790
40	CRYOBIOLOGY	4,661	2.283	0.003850
41	BIOELECTROMAGNETICS	2,549	2.278	0.001530
42	Biology Direct	1,871	2.193	0.002560
43	Journal of Biological Research-Thessaloniki	354	2.121	0.000650
44	MICROSCOPY RESEARCH AND TECHNIQUE	5,133	2.117	0.002830
45	Biology Open	2,992	2.029	0.009650
46	International Journal of Astrobiology	749	2.026	0.001410
47	BRAZILIAN JOURNAL OF MEDICAL AND BIOLOGICAL RESEARCH	5,524	2.023	0.004170
48	JOURNAL OF RADIATION RESEARCH	2,892	1.950	0.003960
49	JOURNAL OF MATHEMATICAL BIOLOGY	5,107	1.939	0.005980
50	COMPTES RENDUS BIOLOGIES	2,442	1.904	0.001840
51	COMPUTATIONAL BIOLOGY AND CHEMISTRY	1,929	1.850	0.002910
52	ELECTROMAGNETIC BIOLOGY AND MEDICINE	683	1.820	0.000670
53	ORIGINS OF LIFE AND EVOLUTION OF BIOSPHERES	1,756	1.814	0.001220
54	BULLETIN OF MATHEMATICAL BIOLOGY	4,386	1.812	0.004510
55	BIOSYSTEMS	2,724	1.808	0.002250
56	BIOMETRICS	21,788	1.711	0.011730
57	JOURNAL OF AGRICULTURAL BIOLOGICAL AND ENVIRONMENTAL STATISTICS	1,111	1.650	0.001490
58	MATHEMATICAL BIOSCIENCES	5,742	1.649	0.004210
59	JOURNAL OF BIOSCIENCES	2,782	1.645	0.002070
60	BIOMETRIKA	21,597	1.632	0.012270

Rank	Full Journal Title	Total Cites	Journal Impact Factor	Eigenfactor Score
61	AMERICAN JOURNAL OF HUMAN BIOLOGY	3,287	1.558	0.003650
62	BioScience Trends	1,038	1.553	0.001930
63	ANNALS OF HUMAN BIOLOGY	2,224	1.535	0.002580
64	BIOLOGICAL BULLETIN	4,731	1.527	0.001600
65	MATHEMATICAL MEDICINE AND BIOLOGY-A JOURNAL OF THE IMA	501	1.392	0.000630
66	RADIATION AND ENVIRONMENTAL BIOPHYSICS	1,332	1.321	0.001330
67	THEORY IN BIOSCIENCES	542	1.303	0.000390
68	BRAZILIAN JOURNAL OF BIOLOGY	2,702	1.266	0.002650
69	JOURNAL OF ETHNOBIOLOGY	600	1.092	0.000830
70	JOURNAL OF THE HISTORY OF BIOLOGY	636	0.864	0.000570
71	BIOLOGICAL RHYTHM RESEARCH	816	0.826	0.000860
72	PROCEEDINGS OF THE BIOLOGICAL SOCIETY OF WASHINGTON	1,382	0.816	0.000320
73	BIOLOGIA	2,247	0.811	0.002120
74	INDIAN JOURNAL OF EXPERIMENTAL BIOLOGY	3,018	0.783	0.001000
75	JOURNAL OF BIOLOGICAL EDUCATION	656	0.764	0.000370
76	JOURNAL OF BIOLOGICAL SYSTEMS	442	0.733	0.000350
77	Archives of Biological Sciences	899	0.719	0.000850
78	TURKISH JOURNAL OF BIOLOGY	1,299	0.716	0.001060
79	CRYOLETTERS	925	0.702	0.000610
80	FOLIA BIOLOGICA	520	0.691	0.000420
81	Open Life Sciences	202	0.690	0.000390
82	HUMAN BIOLOGY	1,688	0.629	0.000450
83	ZHURNAL OBSHCHEI BIOLOGII	342	0.606	0.000210
84	ACTA BIOLOGICA HUNGARICA	545	0.585	0.000390
85	BRAZILIAN ARCHIVES OF BIOLOGY AND TECHNOLOGY	2,587	0.579	0.001310
86	FOLIA BIOLOGICA-KRAKOW	362	0.533	0.000340
87	REVISTA DE BIOLOGIA TROPICAL	2,458	0.446	0.001800
88	BIOLOGY BULLETIN	706	0.413	0.000800
89	AMERICAN BIOLOGY TEACHER	684	0.282	0.000410

Rank	Full Journal Title	Total Cites	Journal Impact Factor	Eigenfactor Score
90	Bioscience Journal	990	0.268	0.001260
91	Bulletin de la Societe Linneenne de Lyon	162	0.250	0.000020
92	Theoretical Biology Forum	19	0.167	0.000020
93	Biologia Futura	11	Not Available	0.000000

Olig3 regulates early cerebellar development

Elijah D Lowenstein[1†], Aleksandra Rusanova[2,3†], Jonas Stelzer[2],
Marc Hernaiz-Llorens[1], Adrian E Schroer[2], Ekaterina Epifanova[2,3],
Francesca Bladt[1], Eser Göksu Isik[2], Sven Buchert[1], Shiqi Jia[1,4], Victor Tarabykin[2,3],
Luis R Hernandez-Miranda[1,2‡*]

[1]Max-Delbru¨ck-Centrum in the Helmholtz Association, Berlin, Germany; [2]Institute for Cell Biology and Neurobiology, Charité Universitätsmedizin Berlin, Berlin, Germany; [3]Institute of Neuroscience, Lobachevsky University of Nizhny Novgorod, Nizhny Novgorod, Russian Federation; [4]The First Affiliated Hospital of Jinan University, Guangzhou province, Guangzhou, China

Abstract The mature cerebellum controls motor skill precision and participates in other sophisticated brain functions that include learning, cognition, and speech. Different types of GABAergic and glutamatergic cerebellar neurons originate in temporal order from two progenitor niches, the ventricular zone and rhombic lip, which express the transcription factors Ptf1a and Atoh1, respectively. However, the molecular machinery required to specify the distinct neuronal types emanating from these progenitor zones is still unclear. Here, we uncover the transcription factor Olig3 as a major determinant in generating the earliest neuronal derivatives emanating from both progenitor zones in mice. In the rhombic lip, Olig3 regulates progenitor cell proliferation. In the ventricular zone, Olig3 safeguards Purkinje cell specification by curtailing the expression of Pax2, a transcription factor that suppresses the Purkinje cell differentiation program. Our work thus defines Olig3 as a key factor in early cerebellar development.

Introduction

The cerebellum develops from the dorsal aspect of rhombomere 1, a region known as the cerebellar anlage that in mice becomes apparent at embryonic (E) day 9.5 (*Butts et al., 2014*; *Chizhikov et al., 2006*; *Millet et al., 1996*; *Morales and Hatten, 2006*; *Wingate and Hatten, 1999*). This region contains two distinct germinal zones, the rhombic lip and the ventricular zone, that generate all glutamatergic and GABAergic cerebellar neurons, respectively (*Alder et al., 1996*; *Hallonet et al., 1990*; *Wingate and Hatten, 1999*; *Zervas et al., 2004*). Development of glutamatergic and GABAergic cerebellar neurons largely depends on the differential expression of two basic helix-loop-helix (bHLH) transcription factors: Atonal homolog one transcription factor (Atoh1) and Pancreas-specific transcription factor 1a (Ptf1a) (*Gazit et al., 2004*; *Hoshino et al., 2005*; *Machold and Fishell, 2005*; *Millen et al., 2014*; *Wang et al., 2005*; *Yamada et al., 2014*).

In the rhombic lip, Atoh1 directs the generation of three neuronal derivatives: (i) deep cerebellar nuclei (DCN) neurons (between E10.5 and E13.5), (ii) external granule layer (EGL) cells (between E13.5 and birth), which are the precursors of the internal granule layer cells that develop during early postnatal life, and (iii) unipolar brush cells (between E15.5 and the first days of postnatal life) (*Ben- Arie et al., 1997*; *Englund et al., 2006*; *Fink, 2006*; *Gazit et al., 2004*; *Machold and Fishell, 2005*; *Machold et al., 2011*; *Sekerkova´ et al., 2004*; *Yamada et al., 2014*). In the ventricular zone, Ptf1a instructs the generation of Purkinje cells (between E11.5-E13.5) and all inhibitory interneurons, including Golgi, Stellate, and Basket cells (between E14.5 and birth). Inhibitory interneurons are characterized by the expression of the homeodomain transcription factor Pax2 (*Hashimoto and*

Mikoshiba, 2003; *Hoshino et al., 2005*; *Leto et al., 2006*; *Maricich and Herrup, 1999*). Although the ablation of *Atoh1* and *Ptf1a* severely impairs glutamatergic and GABAergic cerebellar neuron development (*Ben-Arie et al., 1997*; *Hoshino et al., 2005*; *Jensen, 2004*; *Sellick et al., 2004*), less is known about the molecular machinery required for the temporal specification of the different neuronal derivatives emerging from the two cerebellar neurogenic niches.

bHLH transcription factors are master regulators of progenitor cell differentiation during development and are critical players in neuron subtype specification in the nervous system (*Atchley and Fitch, 1997*; *Baker and Brown, 2018*; *Ben-Arie et al., 2000*; *Bertrand et al., 2002*; *Dennis et al., 2019*; *Dokucu et al., 1996*; *Imayoshi and Kageyama, 2014*; *Jones, 2004*; *Mattar et al., 2008*; *Ross et al., 2003*; *Sommer et al., 1996*). Among these factors, Oligodendrocyte factor 3 (Olig3) has been implicated in the specification of dorsally emerging neuron types in the hindbrain and spinal cord (*Hernandez-Miranda et al., 2017b*; *Liu et al., 2008*; *Müller et al., 2005*; *Storm et al., 2009*; *Zechner et al., 2007*). However, its molecular mechanisms and functions outside these regions have been less studied (*Shiraishi et al., 2017*; *Vue et al., 2007*). Although *Olig3* expression was previously reported during cerebellar development, its function there has not yet been explored(*Liu et al., 2010*; *Takebayashi et al., 2002*).

In this study, we sought to identify bHLH factors that contribute to the development of distinct cerebellar neuron types. We report here that Olig3 is crucial for generating the earliest rhombic lip and ventricular zone neuronal derivatives. Our lineage-tracing studies illustrate that the majority of DCN neurons, EGL, granule cells, as well as Purkinje cells emerge from Olig3+ progenitor cells. In contrast, few inhibitory interneurons had a history of *Olig3* expression. Ablation of *Olig3* results in severe cerebellar hypoplasia. In particular, we show that in *Olig3* mutant mice, most DCN neurons as well as half of the EGL cells, granule cells and Purkinje cells are not formed. In contrast, supernumerary inhibitory interneurons develop in *Olig3* mutant animals. Mechanistically, we show that Olig3 cell-autonomously suppresses the development of inhibitory interneurons in the ventricular zone.Olig3 is first expressed in ventricular zone progenitor cells and transiently retained in newborn Purkinje cells to curtail the expression of Pax2, a gene that we found to suppress the Purkinje cell differentiation program. We also show that Olig3 and its close family member Olig2 specify complementary Purkinje cell populations. Altogether, our data provide new insights into the molecular machinery that secures the correct development of cerebellar neurons.

Results

Olig3 is expressed in rhombic lip and ventricular zone progenitor cells during early cerebellar development

About 130 bHLH transcription factors have been found in humans and 117 in mice (*Skinner et al., 2010*; *Stevens et al., 2008*). To identify candidate bHLH factors that contribute to the generation of early versus late derivatives from the rhombic lip and ventricular zone, we first analyzed the expression patterns of 110 bHLH transcription factors annotated in the Human Genome Organization (HuGO; https://www.genenames.org/data/genegroup/#!/group/420) throughout mouse cerebellar development using publically available data from the Allen Developing Mouse Brain Atlas (https://developingmouse.brain-map.org). We found that 51 bHLH genes were expressed during cerebellar development, of which 27 were seen in progenitor niches (rhombic lip, ventricular zone, and/or EGL), and the remainder in postmitotic regions (*Figure 1A*; *Table 1* and *Figure 1—figure supplement 1*). In particular, 9/27 genes displayed differential spatial-temporal expression patterns in the rhombic lip (Atoh1 and Olig3 between E11.5-E13.5), EGL (Atoh1 and Neurod1 between E13.5-birth), and ventricular zone (Ptf1a, Ascl1, Olig3, and Olig2 between E11.5-E13.5; Ptf1a, Neurod6, Neurog1 and Neurog2 between E13.5-E18.5). The remaining (18/27) factors appeared to belong to either a common set of transcription factors expressed in all progenitor niches or they maintained their expression in a particular niche throughout cerebellar development (*Table 1*). Of particular interest was the expression pattern of Olig3, which has not been previously reported to have a function in cerebellar development. However, it is known to participate in the specification of defined hindbrain and spinal cord neurons (*Hernandez-Miranda et al., 2017a*; *Liu et al., 2008*; *Müller et al., 2005*; *Storm et al., 2009*; *Zechner et al., 2007*).
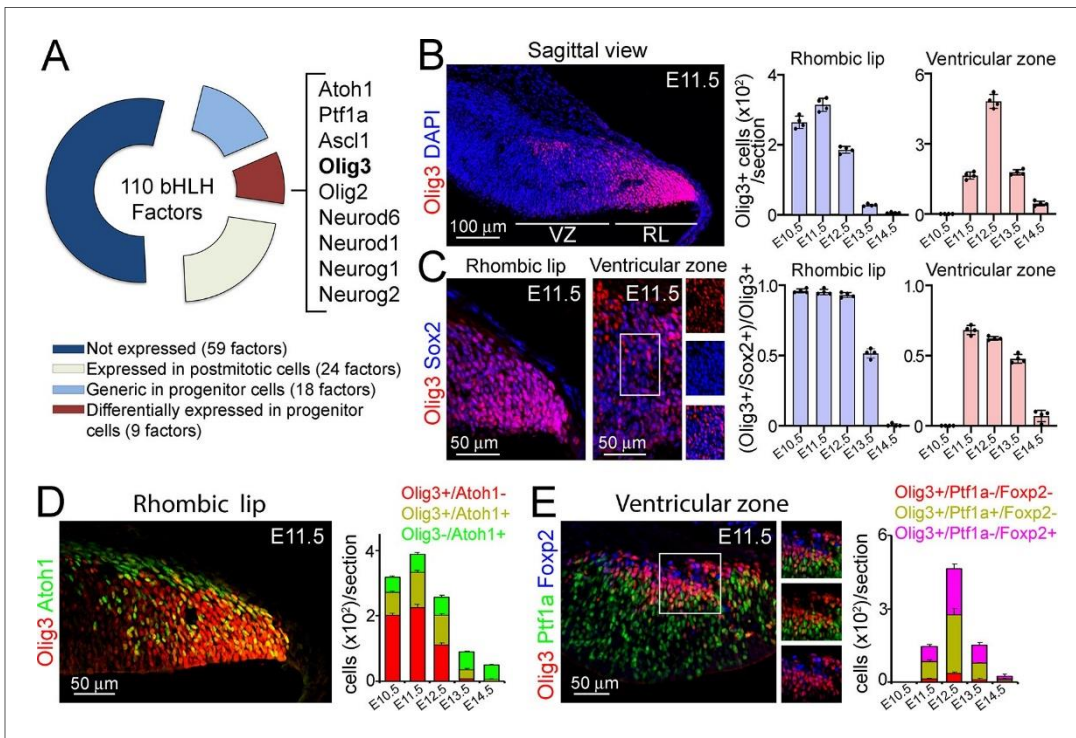
Figure 1. Olig3 marks rhombic lip and ventricular zone progenitor cells during early cerebellar development. (A) Doughnut chart illustrating the expression of 110 bHLH transcription factors during cerebellar development. For details on individual gene names within each category please see *Table 1*. (B) Left, a sagittal section of the cerebellum stained against Olig3 (red) and counterstained with DAPI (blue) at E11.5. Right, quantification of Olig3+ cells in the rhombic lip (RL) and ventricular zone (VZ) between E10.5 and E14.5. See also *Figure 1—figure supplement 2A*. The rhombic lip and ventricular zone domains were defined in this study according to the expression of Atoh1 and Ptf1a, respectively (see *Figure 1—figure supplement 2B*). (C) Left, magnifications of the rhombic lip and ventricular zone of a sagittal cerebellar section stained against Olig3 (red) and Sox2 (blue) at E11.5. The boxed area displayed in the ventricular zone is illustrated to the right of the main photograph. Right, quantification of the proportion of Olig3+ cells co-expressing Sox2 between E10.5 and E14.5. Dots in the graphs represent the mean of individual analyzed animals. (D) Left, immunofluorescence characterization of rhombic lip progenitor cells stained against Olig3 (red) and Atoh1 (green) at E11.5. Right, quantification of the proportion of Olig3+ rhombic lip cells co-expressing Atoh1 between E10.5 and E14.5. (E) Left, immunofluorescence characterization of ventricular zone progenitor cells stained against Olig3 (red), Ptf1a (green), and the Purkinje cell marker Foxp2 (blue) at E11.5. The boxed area on the micrograph is illustrated to the right of the main photograph. Right, quantification of the proportion of Olig3+ ventricular zone cells co-expressing Ptf1a or Foxp2. The mean and SD are plotted in all graphs. n = 4 mice per age. Photomicrographs were acquired using the automatic tile scan modus (10% overlap between tiles) of the Zeiss LSM700 confocal microscope.

The online version of this article includes the following source data and figure supplement(s) for figure 1:

Source data 1. Source data for *Figure 1*.
Figure supplement 1. Expression pattern of selected bHLH factors during cerebellar development.
Figure supplement 2. Characterization of Olig3 expression during cerebellar development.
Figure supplement 2–source data 1. Source data for *Figure 1—figure supplement 2*.

Next, we characterized the expression of *Olig3* during cerebellar development by immunofluorescence. In the rhombic lip, Olig3+ cells were abundant from E10.5 to E12.5, but their numbers declined by E13.5 and were rare by E14.5 (*Figure 1B*; *Figure 1—figure supplement 2A,B*). Almost all (>98%) Olig3+ rhombic lip cells co-expressed the progenitor marker Sox2 between E10.5 and E12.5, but this co-localization, as well as the total number of Olig3+ cells, declined by E13.5 (*Figure 1C*). In addition, most (>95%) proliferative BrdU+ cells in the rhombic lip co-expressed Olig3 (*Figure 1—figure supplement 2C*). Lastly, about 30% of Olig3+ cells in the rhombic lip expressed Atoh1 (Olig3+/Atoh1+ cells; *Figure 1D*). Thus, in the rhombic lip, Olig3+ cells are progenitors, and a third of them co-express Atoh1.

In the ventricular zone, Olig3+ cells were first seen at E11.5. Their numbers peaked by E12.5 and became rare by E14.5 (*Figure 1B*; *Figure 1—figure supplement 2A,B*). Most Olig3+ cells (59%) in the ventricular zone co-expressed the progenitor marker Sox2 at E11.5 and E12.5, but this co-

Table 1. Categorization of bHLH transcription factors expressed or not expressed during cerebellar development in mice.

bHLH factors expressed in cerebellar progenitor niches: Rhombic lip (RL), Ventricular zone (VZ) and/or external granule cell layer (EGL)

Gene name	Expressed in progenitors?	Developmental stage: embryonic (E) day			
		E11.5	E13.5	E15.5	E17.5/E18.5
Ascl1	Yes	VZ	VZ	Weak in VZ	Not expressed
Atoh1	Yes	RL	RL and EGL	RL and EGL	RL and EGL
Hes1	Yes	Not expressed	RL and VZ	Not expressed	Not expressed
Hes5	Yes	RL and VZ	RL and VZ	RL and VZ	Postmitotic cells
Hes6	Yes	RL and VZ	RL, VZ and EGL	EGL	No data
Hes7	Yes	RL and VZ	Weak in RL, VZ	Weak in RL, VZ	Not expressed
Hey1	Yes	Not expressed	Not expressed	EGL	EGL
Hif1a	Yes	RL and VZ	Weak in RL, VZ	Not expressed	Not expressed
Id1	Yes	RL and VZ	In blood vessels	In blood vessels	In blood vessels
Id3	Yes	RL and VZ	RL, VZ and EGL	RL, VZ and EGL	EGL
Max	Yes	Weak in RL and VZ	Not expressed	Not expressed	Not expressed
Mxd3	Yes	RL and VZ	RL, VZ and EGL	EGL	EGL
Mxi1	Yes	Weak in RL and VZ	RL, VZ and EGL	RL, VZ and EGL	Weak in EGL
Mycl	Yes	RL and VZ	RL, VZ and EGL	EGL	EGL
Mycn	Yes	Strong in RL and VZ	Not expressed	Not expressed	Not expressed
Neurod1	Yes	Not expressed	Not expressed	Strong in EGL	Strong in EGL
Neurod6	Yes	Not expressed	Weak in VZ	VZ	Broad expression
Neurog1	Yes	Not expressed	VZ	Not expressed	Not expressed
Neurog2	Yes	Not expressed	Weak in VZ	Strong in VZ	Not expressed
Olig2	Yes	Weak in VZ	Strong in VZ	Postmitotic cells	Postmitotic cells
Olig3	Yes	RL and weak in VZ	RL and VZ	Not expressed	Not expressed
Ptf1a	Yes	Strong in VZ	Strong in VZ	Weak in VZ	Not expressed
Srebf1	Yes	Not expressed	RL, VZ and EGL	Weak in EGL	Not expressed
Srebf2	Yes	Weak in RL and VZ	RL and VZ	Postmitotic cells	Postmitotic cells
Tcf12	Yes	RL and VZ	RL, VZ and EGL	RL, VZ and EGL	RL, VZ and EGL
Tcf3	Yes	RL and VZ	RL, VZ and EGL	RL, VZ and EGL	RL, VZ and EGL
Tcf4	Yes	RL and VZ	RL, VZ and EGL	RL, VZ and EGL	RL, VZ and EGL

Table 1 continued on next page

Table 1 continued

bHLH factors expressed in cerebellar progenitor niches: Rhombic lip (RL), Ventricular zone (VZ) and/or external granule cell layer (EGL)

bHLH factors expressed in postmitotic cerebellar cells during development		bHLH factors not expressed in the cerebellum during development	
Gene name:	Arntl, Arnt2, Bhlhe22, Clock, Epas1, Id2, id4, Mlx, Mnt, Mxd1, Mxd4, Myc, Ncoa1, Ncoa2, Neurod2, Neurog3, Nhlh1, Nhlh2, Npas3, Npas4, Olig1, Scx, Sim2, Usf1 and Usf2	Gene name:	Ahr, Ahrr, Arnt, Arntl2, Ascl2, Ascl3, Ascl4, Ascl5, Atoh7, Atoh8, Bhlha15, Bhlha9, Bhlhb9, Bhlhe23, Bhlhe40, Bhlhe41, Ferd3l, Figla, Hand1, Hand2, Helt, Hes2, Hes3, Hes4, Hey2, Heyl, Hif3a, Lyl1, Mesp1, Mesp2, Mitf, Mlxip, Mlxipl, Msc, Myf5, Myf6, Myod1, Myog, Ncoa3, Neurod4, Npas1, Npas2, Sim1, Sohlh1, Sohlh2, Tal1, Tal2, Tcf15, Tcf21, Tcf23, Tcf24, Tcfl5, Tfap4, Tfe3, Tfeb, Tfec, Twist1 and Twist2

localization, as well as the total number of Olig3+ cells, declined by E13.5 (*Figure 1C*). Furthermore, about one-third of the BrdU+ cells in the ventricular zone co-expressed Olig3 (*Figure 1—figure supplement 2D*). Lastly, 52% of the Olig3+ ventricular zone cells co-expressed Ptf1a, while 41% co-expressed the postmitotic Purkinje cell marker Foxp2 (*Figure 1E*). This indicates that whereas most Olig3+ cells in the ventricular zone are progenitors (Olig3+/Ptf1a+/Foxp2-), Olig3 is transiently retained in early-born Purkinje cells (Olig3+/Ptf1a-/Foxp2+). We conclude that Olig3 is expressed in rhombic lip and ventricular zone progenitor cells during the generation of their earliest neuronal derivatives.

Early derivatives from the rhombic lip and ventricular zone arise from Olig3+ progenitor cells

To obtain a complete picture of the distinct cerebellar neuron types arising from Olig3+ progenitor cells, we first carried out a long-term lineage tracing experiment. This experiment used a tamoxifen- inducible cre recombinase driven by *Olig3* (*Olig3*$^{creERT2/+}$) and the fluorescent reporter *Rosa26*$^{lsl-tdT}$ that expresses a cytoplasmic Tomato fluorescent protein upon cre-mediated recombination (see the genetic strategy in *Figure 2—figure supplement 1A*). Specifically, we induced tamoxifen recombi- nation in *Olig3*$^{creERT2/+}$; *Rosa26*$^{lsl-tdT/+}$ mice at E10.5 and analyzed their brains by lightsheet micros- copy at E19 (see *Video 1*). Three-dimensional reconstructions of recombined brains showed that Tomato+ cells were broadly distributed across the entire cerebellum of *Olig3*$^{creERT2/+}$; *Rosa26*$^{lsl-tdT/+}$ mice (*Figure 2A–B*; *Figure 2—figure supplement 1A–A''*). In particular, we observed Tomato+ cells in the EGL, Purkinje cell layer, and dense groups of Tomato+ cells encompassing the three nuclei formed by DCN neurons: the nucleus dentatus, interpositus, and fastigii (*Figure 2A–C*). Closer
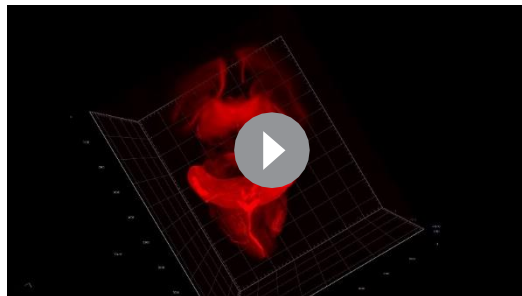
Video 1. Three-dimensional reconstruction of an E19 *Olig3*$^{creERT2/+}$; *Rosa26*$^{lsl-tdT/+}$ mouse brain that was recombined at E10.5. Red fluorescence represents the somas and axons of all cells with a history of Olig3 expression. See also *Figure 2—figure supplement 1A*.
https://elifesciences.org/articles/64684#video1

inspection revealed that Tomato+ cells co-expressed Tbr1 (a marker of Fastigii DCN cells) and Brn2 (a marker of Interpositus and Dentatus DCN cells; *Figure 2D*). Thus, the distribution of cerebellar neurons with a history of *Olig3* expression suggests that Olig3+ progenitor cells generate the earliest set of ventricular zone (Pur-kinje cells) and rhombic lip (DCN neurons) cere-bellar derivatives, and also to the later arising EGL cells from the latter progenitor domain.

We performed a second long-term lineage-tracing experiment to better define the temporal contribution of Olig3+ progenitor cells to spe-cific cerebellar neuron types. In particular, we used *Olig3*^{creERT2} and the reporter *Mapt*^{nLacZ}, which selectively expresses a nuclear b-galactosi-dase (bgal) protein upon cre-mediated recombi-nation in postmitotic (Mapt+) neurons. We
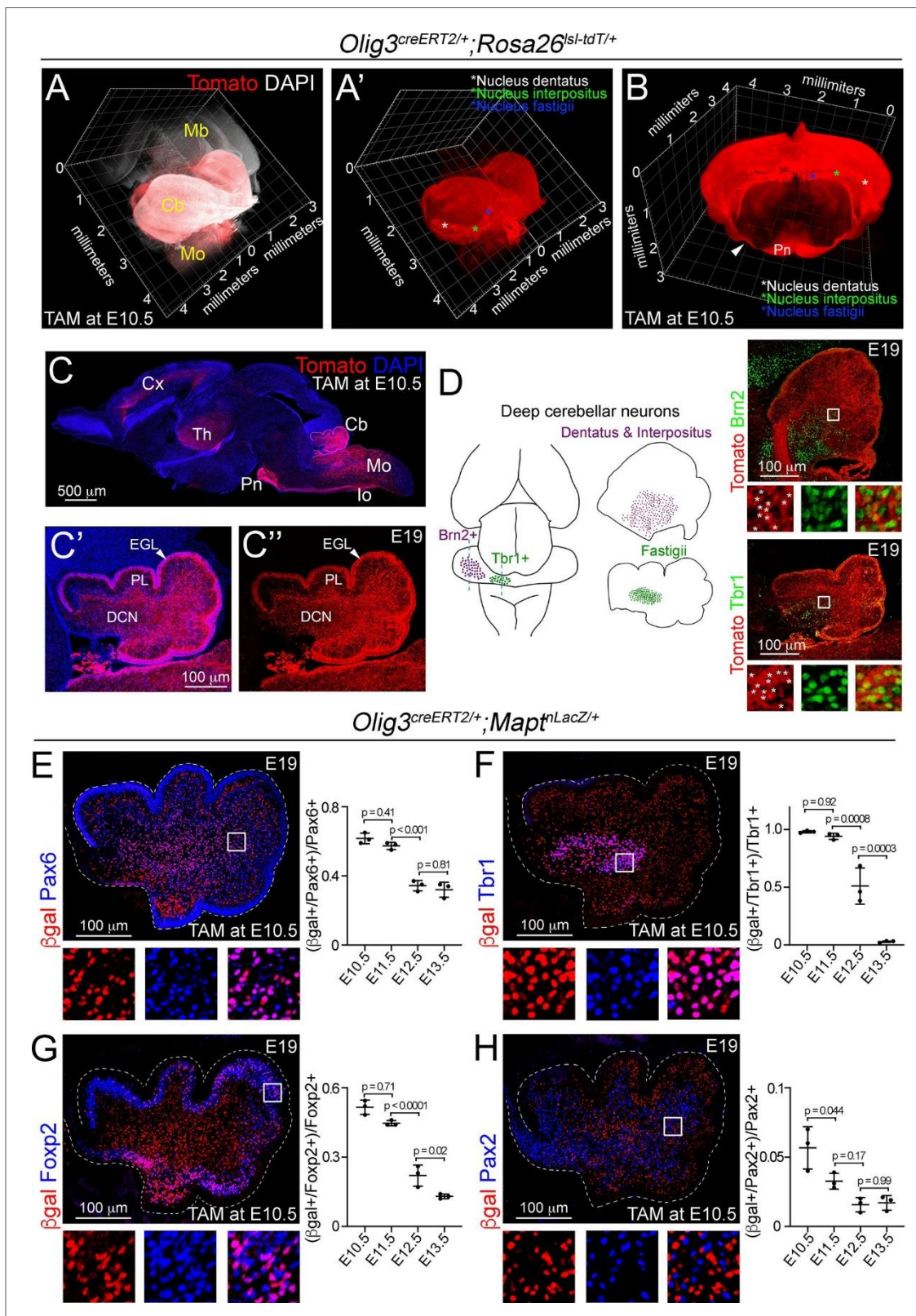
Figure 2. Lineage-tracing of cerebellar neurons arising from Olig3+ progenitor cells. (A-D) Analysis of Tomato+ (red) cells in *Olig3^{creERT2/+};Rosa26^{lsl-tdT/+}* mice that were recombined with tamoxifen (TAM) at E10.5 and imaged at E19. See *Figure 2—figure supplement 1A* and *Video 1* for a description of the genetic strategy and a complete reconstruction of a recombined *Olig3^{creERT2/+};Rosa26^{lsl-tdT/+}* brain. (A, A') A sagittal three-dimensional reconstruction of the cerebellum. Tomato+ cells were broadly distributed across the cerebellum and densely packed in the DCN nuclei

Figure 2 continued on next page

Figure 2 continued

(asterisks in A'). (B) A coronal three-dimensional reconstruction of the cerebellum. DCN nuclei are marked with asterisks. The pontine nuclei (Pn) and their axons (arrowhead), which develop from Olig3+ progenitor cells in the medulla oblongata, are labeled with Tomato. (C) A sagittal section stained against Tomato and DAPI (blue). Other known Olig3 derivatives, such as the thalamus (Th) including its projections to the cortex (Cx), pontine nuclei (Pn), inferior olive (Io) and many neurons in the medulla oblongata (Mo) are marked with Tomato. A magnification of the cerebellum is displayed with (C') or without (C'') DAPI. The external granule cell layer (EGL), Purkinje cell layer (PL), and DCN neurons are labeled with Tomato. (D) Left, schematic display of DCN nuclei positive for Brn2 (dentatus and interpositus) and Tbr1 (fastigii). Right, sagittal cerebellar sections stained against Tomato and Brn2 or Tbr1 (green). The boxed areas are illustrated to the bottom of the main photographs displaying individual and merged fluorescent signals. Asterisks mark double positive cells. (E-H) Analysis of cerebellar neurons with a history of Olig3 (bgal+) expression. *Olig3$^{creERT2/+}$;Mapt$^{nLacZ/+}$* mice were recombined with tamoxifen (TAM) at different embryonic stages and analyzed at E19. See *Figure 2—figure supplement 1B* for a description of the experiment. Sagittal cerebellar sections from these mice were stained against bgal (red) and markers for the EGL and granule cells (Pax6, blue in E), DCN neurons (Tbr1, blue in F), Purkinje cells (Foxp2, blue in G), and inhibitory interneurons (Pax2, blue in H). Double-positive (bgal+/marker+) cells were quantified at E19. The boxed areas on the micrographs are illustrated to the bottom of the main photographs displaying individual and merged fluorescent signals. The mean and SD are plotted in all graphs, and the dots represent the mean of individual animals. n = 3 mice per age. Significance was obtained using one-way ANOVA followed by *post hoc* Tukey's test, see *Table 2* for statistical details. Photomicrographs were acquired using the automatic tile scan modus (10% overlap between tiles) of the Zeiss LSM700 confocal microscope. The main microphotograph displayed in G was mounted on a black frame to maintain figure panel proportions.

The online version of this article includes the following source data and figure supplement(s) for figure 2:

Source data 1. Source data for *Figure 2*.

Figure supplement 1. Lineage-tracing of Olig3-derived cells.

Figure supplement 1–source data 1. Source data for *Figure 2—figure supplement 1*.

---

induced tamoxifen recombination in *Olig3$^{creERT2/+}$;Mapt$^{nLacZ/+}$* mice at distinct embryonic stages from E10.5 to E13.5 and analyzed the cerebella of recombined mice at E19 (*Figure 2—figure supplement 1B–C*). As expected, we did not observe any bgal+ cells in the EGL, as this layer contains granule cell progenitors that do not express Mapt (arrowheads in *Figure 2—figure supplement 1C*). Both EGL and postmitotic granule cells express the transcription factor Pax6 (*Fink, 2006*; *Yeung et al., 2016*). We observed that the majority (62%) of Pax6+ postmitotic cells, outside the EGL, co-expressed bgal when recombination was induced at E10.5 or E11.5, but the proportion of Pax6+/bgal+ cells dropped when recombination was induced at later stages (*Figure 2E*). Furthermore, we found that most Tbr1+ (>99%) DCN neurons, Foxp2+ (51%) Purkinje cells, and Brn2+ (43%) DCN neurons co-expressed bgal when recombination was induced at E10.5 or E11.5, but the proportion of double-positive cells declined when recombination was induced at later stages (*Figure 2F,G*; *Figure 2—figure supplement 1D*). In contrast, few Pax2+ (6%) cells co-expressed bgal when recombination was induced at E10.5, and the number of double-positive cells was minimal when recombination was induced at later stages (*Figure 2H*). Unipolar brush cells (Tbr2+) were also observed to co-express bgal in recombined animals (*Figure 2—figure supplement 1E*). One should note that these cells derive from late rhombic lip progenitor cells at a time point (E15.5-birth) when *Olig3* is no longer expressed, which indicates that these progenitor cells, like those in the EGL, had a history of *Olig3* expression. We conclude that Olig3+ progenitor cells substantially contribute to the generation of the earliest derivatives of the ventricular zone (Purkinje cells) and rhombic lip (DCN neurons), and partially contribute to the later arising EGL cell population.

Cerebellar hypoplasia and loss of early-born cerebellar neurons in *Olig3* mutant mice

We next analyzed the consequences of *Olig3* ablation on cerebellar development. At birth (P0), the cerebella of *Olig3* null (*Olig3$^{-/-}$*) mutant mice were drastically reduced in volume when compared to control (*Olig3$^{+/-}$*) littermates (*Figure 3A,B*). The strongest reduction in volume was observed in the medial portion of the cerebella of *Olig3* mutant mice (*Figure 3—figure supplement 1A*). Closer inspection of *Olig3* mutant cerebella revealed that they had less folia than control littermates (*Figure 3B*). Thus, ablation of *Olig3* results in severe cerebellar hypoplasia. Furthermore, the number of Tbr1+, Brn2+, Pax6+, and Foxp2+ neurons was greatly reduced in *Olig3* mutant mice (*Figure 3C–E*; *Figure 3—figure supplement 1B*). In contrast, the number of Pax2+ inhibitory inter- neurons increased in mutant mice (*Figure 3F*). Late born derivatives from the rhombic lip, such as Tbr2+ unipolar brush cells, were correctly specified in *Olig3* mutant mice (*Figure 3—figure*

supplement 1C). Together these data show that Olig3 is critically involved in cerebellar development and the generation of DCN neurons, EGL cells (including their granule cell derivatives) and Purkinje cells.

To define the developmental onset of the cerebellar deficiencies seen in *Olig3* mutant mice, we carried out a short-term lineage-tracing experiment using a knock-in mouse strain that expresses GFP from the *Olig3* locus (*Olig3^GFP*) (*Müller et al., 2005*). We compared control (*Olig3^GFP/+*) and *Olig3* mutant (*Olig3^GFP/GFP*) mice at E13.5. In control mice at this stage, DCN neurons have already migrated away from the rhombic lip and accumulated in the nuclear transitory zone, EGL cells have formed their characteristic subpial layer, and Purkinje cells have completed their specification (*Figure 3—figure supplement 2*). Compared to control littermates, E13.5 *Olig3* mutant mice showed a severe reduction in the number of DCN and EGL cells but no significant reduction in the number of Purkinje cells (*Figure 3—figure supplement 2*). Therefore, while the deficits observed in DCN neurons and EGL cells arise early during cerebellar development in *Olig3* mutant mice, the reduction in Purkinje cell numbers occurs at a later developmental stage than E13.5 (see below).
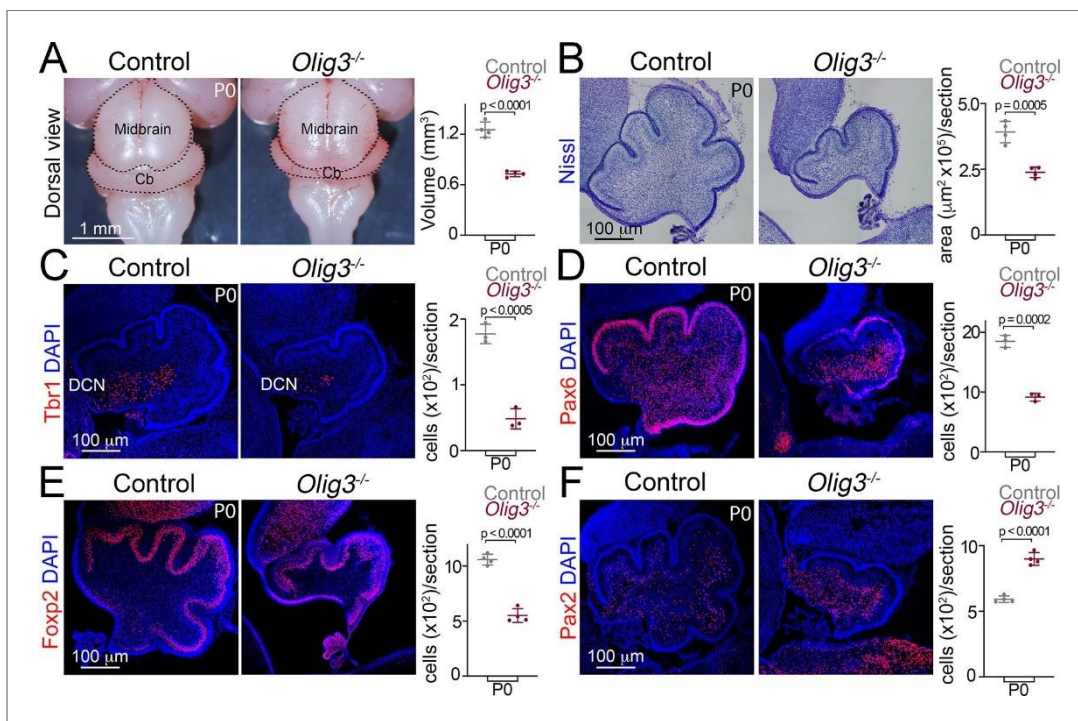
Figure 3. Severe cerebellar hypoplasia and neuronal loss in *Olig3* mutant mice. (A) Left, dorsal views of control (*Olig3^+/-*) and *Olig3* mutant (*Olig3^-/-*) cerebella at birth (P0). Right, quantification of cerebellar volume in newborn control and *Olig3^-/-* mice. (B) Left, sagittal sections of newborn control and *Olig3^-/-* cerebella stained with Nissl. Right, quantification of cerebellar area in newborn control and *Olig3^-/-* mice. (C–F) Immunofluorescence characterization and quantification of Tbr1+ DCN neurons (C, in red), Pax6+ EGL and granule cells (D, in red), Foxp2+ Purkinje cells (E, in red) and Pax2 + inhibitory interneurons (F, in red) in newborn control and *Olig3^-/-* mice. All cerebellar sagittal sections were counterstained with DAPI (blue). The mean and SD are plotted in all graphs, and the dots represent the mean of individual animals. n = 4 mice per genotype in A, B, E, and F; n = 3 mice per genotype in C and D. Two-tailed t-tests were performed to determine statistical significance. See *Table 2* for statistical details. Photographs in A and B were acquired with a conventional bright-field microscope and photomicrographs in C-F were acquired using the automatic tile scan modus (10% overlap between tiles) of the Zeiss LSM700 confocal microscope.

The online version of this article includes the following source data and figure supplement(s) for figure 3:

Source data 1. Source data for *Figure 3*.

Figure supplement 1. Hypoplasia and loss of defined neurons in the cerebellum of *Olig3* mutant mice.

Figure supplement 1–source data 1. Source data for *Figure 3—figure supplement 1*.

Figure supplement 2. Cerebellar neuron loss in *Olig3* mutant embryos.

Figure supplement 2–source data 1. Source data for *Figure 3—figure supplement 2*.

Figure supplement 3. Deficits of rhombic progenitor cells in *Olig3* mutant embryos.

Figure supplement 3–source data 1. Source data for *Figure 3—figure supplement 3*.

We next analyzed whether Atoh1 and/or Ptf1a progenitor cell numbers changed in *Olig3* mutant mice at early embryonic stages. Analysis of *Olig3* mutant mice at E11.5 and E12.5 revealed reduced numbers of Atoh1+ cells in the rhombic lip, but no change in the number of Ptf1a+ cells in the ventricular zone (*Figure 3—figure supplement 3A,B*). We then asked whether the ablation of *Olig3* might affect the proliferation of rhombic lip and ventricular zone progenitor cells and/or their viability. In the rhombic lip, the number of proliferative (BrdU+) cells was reduced in *Olig3* mutant animals (*Figure 3—figure supplement 3C*). However, no change in the number of Tunel+ apoptotic bodies (puncta) were seen at any of the analyzed embryonic stages (*Figure 3—figure supplement 3E*). In the ventricular zone of *Olig3* mutant animals neither the number of BrdU+ or Tunel+ apoptotic bodies changed (*Figure 3—figure supplement 3D,E*). Thus, the mutation of *Olig3* impairs progenitor proliferation in the rhombic lip but not in the ventricular zone, illustrating that Olig3's function in the ventricular zone differs from that in the rhombic lip.

Ablation of *Olig3* misspecifies Purkinje cells that transform into inhibitory interneurons

1. We next compared the development of Foxp2+ Purkinje cells and Pax2+ inhibitory interneurons in *Olig3* mutant mice. In wildtype and heterozygous *Olig3*^{GFP/+} mice, Pax2+ cells first appeared at E13.5 in a rostral domain of the ventricular zone that lacked expression of Olig3, and by E14.5 occupied most of the ventricular zone (*Figure 4A*). The spread of Pax2+ cells from rostral to caudal coincided with the receding of Olig3+ cells (schematically displayed in *Figure 4B*). In sharp contrast to wildtype and heterozygous *Olig3*^{GFP/+} mice, we found supernumerary Pax2+ cells in *Olig3*^{GFP/GFP} mutant mice from E13.5 to P0 (*Figure 4C*; *Figure 4—figure supplements 1* and *2*; quantified in *Figure 4D*). Many of the supernumerary Pax2+ cells co-expressed GFP at E13.5 and E14.5 (see magnifications in *Figure 4C* and *Figure 4—figure supplement 2A*). Thus, the ablation of *Olig3* derepresses Pax2 in the early developing cerebellum.

Surprisingly at E13.5, most Foxp2+ cells (52%) co-expressed Pax2 in *Olig3* mutant mice (*Figure 4C*, quantified in *Figure 4E*), vice versa, roughly 90% of the Pax2+ cells co-expressed Foxp2 (*Figure 4—figure supplement 2B*). Interestingly, the proportion of misspecified Foxp2+/Pax2+ (or Pax2+/Foxp2+) cells declined by E14.5 and became rare by P0 (quantified in *Figure 4E* and *Figure 4—figure supplement 2B*). The decrease of misspecified (Foxp2+/Pax2+) cells coincided with the increase of inhibitory (Foxp2-/Pax2+) interneurons seen in *Olig3* mutant animals (compare *Figure 4D* and *Figure 4E*). We thus hypothesized that misspecified (Foxp2+/Pax2+) cells in *Olig3* mutant animals might undergo a fate shift and adopt an inhibitory (Foxp2-/Pax2+) interneuron identity. To assess this hypothesis, we carried out a long-term lineage-tracing experiment using *Olig3-*^{creERT2} and the *Mapt*^{nLacZ} reporter in an *Olig3* mutant background (*Olig3*^{creERT2/GFP};*Mapt*^{nLacZ/+} mice) and analyzed bgal expression in Pax2+ inhibitory interneurons. Tamoxifen recombination in *Olig3-*^{creERT2/GFP};*Mapt*^{nLacZ/+} mice was induced at E10.5. We found an increase in the proportion of Pax2+/bgal+ cells in *Olig3*^{creERT2/GFP};*Mapt*^{nLacZ/+} mice when compared to *Olig3*^{creERT2/+};*Mapt*^{nLacZ/+} control littermates (*Figure 4F*). Notably, ectopic Pax2+/bgal+ cells in *Olig3*^{creERT2/GFP};*Mapt*^{nLacZ/+} mice not only adopt an inhibitory interneuron identity (Pax2 expression), but also intermingle with Pax2+/bgal- cells underneath the Purkinje cell layer at E19 (compare inserts 1 and 2 in *Figure 4F*). Taken together, we conclude that ablation of *Olig3* in the ventricular zone results in the misspecification of Purkinje cells. These cells later change their fate and adopt an inhibitory interneuron identity (schematically displayed in *Figure 4G*).

Olig3 cell-autonomously curtails Pax2 expression to secure Purkinje cell differentiation

To experimentally assess whether Pax2 cell-autonomously suppresses *Foxp2* expression to induce an inhibitory interneuron differentiation program, we electroporated *in utero* a Pax2-IRES-GFP-expressing vector in the ventricular zone of wildtype animals at E12.5. This is a timepoint during which Foxp2+ cells are abundant and Pax2+ cells are absent (see *Figure 5A* for a schematic display of the experimental conditions). Electroporated pCAG-Pax2-IRES-GFP (*Pax2* overexpressing) and pCAG-GFP + Empty-IRES-GFP (control) embryos were analyzed at E14.5. In pCAG-Pax2-ires-GFP electroporated mice, no GFP+/Pax2+ cell co-expressed Foxp2, whereas in pCAG-GFP + Empty-IRES-GFP electroporated mice about 72% of the GFP+ cells were also Foxp2+ (*Figure 5B*). Calcium-binding
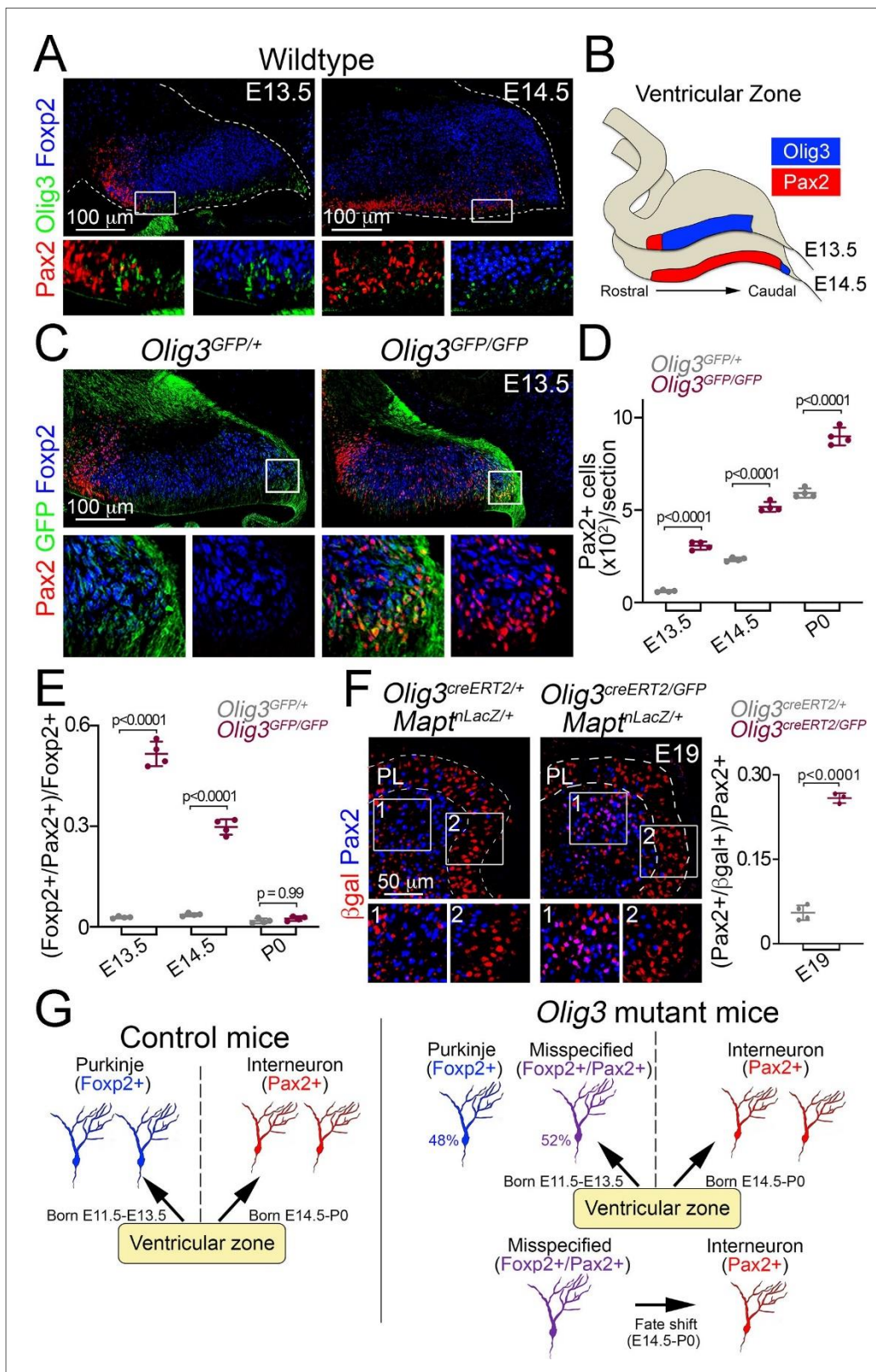
Figure 4. Ablation of *Olig3* misspecifies Purkinje cells which become inhibitory interneurons. (A) Immunofluorescence characterization of Foxp2+ (blue) Purkinje cells, Pax2+ (red) inhibitory interneurons and Olig3+ (green) progenitor cells in wildtype mice at the indicated stages. Boxed areas are magnified underneath the main photographs. (B) Schema illustrating the development of Pax2+ inhibitory interneurons. At E13.5, inhibitory interneurons develop in a rostral domain of the ventricular zone that lacks Olig3 expression. At E14.5, Pax2+ cells span most of the ventricular zone as

Figure 4 continued on next page

Figure 4 continued

Olig3 expression becomes extinguished. (C) Immunofluorescence characterization of Foxp2+ (blue) Purkinje cells and Pax2+ (red) inhibitory interneurons in E13.5 control (*Olig3*$^{GFP/+}$) and *Olig3* mutant (*Olig3*$^{GFP/GFP}$) mice. All cerebellar sagittal sections were stained against GFP (green). Boxed areas are magnified underneath the main photographs. Note that GFP+ and Foxp2+ cells ectopically express Pax2 in *Olig3*$^{GFP/GFP}$ mice. See *Figure 4—figure supplement 1* for additional examples and magnifications illustrating the co-expression of Pax2 and Foxp2 in *Olig3*$^{GFP/GFP}$ mice. (D) Quantification of Pax2+ cells in *Olig3*$^{GFP/+}$ and *Olig3*$^{GFP/GFP}$ mice at the indicated stages. (E) Quantification of the proportion of Foxp2+ Purkinje cells co-expressing Pax2+ in *Olig3*$^{GFP/+}$ and *Olig3*$^{GFP/GFP}$ mice at the indicated stages. (F) Immunofluorescence characterization and quantification of the proportion of Pax2+ (blue) inhibitory interneurons co-expressing bgal (red) in E19 control (*Olig3*$^{creERT2/+}$;*Mapt*$^{nLacZ/+}$) and *Olig3* mutant (*Olig3*$^{creERT2/GFP}$; *Mapt*$^{nLacZ/+}$) mice that were recombined at E10.5. (G) Schema illustrating the above findings. In control mice, the ventricular zone generates two sets of GABAergic neurons: Foxp2+ Purkinje cells (E11.5-E13.5) and Pax2+ inhibitory interneurons (E14.5- P0). In *Olig3* mutant mice, about half of the Foxp2+ cells are misspecified and co-expressed Pax2. These cells subsequently undergo a fate shift and transform into inhibitory interneurons. The mean and SD are plotted in all graphs, and the dots represent the mean of individual animals. n = 4 mice per genotype in D and E; n = 4 control mice and n = 3 *Olig3* mutant mice in F. Significance was determined using a one-way ANOVA followed by post hoc Tukey's (in D and E) or two-tailed t-test (in F) analyses, see *Table 2* for statistical details. Photomicrographs were acquired using the automatic tile scan modus (10% overlap between tiles) of the Zeiss spinning disk confocal microscope (in A and C) and the Zeiss LSM700 confocal microscope (in F).
The online version of this article includes the following source data and figure supplement(s) for figure 4:

Source data 1. Source data for *Figure 4*.
Figure supplement 1. Misspecification of Foxp2+ Purkinje cells in *Olig3* mutant mice.
Figure supplement 2. Misspecified Foxp2+/Pax2+ cell numbers decline over the time in *Olig3* mutant mice.
Figure supplement 2–source data 1. Source data for *Figure 4—figure supplement 2*.

proteins are characteristic of inhibitory interneurons in the central nervous system, among which we found Parvalbumin expression to coincide with the onset of cerebellar interneuron specification and to be virtually absent in Foxp2+ cells at E14.5 (*Figure 5—figure supplement 1A*). Next, we evaluated whether Pax2 electroporated cells acquire an inhibitory interneuron identity using the same conditions described above. In pCAG-Pax2-ires-GFP electroporated mice, a third of the Parvalbumin + cells co-expressed GFP, whereas in pCAG-GFP + Empty-IRES-GFP electroporated mice about 4% of the GFP+ cells were also Parvalbumin+ (*Figure 5—figure supplement 1B*). We conclude that Pax2 is an efficient suppressor of Foxp2 expression and that its expression seems to induce a differ- entiation program characteristic of inhibitory interneurons.

To assess whether Olig3 cell-autonomously suppresses *Pax2* expression, we forced the ectopic expression of *Olig3* in the ventricular zone of wildtype mice at E14, a timepoint when *Olig3* expres- sion is almost absent and Pax2+ cells initiate their specification. Electroporated Olig3-IRES-GFP (*Olig3* overexpressing) and pCAG-GFP + Empty-IRES-GFP (control) embryos were analyzed at E15.5. The proportion of GFP+ cells that co-expressed Pax2 was greatly reduced in the ventricular zone of *Olig3*-overexpressing embryos when compared to control electroporated mice (*Figure 5C*, *Figure 5—figure supplement 2*). Thus, expression of *Olig3* is sufficient to cell-autonomously sup- press Pax2 expression. We conclude that during early development, Olig3 in the ventricular zone suppresses *Pax2* in newborn Purkinje cells to prevent their misspecification and secure their identity.

Olig3 and Olig2 specify complementary Purkinje cell populations

Our analysis of bHLH factors expressed throughout cerebellar development showed that in addition to *Olig3* and *Ptf1a*, *Ascl1* and *Olig2* are also expressed in the ventricular zone during Purkinje cell generation (*Table 1*). While ablation of *Ascl1* does not interfere with Purkinje cell development (*Grimaldi et al., 2009*; *Sudarov et al., 2011*), the exact role of Olig2 in the generation of GABAer- gic derivatives is unclear (*Ju et al., 2016*; *Seto et al., 2014*). In order to clarify the function of Olig2 we analyzed *Olig2* null mutant mice and found a reduction in Purkinje cell numbers and a modest increase in inhibitory interneurons (*Figure 6—figure supplement 1A,B*). We next carried out a long-term lineage-tracing experiment using *Olig2*^{cre} and *Mapt*^{nLacZ} alleles (*Olig2*$^{cre/+}$;*Mapt*$^{nLacZ/+}$ mice) to determine the contribution of Olig2 to cerebellar GABAergic neurons. This showed that while roughly half of the Foxp2+ Purkinje cell population had a history of *Olig2* expression, few inhibitory interneurons were generated from Olig2+ progenitors (*Figure 6—figure supplement 1C*). We thus conclude that the phenotypes of *Olig3* and *Olig2* mutant mice partially overlap (summarized in *Figure 6A*; *Figure 6—figure supplement 1D*).
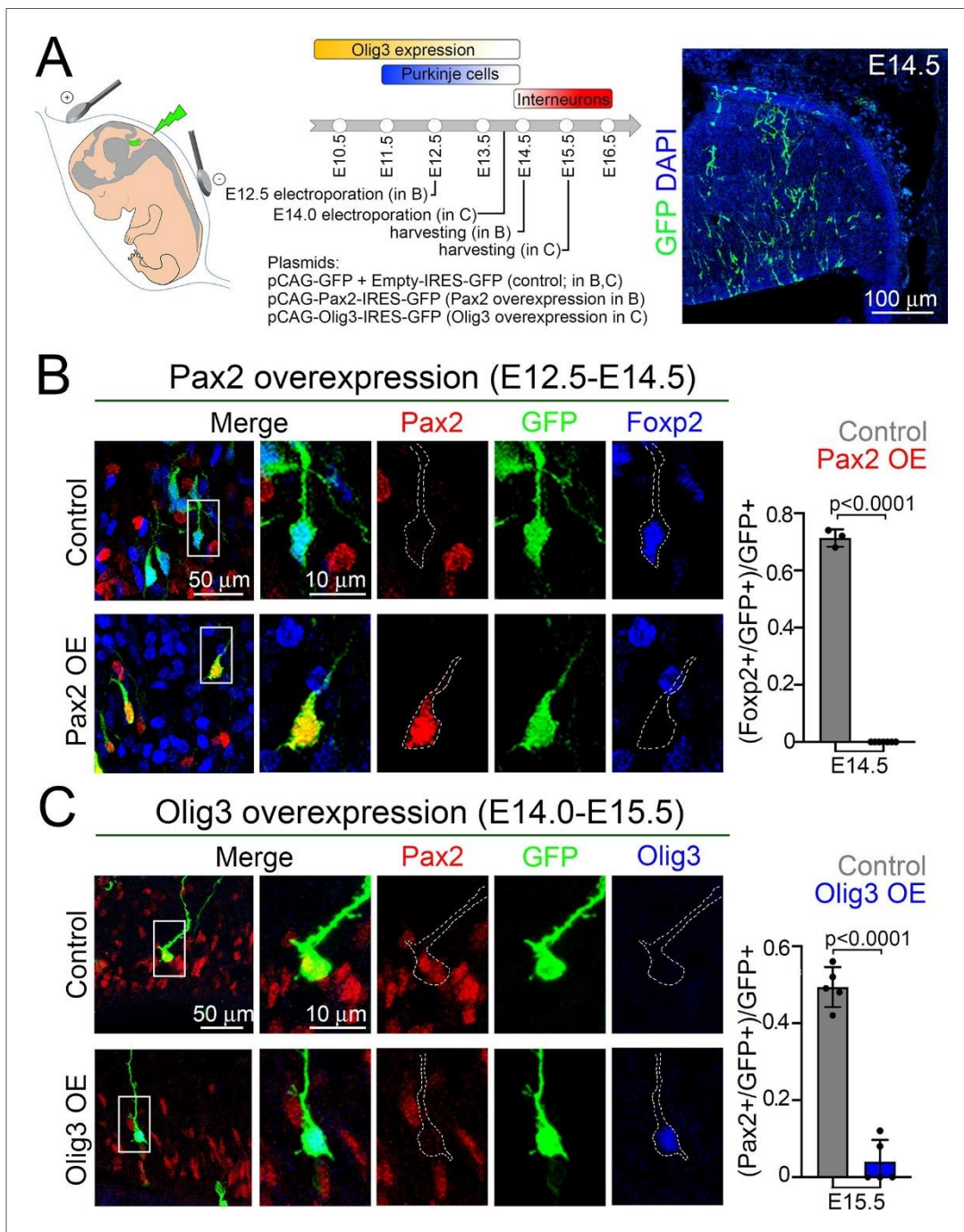
Figure 5. Olig3 cell-autonomously curtails *Pax2* expression to prevent the suppression of Foxp2 in newborn Purkinje cells. (A) Strategy to force *Olig3* and *Pax2* expression in the ventricular zone of wildtype mouse embryos. Left, illustration of the electrode position required to target the ventricular zone. Middle top, schema illustrating the temporal expression of Olig3, and the generation of Purkinje cells and inhibitory interneurons. Middle bottom, *Pax2* and *Olig3* expressing vectors were electroporated at E12.5 and E14.0, respectively. Electroporated embryos were harvested at the indicated stages. Electroporated plasmids are shown. Right, a representative cerebellar section stained with GFP (green) and DAPI (blue) of an E14.5 mouse that was electroporated with control plasmids at E12.5. (B) Analysis of E14.5 wildtype mice that were electroporated at E12.5 with control (pCAG-GFP + Empty-IRES-GFP) or Pax2-overexpression (pCAG-Pax2-IRES-GFP) plasmids. Left, representative analyzed cells in the cerebellum of electroporated embryos that were stained against Pax2 (red), GFP (green), and Foxp2 (blue). Right, quantification of the proportion of GFP+ cells co-expressing Foxp2 in electroporated control (Pax2-; n = 3) and Pax2-overexpressing (Pax2+; n = 7) mice. (C) Analysis of E15.5 wildtype mice that were electroporated at E14.0 with control (pCAG-GFP + Empty-IRES-GFP) or Olig3-overexpression (pCAG-Olig3-IRES-GFP) plasmids. Left, representative analyzed cells in the cerebellum of electroporated embryos that were stained against Pax2 (red), GFP (green) and Olig3 (blue). Right, quantification of the proportion of GFP+ cells co-expressing Pax2 in electroporated control (Olig3-; n = 5) and Olig3-overexpressing (Olig3+; n = 5) mice. See

Figure 5 continued on next page

Olig3 and Olig2 are known to specify non-overlapping neuron populations during the development of the hindbrain and spinal cord (*Takebayashi et al., 2002*; *Takebayashi et al., 2000*). To determine whether Olig3 and Olig2 mark complementary ventricular zone progenitor cells that specify distinct Foxp2+ Purkinje cells, we stained the cerebella of E10.5-E14.5 wildtype embryos with antibodies against these two factors. We observed that roughly 58% of Olig3+ cells in the ventricular zone co-expressed Olig2 but not Foxp2, while the remaining 42% of the Olig3+ cells co-expressed Foxp2 but not Olig2 (*Figure 6B*). Notably, we observed no Olig3-/Olig2+ cells that co-expressed Foxp2, illustrating that differentiated Purkinje cells retain *Olig3* but not *Olig2* expression.

We then asked whether ablation of *Olig3* might affect the expression of *Olig2* in ventricular zone progenitors, and vice versa we assessed whether mutation of *Olig2* might compromise the expres- sion of *Olig3*. Mutation of *Olig3* did not affect the expression of *Olig2*, and neither did mutation of *Olig2* affect the expression of *Olig3* in progenitor cells of the ventricular zone (*Figure 6C and D*; *Fig- ure 6— figure supplement 1E,F*). These data demonstrate that the expression of *Olig3* and *Olig2* in ventricular zone progenitor cells is independent of the other factor. Next, we assessed whether mutation of *Olig2* might also de-repress Pax2 in newborn Purkinje cells in a similar manner as the ablation of *Olig3*. Indeed, we observed numerous Foxp2+/Pax2+ misspecified cells in *Olig2* mutant animals at E13.5 (*Figure 6E*, quantified in *Figure 6F*), but unlike in *Olig3* mutant embryos, these cells were only located in the rostral-most part of the ventricular zone (compare insets in *Figure 6E*). These data demonstrate that Olig2 specifically suppresses *Pax2* in rostrally generated Purkinje cells, while Olig3 has a broader function in the suppression of *Pax2* in most of the Purkinje cell population. We therefore conclude that Olig3 and Olig2 complementarily contribute to the correct specification of Purkinje cells by curtailing the expression of *Pax2* (schematically displayed in *Figure 6G*).

Discussion

bHLH transcription factors are highly conserved in evolution and function as principal regulators of cell differentiation and neuronal specification (*Atchley and Fitch, 1997*; *Baker and Brown, 2018*; *Ben-Arie et al., 2000*; *Bertrand et al., 2002*; *Dennis et al., 2019*; *Dokucu et al., 1996*; *Jones, 2004*; *Sommer et al., 1996*). In this study, we sought to identify bHLH factors that regulate the specifica-tion of distinct cerebellar neuron types. We report here that Olig3 is a key player in cerebellar devel- opment and the generation of its earliest neuronal derivatives. Ablation of *Olig3* results in pronounced cerebellar hypoplasia at birth and the massive loss of DCN neurons, EGL cells including their granule cell derivatives, and Purkinje cells. These deficits are accompanied by an increase in the number of inhibitory interneurons. Our data illustrate that Olig3 regulates progenitor cell prolifera-tion in the rhombic lip, whereas in the ventricular zone Olig3 cell-autonomously suppresses the development of inhibitory interneurons by curtailing the expression of *Pax2*. We demonstrate that Pax2 acts as an effective suppressor of the Purkinje cells differentiation program. In addition, we show that Olig3 and its close family member Olig2 specify complementary Purkinje cell populations.

Here, we show that Olig3 is critically involved in the generation of EGL cells as well as DCN neu-rons. Earlier studies revealed that these rhombic lip derivatives depend on Atoh1 for their develop- ment, as loss of Atoh1 results in the severe reduction of EGL cells and impairs the development of DCN neurons (*Ben-Arie et al., 1997*; *Gazit et al., 2004*; *Jensen, 2004*; *Machold and Fishell, 2005*; *Machold et al., 2011*; *Wang et al., 2005*; *Yamada et al., 2014*). Our long-term lineage-tracing stud- ies demonstrated that most EGL and DCN cells have a history of *Olig3* expression, ablation of which massively reduced their cell numbers. In the early rhombic lip (E10.5-E13.5), we found that most
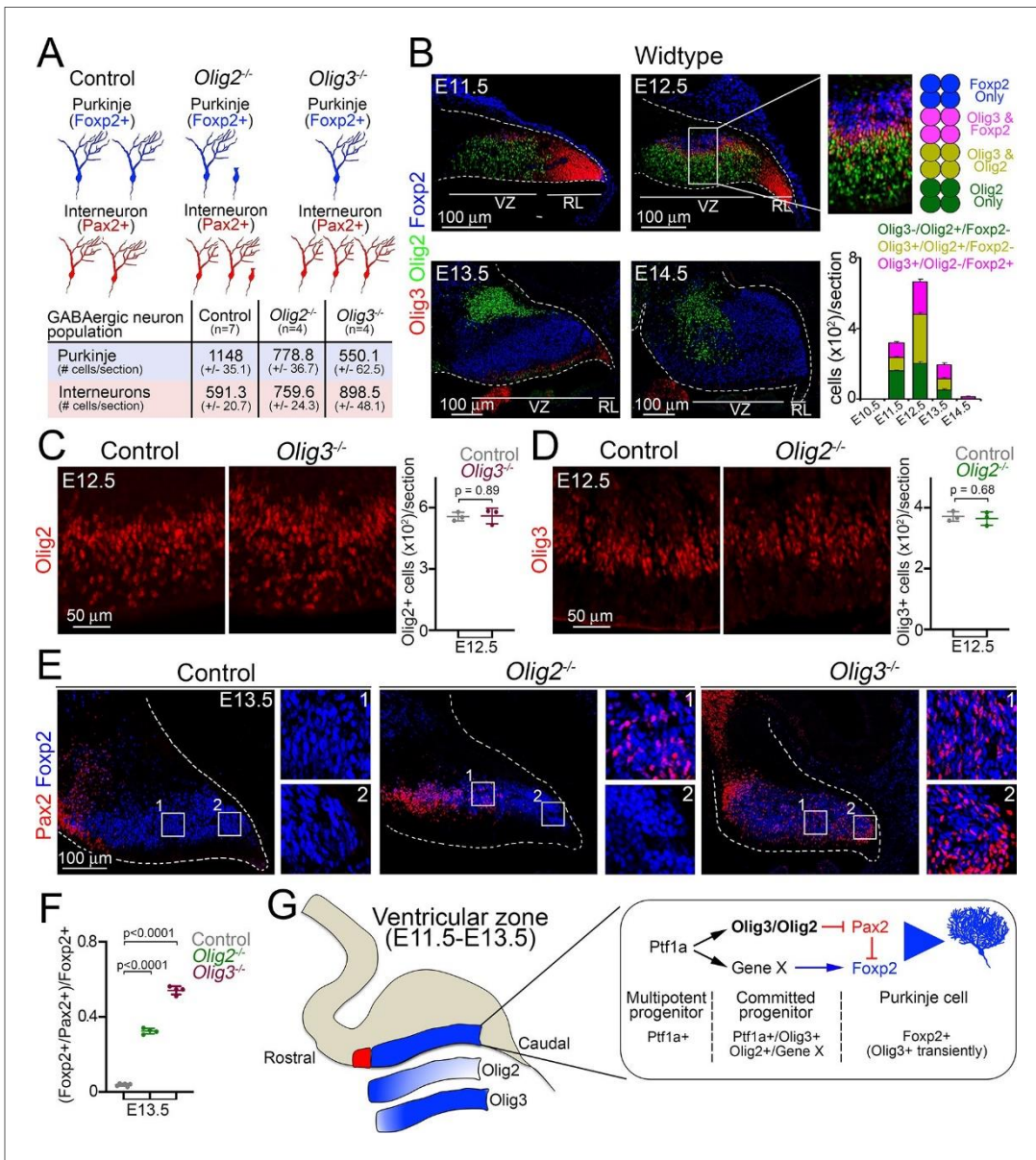
Figure 6. Complementary functions of Olig3 and Olig2 during Purkinje cell development. (A) Schema and quantification of the phenotypes observed in *Olig2* and *Olig3* mutant mice with respect to the development of GABAergic cerebellar neurons. See also *Figure 3E and F* (*Olig3* mutant analysis) and *Figure 6—figure supplement 1A and B*. (*Olig2* mutant analysis). n numbers are indicated in the brackets. (B) Immunofluorescence characterization and quantification of Olig3+ (red), Olig2+ (green), and Foxp2+ (blue) cells in the ventricular zone at indicated embryonic stages (n = 4 mice per age). (C) Immunofluorescence characterization and quantification of Olig2+ (red) cells in the ventricular zone of *Olig3* (*Olig3$^{-/-}$*) mutant mice at E12.5 (n = 3 mice per genotype). See also *Figure 6—figure supplement 1E* (D) Immunofluorescence characterization and quantification of Olig3+ (red) cells in the ventricular zone of *Olig2* (*Olig2$^{-/-}$*) mutant mice at E12.5 (n = 3 mice per genotype). See also *Figure 6—figure supplement 1F*. (E) Immunofluorescence comparison of Foxp2+ (blue) Purkinje cells and Pax2+ (red) inhibitory neurons in control versus *Olig2$^{-/-}$* and *Olig3$^{-/-}$* mutant mice at E13.5. Numbered boxed areas are displayed to the right of the main photographs. (F) Quantification of the proportion of Foxp2+ cells co-expressing Pax2 in control (n = 6), *Olig2$^{-/-}$* (n = 4), and *Olig3$^{-/-}$* (n = 4) mutant mice at E13.5. (G) Schematic summary explaining the function of Olig3 and Olig2 in the ventricular zone during the specification of Purkinje cells. Induction of Olig3 and Olig2, in committed Ptf1a+ progenitor cells, curtails the expression of Pax2 to allow for the correct specification of Purkinje cells. Olig2 predominantly operates in the rostral ventricular zone, whereas Olig3 has a broader function and is transiently retained in newborn Purkinje cells. The suppression of Pax2 is critical for Purkinje cell development, as it can override the Purkinje cell differentiation program. The mean and SD are plotted in all graphs, and the dots represent the mean of individual animals. Significance was determined using a one-way ANOVA followed by post hoc Tukey (in F) or two-tailed t-test (in C and D) analyses, see *Table 2* for statistical details. Photomicrographs were acquired using the automatic tile scan modus (10% overlap between tiles) of the Zeiss spinning disk confocal microscope (in C–E) and the Zeiss LSM700 confocal microscope (in B).

Figure 6 continued on next page

proliferative progenitor cells (Sox2+/BrdU+) co-expressed Olig3 and a third of them co-expressed Atoh1 (Olig3+/Atoh1+ cells). This temporal window overlaps with the generation of DCN cells (*Fink, 2006*; *Sekerkova´ et al., 2004*; *Wang et al., 2005*; *Yamada et al., 2014*), which are the most reduced neuron type in *Olig3* mutant mice (this study). Thus, Olig3 is essential for DCN neuron development. Ablation of *Olig3* reduced the number of BrdU+ (proliferative) progenitor cells in the rhombic lip, and consequently decreased the number of Atoh1+ cells. This impairment led to smaller numbers of EGL cells and, therefore, to fewer differentiated granule cells. The severe loss of EGLcells and their granule cell derivatives seems to largely account for the pronounced cerebellar hypo- plasia observed in *Olig3* mutant mice, and has also been observed after the loss of EGL cells in other studies (*Ben-Arie et al., 1997*). One should note, however, that the reduced numbers of granulecells in *Olig3* mutant mice might be mainly independent of Olig3 and due to the reduction of instructive signals emanating from Purkinje cells, which are severely affected in these mutant mice. Indeed, available evidence shows that Purkinje cells regulate EGL proliferation and the differentia-tion of granule cells via sonic hedgehog signaling (*Dahmane and Ruiz i Altaba, 1999*; *Wal- lace, 1999*; *Wechsler-Reya and Scott, 1999*).

During the development of rhombomeres 2-7, there exists a dorsal progenitor domain (called dA1) that also co-expresses Olig3 and Atoh1 (*Hernandez-Miranda et al., 2017a*; *Liu et al., 2008*; *Storm et al., 2009*). This domain generates the mossy fiber precerebellar (pontine, lateral reticular, external cuneate) nuclei. Like in the rhombic lip, ablation of *Olig3* greatly reduces the number of Atoh1+ cells in this area and their derivatives (*Liu et al., 2008*; *Storm et al., 2009*). This phenome-non also occurs in the spinal cord when *Olig3* is ablated (*Müller et al., 2005*). Thus, Olig3 has a con-served function in the proliferation of Atoh1+ progenitor cells.

We also show that the ablation of *Olig3* results in the development of supernumerary inhibitory interneurons. Both Purkinje cells and inhibitory interneurons depend on Ptf1a for their development (*Hashimoto and Mikoshiba, 2003*; *Hoshino et al., 2005*; *Leto et al., 2006*; *Yamada et al., 2014*). We predominantly found expression of Olig3 in the ventricular zone between E11.5 and E13.5, the temporal window during which Purkinje cells are specified. In the ventricular zone, about half of the Olig3+ cells co-express Ptf1a, while the rest co-express the Purkinje cell marker Foxp2. This shows that Olig3 expression is initiated in progenitors and transiently retained in newborn Purkinje cells. Ablation of *Olig3* neither impaired the number of Ptf1a+ cells nor their proliferation. Strikingly, around half of newborn Purkinje cells erroneously co-expressed Pax2 in *Olig3* mutant mice at E13.5, illustrating that ablation of *Olig3* misspecifies newborn Purkinje cells. In *Olig3* mutant mice, the num-ber of misspecified cells declined over time and became rare by P0. This decline correlated with a parallel increase in the number of inhibitory interneurons. Thus, the primary function of Olig3 in the ventricular zone is to secure the development of Purkinje cells by cell-autonomously suppressing an alternative program that specifies inhibitory interneurons. In this context, our functional data demon-strate that forced expression of *Olig3*, during the temporal generation of inhibitory interneurons, is sufficient to curtail *Pax2* expression. Furthermore, our functional data demonstrate that Pax2 acts as an effective suppressor of Foxp2 and the Purkinje differentiation cell program. In agreement with our findings, it was previously shown that supernumerary inhibitory neurons become specified at the expense of excitatory neurons in the hindbrain and spinal cord of *Olig3* mutant mice (*Müller et al., 2005*; *Storm et al., 2009*; *Zechner et al., 2007*). Interestingly, there is a unique progenitor domain in rhombomere 7 (called dA4) that co-expresses Olig3 and Ptf1a, which generates the pre-cerebellar climbing fiber neurons of the inferior olive (reviewed in *Hernandez-Miranda et al., 2017a*). In the absence of Olig3, inferior olive neurons and many spinal cord excitatory neurons seem to change their fate and erroneously adopt an inhibitory interneuron identity (*Liu et al., 2008*; *Müller et al., 2005*; *Storm et al., 2009*). This suggests that inhibitory interneurons are the default neuronal type generated from the brainstem, spinal cord and the ventricular zone of the cerebellum.

Based on short-term lineage-tracing experiments, *Seto et al., 2014* postulated a 'temporal identity transition' model in which Olig2+ Purkinje cell progenitors transition into inhibitory interneuron progenitors (*Seto et al., 2014*). From this model, one would expect that inhibitory interneurons would have a history of *Olig2* expression. In keeping with observations made by *Ju et al., 2016*, our long-term lineage-tracing experiments using *Olig2^cre^* and *Olig3^creERT2^* mice showed that Pax2+ inhibitory interneurons rarely have a history of *Olig2* or *Olig3* expression. This casts doubt on the 'temporal identity transition' model as both factors are abundantly expressed in Ptf1a+ progenitors during the specification of Purkinje cells (this work and *Seto et al., 2014*). Our data unambiguously show that neither Olig2 nor Olig3 control the transition of early (Purkinje) to late (inhibitory interneu- ron) ventricular zone progenitor cells. Rather, our work demonstrates that these factors are essential for the correct specification of Purkinje cells by curtailing an inhibitory interneuron transcriptional program.

Development of the central nervous system is characterized by molecular 'grids' of combinatorial transcription factor expression that single out distinct progenitor domains. It is from here that the enormous diversity of neuron types is generated (reviewed in *Alaynick et al., 2011*; *Hernandez-Miranda et al., 2017a*; *Herna´ndez-Miranda et al., 2010*; *Jessell, 2000*). Here, we show that cerebellar DCN neurons and internal granule cells develop from Olig3+/Atoh1+ rhombic lip progenitor cells, whereas Purkinje cells derive from Olig3+/Ptf1a+ ventricular zone progenitors. In the mature cerebellum, DCN neurons and granule cells receive input from brainstem precerebellar mossy fiber neurons that originate from progenitor cells that co-express Olig3 and Atoh1, whilst Purkinje cells receive input from climbing fiber neurons that emerge from progenitors that co-express Olig3 and Ptf1a (*Liu et al., 2008*; *Storm et al., 2009*). The question of how these progenitor cells, located at such distant positions, acquire similar molecular signatures to specify both targets and inputs that in turn form functional cerebellar circuits remains to be elucidated.

Materials and methods

Key resources table

Reagent type (species) or resource	Designation	Source or reference	Identifiers	Additional information
Strain, strain background (*M. musculus*)	*Olig3^CreERT2^*	*Storm et al., 2009*.	RRID:MGI:3833734	
Strain, strain background (*M. musculus*)	*Olig3^GFP^*	*Müller et al., 2005*.		
Strain, strain background (*M. musculus*)	*Mapt^nLacZ^*	*Hippenmeyer et al., 2005*.	The Jackson Laboratory, Stock No: 021162	
Strain, strain background (*M. musculus*)	*Rosa26^lsl-tdT^ (Ai14)*	*Madisen et al., 2010*.	The Jackson Laboratory, Stock No. 007908	
Strain, strain background (*M. musculus*)	*Olig2^Cre^*	*Dessaud et al., 2007*.		
Antibody	Anti-b-gal (Chicken polyclonal)	Abcam	ab9361 RRID:AB_307210	(1:1,000)
Antibody	Anti-GFP (Chicken polyclonal)	Abcam	ab13970 RRID:AB_300798	(1:500)
Antibody	Anti-Brn2 (Goat polyclonal)	Abcam	ab101726 RRID:AB_10710183	(1:1,000)
Antibody	Anti-Foxp2 (Goat polyclonal)	Abcam	ab58599 RRID:AB_941649	(1:1,000)
Antibody	Anti-Olig3 (Guinea pig polyclonal)	Gift from T. Muller	Homemade	(1:5,000)

Continued on next page

Continued

Reagent type (species) or resource	Designation	Source or reference	Identifiers	Additional information
Antibody	Anti-Foxp2 (Rabbit polyclonal)	Abcam	ab16046 RRID:AB_2107107	(1:1,000)
Antibody	Anti-GFP (Rabbit polyclonal)	Abcam	ab290 RRID:AB_303395	(1:500)
Antibody	Anti-Pax2 (Rabbit monoclonal)	Abcam	EP3251 RRID:AB_1603338	(1:1,000)
Antibody	Anti-Sox2 (Rabbit polyclonal)	Abcam	ab97959 RRID:AB_2341193	(1:1,000)
Antibody	Anti-Tbr1 (Rabbit polyclonal)	Abcam	ab31940 RRID:AB_2200219	(1:1,000)
Antibody	Anti-Tbr2 (Rabbit polyclonal)	Abcam	ab23345 RRID:AB_778267	(1:1,000)
Antibody	Anti-Ptf1a (Rabbit polyclonal)	Gift from J. Johnson	Homemade	(1:5,000)
Antibody	Anti-Olig2 (Rabbit polyclonal)	Merck Millipore	AB9610 RRID:AB_570666	(1:1,000)
Antibody	Anti-Pax6 (Rabbit polyclonal)	Merck Millipore	AB2237 RRID:AB_1587367	(1:1,000)
Antibody	Anti-RFP (Rabbit polyclonal)	Rockland	600-401-379 RRID:AB_2209751	(1:500)
Antibody	Anti-Caspase-3 (Rabbit polyclonal)	R and D Systems	AF835 RRID:AB_2243952	(1:1,000)
Antibody	Anti-Parvalbumin (Rabbit polyclonal)	Swant	PV 27 RRID:AB_2631173	(1:3,000)
Antibody	Anti-Atoh1 (Rabbit polyclonal)	Gift from T. Jessell	Homemade	(1:10,000)
Antibody	Anti-BrdU (Rat monoclonal)	Abcam	ab6326 RRID:AB_305426	(1:2,000)
Antibody	Anti-GFP (Rat monoclonal)	Nacalai Tesque	GF090R RRID:AB_10013361	(1:2,000)
Antibody	Donkey anti-species Alexa Fluor 488/568/647	Jackson ImmunoResearch	Various	(1:500)
Commercial Assay or kit	BrdU	Sigma-Aldrich	B5002-1G	16 mg/ml in 0.9% saline solution
Recombinant DNA reagent	pCAG-GFP	Addgene	Plasmid #11150 RRID:Addgene_11150	
Recombinant DNA reagent	pCAG-Empty-IRES-GFP	This paper		
Recombinant DNA reagent	pCAG-Olig3-IRES-GFP	This paper		vector: pCAG; cDNA fragment: mouse *Olig3*
Recombinant DNA reagent	pCAG-Pax2-IRES-GFP	This paper		vector: pCAG; cDNA fragment: mouse *Pax2*
Sequence-based reagent (*M. musculus*)	Mouse *Olig3* forward primer	Olig3FW	PCR Primer	ATGAATTCTGATTCGAGC
Sequence-based reagent (*M. musculus*)	Mouse *Olig3* reverse primer	Olig3RV	PCR Primer	TTAAACCTTATCGTCGTC
Sequence-based reagent (*M. musculus*)	Mouse *Pax2* forward primer	Pax2FW	PCR Primer	ATGGATATGCACTGCAAAGCAG
Sequence-based reagent (*M. musculus*)	Mouse *Pax2* reverse primer	Pax2RV	PCR Primer	GTGGCGGTCATAGGCAGC

Continued on next page

Continued

Reagent type (species) or resource	Designation	Source or reference	Identifiers	Additional information
Software, algorithm	GraphPad Prism	GraphPad Software	RRID:SCR_002798	Prism 8
Software, algorithm	Adobe Photoshop	Adobe	RRID:SCR_014199	Adobe Photoshop CS6
Software, algorithm	ImageJ	NIH	RRID:SCR_002285	
Software, algorithm	Arivis Vision4D	Arivis	RRID:SCR_018000	Arivis Vision4D 3.2

Animals

All animal experimental procedures were done in accordance to the guidance and policies of the Charite Universitatsmedizin, Berlin, Germany; Max-Delbru¨ ck-Center for Molecular Medicine, Berlin, Germany; and the Institute of Neuroscience, Lobachevsky University of Nizhny Novgorod, Russian Federation. Mouse strains used for this study were: *Olig3creERT2* (*Storm et al., 2009*), *Olig3GFP* (*Müller et al., 2005*), *MaptnLacZ* (*Hippenmeyer et al., 2005*), *Rosa26lsl-tdT* (*Madisen et al., 2010*), and *Olig2cre* (*Dessaud et al., 2007*). All strains were maintained in a mixed genetic background.

For tamoxifen treatment, pregnant dams were treated with tamoxifen (Sigma-Aldrich; 20 mg/ml dissolved in sunflower oil) as described previously (*Hernandez-Miranda et al., 2017b*; *Storm et al., 2009*). Tamoxifen delays labor in rodents and humans (*Lizen et al., 2015*). Therefore, offspring from tamoxifen-treated dams were delivered by caesarean section at E19.

Histology and cell quantifications

Immunofluorescence and tissue processing were performed as previously described (*Herna´ndez-Miranda et al., 2011*). Briefly, mouse tissue (E10.5-P0) was fixed in 4% paraformaldehyde (PFA), made in phosphate buffered saline (PBS), for 3 hr at 4˚C. After fixation, brains were cryoprotected overnight in 30% sucrose in PBS, embedded and frozen in Tissue-Tek OCT (Sakura Finetek), and sec-tioned at 20 mm using a cryostat. Sections were washed in PBS and blocked in PBS containing 5% normal goat serum (Sigma-Aldrich) (v/v) and 0.1% Triton X-100 (v/v) (Sigma-Aldrich) at room temper- ature for 1 hr. They were subsequently incubated in primary antibodies at room temperature over- night. After incubation in primary antibodies, sections were washed in PBS and then incubated in secondary antibodies for 2 hr at room temperature. Primary and secondary antibodies used in this study are displayed in the Key Resources Table. For a 45 min BrdU pulse labeling, BrdU (Sigma- Aldrich) was diluted to a concentration of 16 mg/ml in saline solution and injected intraperitoneally.

Cell quantifications were performed in a non-blind manner on non-consecutive 20-mm-thick brain sections encompassing the complete lateral-medial cerebellar axis. On average six to ten sections per animal were used for quantifications. E12.5 whole-mount embryos were analysed for b-gal activ- ity with X-gal (0.6 mg/ml; Merck Millipore, B4252) in PBS buffer containing 4 mM potassium ferricya- nide, 4 mM potassium ferrocyanide, 0.02% NP-40 and 2 mM MgCl2 as previously described (*Comai and Tajbakhsh, 2014*). For the estimation of the cerebellar volume and area, consecutive 20-mm-thick sagittal sections were collected encompassing the whole cerebellum and stained with Nissl. Roughly 32-35 sections of the cerebellum were obtained per animal (four animals/genotype). The area of every section was measured using ImageJ; NIH, version 1.34 n. Estimation of the total volume of the cerebellum was obtained by application of Cavalieri's method (*West, 2012*). Fluores- cence images were acquired using: (i) a Zeiss LSM 700 confocal microscope using the automatic tile scan modus (10% overlap between tiles) and assembled using ZEN2012, (ii) a Zeiss spinning disk confocal microscope using the automatic tile scan modus (10% overlap between tiles) and assem- bled using ZEN2012, and (iii) a Leica SPL confocal microscope. Photographs obtained with the Leica SPL confocal microscope were manually acquired and these were assembled using Image J. Unless otherwise specified all photomicrographs were acquired in a non-blind manner.

Brain clearing, lightsheet microscopy and analysis

Brains were cleared using the CUBIC protocol (*Susaki et al., 2015*). Briefly, brains were dissected and fixed overnight at 4˚C in 4% paraformaldehyde made in PBS. After washing overnight in PBS, lipids were removed using Reagent-1 (25% urea, 25% Quadrol, 15% Triton X-100, 35% dH2O) at 37˚C until brains were transparent (4 days). The brains were then washed overnight at 4˚C in PBS to

Table 2. Description of the statistical analyses used in this study.

Fig.	N	Descriptive statistics	Test used	p Value	Degrees of freedom and F/t/z/R/ETC	Pos hoc analysis	Adjusted p value
2E	Three mice (E10.5) three mice (E11.5) three mice (E12.5) three mice (E13.5)	Mean and SD	Ordinary one-way ANOVA	<0.0001	F: 67.20 F(DFn, DFd): 0.1441 (3, 8)	Tukey's multiple comparative test	As indicated in the figure
2F	Three mice (E10.5) three mice (E11.5) three mice (E12.5) three mice (E13.5)	Mean and SD	Ordinary one-way ANOVA	<0.0001	F: 93.57 F(DFn, DFd): 1.868 (3, 8)	Tukey's multiple comparative test	As indicated in the figure
2G	Three mice (E10.5) three mice (E11.5) three mice (E12.5) three mice (E13.5)	Mean and SD	Ordinary one-way ANOVA	<0.0001	F: 122.2 F(DFn, DFd): 1.096 (3, 8)	Tukey's multiple comparative test	As indicated in the figure
2H	Three mice (E10.5) three mice (E11.5) three mice (E12.5) three mice (E13.5)	Mean and SD	Ordinary one-way ANOVA	<0.0001	F: 13.65 F(DFn, DFd): 0.8851 (3, 8)	Tukey's multiple comparative test	As indicated in the figure
3A	Four control mice four mutant mice	Mean and SD	Unpaired t-test (two-tailed)	<0.0001	t = 15.13; df = 6	-	-
3B	Four control mice four mutant mice	Mean and SD	Unpaired t-test (two-tailed)	0.0005	t = 6.742; df = 6	-	-
3C	Three control mice three mutant mice	Mean and SD	Unpaired t-test (two-tailed)	0.0005	t = 10.47; df = 4	-	-
3D	Three control mice three mutant mice	Mean and SD	Unpaired t-test (two-tailed)	0.0002	t = 13.45; df = 4	-	-
3E	Four control mice four mutant mice	Mean and SD	Unpaired t-test (two-tailed)	<0.0001	t = 16.89; df = 6	-	-
3F	Four control mice four mutant mice	Mean and SD	Unpaired t-test (two-tailed)	<0.0001	t = 11.26; df = 6	-	-
4D	Four control (E13.5) four mutant (E13.5) four control (E14.5) four mutant (E14.5) four control (P0) four mutant (P0)	Mean and SD	Ordinary one-way ANOVA	<0.0001	F: 498.6 F(DFn, DFd): 1.252 (5, 18)	Tukey's multiple comparative test	As indicated in the figure
4E	Four control (E13.5) four mutant (E13.5) four control (E14.5) four mutant (E14.5) four control (P0) four mutant (P0)	Mean and SD	Ordinary one-way ANOVA	<0.0001	F: 514.2 F(DFn, DFd): 7.873 (5, 18)	Tukey's multiple comparative test	As indicated in the figure
4F	Four control mice three mutant mice	Mean and SD	Unpaired t-test (two-tailed)	<0.0001	t = 22.92; df = 5	-	-
5B	Three control-OE mice 7 Pax2-OE mice	Mean and SD	Unpaired t-test (two-tailed)	<0.0001	t = 67.67; df = 8	-	-
5C	Five control-OE mice 5 Olig3-OE mice	Mean and SD	Unpaired t-test (two-tailed)	0.0001	t = 13.24; df = 8	-	-
6C	Three control mice three mutant mice	Mean and SD	Unpaired t-test (two-tailed)	0.8969	t = 0.1380; df = 4	-	-
6D	Three control mice three mutant mice	Mean and SD	Unpaired t-test (two-tailed)	0.6835	t = 0.4387; df = 4	-	-

Table 2 continued on next page

Table 2 continued

Fig.	N	Descriptive statistics	Test used	p Value	Degrees of freedom and F/t/z/R/ETC	Pos hoc analysis	Adjusted p value
6F	Four control 4 Olig3 mutant 4 Olig2 mutant	Mean and SD	Ordinary one-way ANOVA	<0.0001	F: 1416 F(DFn, DFd): 0.8767 (2, 11)	Tukey's multiple comparative test	As indicated in the figure
2-fs 1C	Three mice (E10.5) three mice (E11.5) three mice (E12.5) three mice (E13.5)	Mean and SD	Ordinary one-way ANOVA	<0.0001	F: 299.8 F(DFn, DFd): 0.3133 (3, 8)	Tukey's multiple comparative test	As indicated in the figure
2-fs 1D	Three mice (E10.5) three mice (E11.5) three mice (E12.5) three mice (E13.5)	Mean and SD	Ordinary one-way ANOVA	<0.0001	F: 100.9 F(DFn, DFd): 0.2601 (3, 8)	Tukey's multiple comparative test	As indicated in the figure
2-fs 1E	Three mice (E10.5) three mice (E11.5) three mice (E12.5) three mice (E13.5)	Mean and SD	Ordinary one-way ANOVA	<0.0001	F: 85.64 F(DFn, DFd): 0.08333 (3, 8)	Tukey's multiple comparative test	As indicated in the figure
3-fs 1B	Three control mice three mutant mice	Mean and SD	Unpaired t-test (two-tailed)	0.0093	t = 4.707; df = 4	-	-
3-fs 1C	Three control mice three mutant mice	Mean and SD	Unpaired t-test (two-tailed)	0.2799	t = 1.249; df = 4	-	-
3-fs 2A	Three control mice three mutant mice	Mean and SD	Unpaired t-test (two-tailed)	<0.0001	t = 16.84; df = 4	-	-
3-fs 2B	Three control mice three mutant mice	Mean and SD	Unpaired t-test (two-tailed)	<0.0001	t = 17.51; df = 4	-	-
3-fs 2C	Three control mice three mutant mice	Mean and SD	Unpaired t-test (two-tailed)	0.0801	t = 2.331; df = 4	-	-
3-fs 3A	Four control (E11.5) four mutant (E11.5) four control (E12.5) four mutant (E12.5)	Mean and SD	Ordinary one-way ANOVA	<0.0001	F: 139.7 F(DFn, DFd): 2.328 (3, 12)	Tukey's multiple comparative test	As indicated in the figure
3-fs 3B	Three control (E11.5) four mutant (E11.5) four control (E12.5) four mutant (E12.5)	Mean and SD	Ordinary one-way ANOVA	<0.0001	F: 118.9 F(DFn, DFd): 0.3083 (3, 11)	Tukey's multiple comparative test	As indicated in the figure
3-fs 3C	Three control (E11.5) four mutant (E11.5) three control (E12.5) four mutant (E12.5)	Mean and SD	Ordinary one-way ANOVA	<0.0001	F: 232.2 F(DFn, DFd): 0.4627 (3, 10)	Tukey's multiple comparative test	As indicated in the figure
3-fs 3D	Four control (E11.5) four mutant (E11.5) four control (E12.5) four mutant (E12.5)	Mean and SD	Ordinary one-way ANOVA	<0.0001	F: 156.3 F(DFn, DFd): 0.9549 (3, 12)	Tukey's multiple comparative test	As indicated in the figure
3-fs 3E	Four control (E11.5) four mutant (E11.5) four control (E12.5) four mutant (E12.5)	Mean and SD	Ordinary one-way ANOVA	0.1739	F: 1.960 F(DFn, DFd): 0.4100 (3, 12)	Tukey's multiple comparative test	As indicated in the figure
4-fs 2B	Four control (E13.5) four mutant (E13.5) four control (E14.5) four mutant (E14.5) four control (P0) four mutant (P0)	Mean and SD	Ordinary one-way ANOVA	<0.0001	F: 850.2 F(DFn, DFd): 3.630 (5, 18)	Tukey's multiple comparative test	As indicated in the figure

Table 2 continued on next page

Table 2 continued

Fig.	N	Descriptive statistics	Test used	p Value	Degrees of freedom and F/t/z/R/ETC	Pos hoc analysis	Adjusted p value
5-fs 1B	Three control-OE mice 3 Pax2-OE mice	Mean and SD	Unpaired t-test (two-tailed)	<0.0001	t = 22.79; df = 4	-	-
6-fs 1A	Three control mice four mutant mice	Mean and SD	Unpaired t-test (two-tailed)	<0.0001	t = 12.82; df = 5	-	-
6-fs 1B	Three control mice four mutant mice	Mean and SD	Unpaired t-test (two-tailed)	0.0002	t = 10.1; df = 5	-	-

OE, overexpression; fs, figure supplement.

remove Reagent-1 and then placed into Reagent-2 (25% urea, 50% sucrose, 10% triethanolamine, 15% dH_2O) at 37°C for refractive index matching (3 days). Once the brains were cleared, they were imaged using a Zeiss Lightsheet Z.1 microscope. 3D reconstruction, photos and videos were created with arivis Vision4D.

In utero electroporation

In utero electroporation was performed as previously described (*Saito and Nakatsuji, 2001*). Briefly, DNA plasmids were mixed with Fast Green and injected into the fourth ventricle of embryonic brains from outside the uterus with a glass micropipette. Holding the embryo in utero with forceps-type electrodes (NEPA GENE), 50 ms of 40 V electronic pulses were delivered five times at intervals of 950 ms with a square electroporator (Nepa Gene, CUY21). The plasmids used in this study are displayed in the Key Resource table. The primer sequences to clone to clone the mouse *Olig3* (NM_053008.3) and *Pax2* (NM_011037.5) genes are displayed in in the Key Resource table. The electroporated plasmid DNA mixtures were as follows: (i) for the control experiment, pCAG-GFP (0.5 mg ml^{-1}) + pCAG-Empty-IRES-GFP (0.5 mg ml^{-1}); (ii) for the *Olig3* overexpression experiment, pCAG-Olig3-IRES-GFP (0.5 mg ml^{-1}); and (iii) for the *Pax2* overexpression experiment, pCAG-Pax2-IRES-GFP (0.5 mg ml^{-1}).

Statistics

Statistical analyses were performed using Prism 8 (GraphPad). Data are plotted in scatter dot plots or column dot plots with means and standard deviations (SD) displayed. The statistical significance between group means was tested by one-way ANOVA, followed by Tukey's post hoc test (for multi-ple-comparison tests), or two-tailed t-test (for pair comparison tests). Degrees of Freedom as wellas F and t values are provided in *Table 2*. No statistical method was used to pre-determine the sam-ple size. No randomization or blinding was used for *in vivo* studies.

Author contributions

Elijah D Lowenstein, Conceptualization, Formal analysis, Investigation, Visualization, Methodology, Writing - review and editing; Aleksandra Rusanova, Jonas Stelzer, Investigation, Visualization, Methodology; Marc Hernaiz-Llorens, Adrian E Schroer, Francesca Bladt, Sven Buchert, Shiqi Jia, Investigation; Ekaterina Epifanova, Methodology; Eser Göksu Isik, Investigation, Visualization; Victor Tarabykin, Methodology, Visualization; Luis R Hernandez-Miranda, Conceptualization, Formal analysis, Supervision, Funding acquisition, Investigation, Visualization, Methodology, Writing - originaldraft, Project administration, Writing - review and editing

Author ORCIDs

Elijah D Lowenstein https://orcid.org/0000-0003-3755-0818
Marc Hernaiz-Llorens http://orcid.org/0000-0003-1052-9613
Luis R Hernandez-Miranda https://orcid.org/0000-0002-0498-708X

Ethics

Animal experimentation: Animal experiments were approved by the local ethics committee LaGeSo (Landesamt fu¨ r Gesundheit und Soziales) Berlin under animal experiment licenses G0026/14, and in accordance to the guidance and policies of the Charite Universitatsmedizin, Berlin, Germany; Max-Delbru¨ ck-Center for Molecular Medicine, Berlin, Germany; and the Institute of Neuroscience, Lobachevsky University of Nizhny Novgorod, Russian Federation.

Decision letter and Author response

Decision letter https://doi.org/10.7554/eLife.64684.sa1
Author response https://doi.org/10.7554/eLife.64684.sa2

Additional files

Supplementary files

◦ Transparent reporting form

Data availability

All data generated or analysed during this study are included in the manuscript and supporting files.

References

Alaynick WA, Jessell TM, Pfaff SL. 2011. SnapShot: spinal cord development. *Cell* 146:178–. DOI: https://doi.org/10.1016/j.cell.2011.06.038, PMID: 21729788

Alder J, Cho NK, Hatten ME. 1996. Embryonic precursor cells from the rhombic lip are specified to a cerebellar granule neuron identity. *Neuron* 17:389-399. DOI: https://doi.org/10.1016/S0896-6273(00)80172-5, PMID: 8816703

Atchley WR, Fitch WM. 1997. A natural classification of the basic helix-loop-helix class of transcription factors. *PNAS* 94:5172-5176. DOI: https://doi.org/10.1073/pnas.94.10.5172, PMID: 9144210

Baker NE, Brown NL. 2018. All in the family: proneural bHLH genes and neuronal diversity. *Development* 145: dev159426. DOI: https://doi.org/10.1242/dev.159426, PMID: 29720483

Ben-Arie N, Bellen HJ, Armstrong DL, McCall AE, Gordadze PR, Guo Q, Matzuk MM, Zoghbi HY. 1997. Math1 is essential for genesis of cerebellar granule neurons. *Nature* 390:169-172. DOI: https://doi.org/10.1038/36579, PMID: 9367153

Ben-Arie N, Hassan BA, Bermingham NA, Malicki DM, Armstrong D, Matzuk M, Bellen HJ, Zoghbi HY. 2000. Functional conservation of atonal and Math1 in the CNS and PNS. *Development* 127:1039-1048. PMID: 10662643

Bertrand N, Castro DS, Guillemot F. 2002. Proneural genes and the specification of neural cell types. *Nature Reviews Neuroscience* 3:517-530. DOI: https://doi.org/10.1038/nrn874, PMID: 12094208

Butts T, Green MJ, Wingate RJ. 2014. Development of the cerebellum: simple steps to make a 'little brain'. *Development* 141:4031-4041. DOI: https://doi.org/10.1242/dev.106559, PMID: 25336734

Chizhikov VV, Lindgren AG, Currle DS, Rose MF, Monuki ES, Millen KJ. 2006. The roof plate regulates cerebellar cell-type specification and proliferation. *Development* 133:2793–2804. DOI: https://doi.org/10.1242/dev.02441, PMID: 16790481

Comai G, Tajbakhsh S. 2014. Molecular and cellular regulation of skeletal myogenesis. *Current Topics in Developmental Biology* 110:1-73. DOI: https://doi.org/10.1016/B978-0-12-405943-6.00001-4, PMID: 25248473

Dahmane N, Ruiz i Altaba A. 1999. Sonic hedgehog regulates the growth and patterning of the cerebellum. *Development* 126:3089-3100. PMID: 10375501

Dennis DJ, Han S, Schuurmans C. 2019. bHLH transcription factors in neural development, disease, and reprogramming. *Brain Research* 1705:48-65. DOI: https://doi.org/10.1016/j.brainres.2018.03.013, PMID: 29544733

Dessaud E, Yang LL, Hill K, Cox B, Ulloa F, Ribeiro A, Mynett A, Novitch BG, Briscoe J. 2007. Interpretation of the sonic hedgehog morphogen gradient by a temporal adaptation mechanism. *Nature* 450:717-720. DOI: https://doi.org/10.1038/nature06347

Dokucu ME, Zipursky SL, Cagan RL. 1996. Atonal, rough and the resolution of proneural clusters in the developing *Drosophila* retina. *Development* 122:4139-4147. PMID: 9012533

Englund C, Kowalczyk T, Daza RA, Dagan A, Lau C, Rose MF, Hevner RF. 2006. Unipolar brush cells of the cerebellum are produced in the rhombic lip and migrate through developing white matter. *Journal of Neuroscience* 26:9184-9195. DOI: https://doi.org/10.1523/JNEUROSCI.1610-06.2006, PMID: 16957075

Fink AJ. 2006. Development of the deep cerebellar nuclei: transcription factors and cell migration from the rhombic lip. *Journal of Neuroscience* 26:3066-3076. DOI: https://doi.org/10.1523/JNEUROSCI.5203-05.2006

Gazit R, Krizhanovsky V, Ben-Arie N. 2004. Math1 controls cerebellar granule cell differentiation by regulating multiple components of the notch signaling pathway. *Development* 131:903-913. DOI: https://doi.org/10.1242/dev.00982, PMID: 14757642

Grimaldi P, Parras C, Guillemot F, Rossi F, Wassef M. 2009. Origins and control of the differentiation of inhibitory interneurons and Glia in the cerebellum. *Developmental Biology* 328:422-433. DOI: https://doi.org/10.1016/j.ydbio.2009.02.008, PMID: 19217896

Hallonet ME, Teillet MA, Le Douarin NM. 1990. A new approach to the development of the cerebellum provided by the quail-chick marker system. *Development* 108:19-31.

Hashimoto M, Mikoshiba K. 2003. Mediolateral compartmentalization of the cerebellum is determined on the "birth date" of Purkinje cells. *The Journal of Neuroscience* 23:11342-11351. DOI: https://doi.org/10.1523/JNEUROSCI.23-36-11342.2003, PMID: 14672998

Hernández-Miranda LR, Parnavelas JG, Chiara F. 2010. Molecules and mechanisms involved in the generation and migration of cortical interneurons. *ASN Neuro* 2::AN20090053. DOI: https://doi.org/10.1042/AN20090053

Hernández-Miranda LR, Cariboni A, Faux C, Ruhrberg C, Cho JH, Cloutier JF, Eickholt BJ, Parnavelas JG, Andrews WD. 2011. Robo1 regulates semaphorin signaling to guide the migration of cortical interneurons through the ventral forebrain. *Journal of Neuroscience* 31:6174-6187. DOI: https://doi.org/10.1523/JNEUROSCI.5464-10.2011, PMID: 21508241

Hernandez-Miranda LR, Mu¨ller T, Birchmeier C. 2017a. The dorsal spinal cord and hindbrain: from developmental mechanisms to functional circuits. *Developmental Biology* 432:34-42. DOI: https://doi.org/10.1016/j.ydbio.2016.10.008, PMID: 27742210

Hernandez-Miranda LR, Ruffault PL, Bouvier JC, Murray AJ, Morin-Surun MP, Zampieri N, Cholewa-Waclaw JB, Ey E, Brunet JF, Champagnat J, Fortin G, Birchmeier C. 2017b. Genetic identification of a hindbrain nucleus essential for innate vocalization. *PNAS* 114:8095-8100. DOI: https://doi.org/10.1073/pnas.1702893114, PMID: 28698373

Hippenmeyer S, Vrieseling E, Sigrist M, Portmann T, Laengle C, Ladle DR, Arber S. 2005. A developmental switch in the response of DRG neurons to ETS transcription factor signaling. *PLOS Biology* 3:e159. DOI: https://doi.org/10.1371/journal.pbio.0030159, PMID: 15836427

Hoshino M, Nakamura S, Mori K, Kawauchi T, Terao M, Nishimura YV, Fukuda A, Fuse T, Matsuo N, Sone M, Watanabe M, Bito H, Terashima T, Wright CV, Kawaguchi Y, Nakao K, Nabeshima Y. 2005. Ptf1a, a bHLH transcriptional gene, defines GABAergic neuronal fates in cerebellum. *Neuron* 47:201-213. DOI: https://doi.org/10.1016/j.neuron.2005.06.007, PMID: 16039563

Imayoshi I, Kageyama R. 2014. bHLH factors in self-renewal, Multipotency, and fate choice of neural progenitor cells. *Neuron* 82:9-23. DOI: https://doi.org/10.1016/j.neuron.2014.03.018, PMID: 24698265

Jensen P. 2004. Analysis of cerebellar development in math1 null embryos and chimeras. *Journal of Neuroscience* 24:2202-2211. DOI: https://doi.org/10.1523/JNEUROSCI.3427-03.2004

Jessell TM. 2000. Neuronal specification in the spinal cord: inductive signals and transcriptional codes. *Nature Reviews Genetics* 1:20-29. DOI: https://doi.org/10.1038/35049541, PMID: 11262869

Jones S. 2004. An overview of the basic helix-loop-helix proteins. *Genome Biology* 5:226. DOI: https://doi.org/10.1186/gb-2004-5-6-226, PMID: 15186484

Ju J, Liu Q, Zhang Y, Liu Y, Jiang M, Zhang L, He X, Peng C, Zheng T, Lu QR, Li H. 2016. Olig2 regulates purkinje cell generation in the early developing mouse cerebellum. *Scientific Reports* 6:30711. DOI: https://doi.org/10.1038/srep30711, PMID: 27469598

Leto K, Carletti B, Williams IM, Magrassi L, Rossi F. 2006. Different types of cerebellar GABAergic interneurons originate from a common pool of multipotent progenitor cells. *Journal of Neuroscience* 26:11682-11694. DOI: https://doi.org/10.1523/JNEUROSCI.3656-06.2006, PMID: 17093090

Liu Z, Li H, Hu X, Yu L, Liu H, Han R, Colella R, Mower GD, Chen Y, Qiu M. 2008. Control of precerebellar neuron development by Olig3 bHLH transcription factor. *Journal of Neuroscience* 28:10124-10133. DOI: https://doi.org/10.1523/JNEUROSCI.3769-08.2008, PMID: 18829970

Liu ZR, Shi M, Hu ZL, Zheng MH, Du F, Zhao G, Ding YQ. 2010. A refined map of early gene expression in the dorsal rhombomere 1 of mouse embryos. *Brain Research Bulletin* 82:74-82. DOI: https://doi.org/10.1016/j.brainresbull.2010.02.010, PMID: 20206242

Lizen B, Claus M, Jeannotte L, Rijli FM, Gofflot F. 2015. Perinatal induction of cre recombination with tamoxifen. *Transgenic Research* 24:1065-1077. DOI: https://doi.org/10.1007/s11248-015-9905-5, PMID: 26395370

Machold R, Klein C, Fishell G. 2011. Genes expressed in Atoh1 neuronal lineages arising from the r1/isthmus rhombic lip. *Gene Expression Patterns* 11:349-359. DOI: https://doi.org/10.1016/j.gep.2011.03.007, PMID: 21440680

Machold R, Fishell G. 2005. Math1 is expressed in temporally discrete pools of cerebellar rhombic-lip neural progenitors. *Neuron* 48:17-24. DOI: https://doi.org/10.1016/j.neuron.2005.08.028, PMID: 16202705

Madisen L, Zwingman TA, Sunkin SM, Oh SW, Zariwala HA, Gu H, Ng LL, Palmiter RD, Hawrylycz MJ, Jones AR, Lein ES, Zeng H. 2010. A robust and high-throughput cre reporting and characterization system for the whole mouse brain. *Nature Neuroscience* 13:133-140. DOI: https://doi.org/10.1038/nn.2467, PMID: 20023653

Maricich SM, Herrup K. 1999. Pax-2 expression defines a subset of GABAergic interneurons and their precursors in the developing murine cerebellum. *Journal of Neurobiology* 41:281-294. DOI: https://doi.org/10.1002/(SICI)1097-4695(19991105)41:2<281::AID-NEU10>3.0.CO;2-5, PMID: 10512984

Mattar P, Langevin LM, Markham K, Klenin N, Shivji S, Zinyk D, Schuurmans C. 2008. Basic helix-loop-helix transcription factors cooperate to specify a cortical projection neuron identity. *Molecular and Cellular Biology* 28:1456-1469. DOI: https://doi.org/10.1128/MCB.01510-07, PMID: 18160702

Millen KJ, Steshina EY, Iskusnykh IY, Chizhikov VV. 2014. Transformation of the cerebellum into more ventral brainstem fates causes cerebellar agenesis in the absence of Ptf1a function. *PNAS* 111:E1777-E1786. DOI: https://doi.org/10.1073/pnas.1315024111, PMID: 24733890

Millet S, Bloch-Gallego E, Simeone A, Alvarado-Mallart RM. 1996. The caudal limit of Otx2 gene expression as a marker of the midbrain/hindbrain boundary: a study using in situ hybridisation and chick/quail homotopic grafts. *Development* 122:3785-3797. PMID: 9012500

Morales D, Hatten ME. 2006. Molecular markers of neuronal progenitors in the embryonic cerebellar anlage. *Journal of Neuroscience* 26:12226-12236. DOI: https://doi.org/10.1523/JNEUROSCI.3493-06.2006, PMID: 17122047

Müller T, Anlag K, Wildner H, Britsch S, Treier M, Birchmeier C. 2005. The bHLH factor Olig3 coordinates the specification of dorsal neurons in the spinal cord. *Genes & Development* 19:733-743. DOI: https://doi.org/10.1101/gad.326105, PMID: 15769945

Ross SE, Greenberg ME, Stiles CD. 2003. Basic helix-loop-helix factors in cortical development. *Neuron* 39:13-25. DOI: https://doi.org/10.1016/S0896-6273(03)00365-9, PMID: 12848929

Saito T, Nakatsuji N. 2001. Efficient gene transfer into the embryonic mouse brain using in vivo electroporation. *Developmental Biology* 240:237-246. DOI: https://doi.org/10.1006/dbio.2001.0439, PMID: 11784059

Sekerková G, Ilijic E, Mugnaini E. 2004. Time of origin of unipolar brush cells in the rat cerebellum as observed by prenatal bromodeoxyuridine labeling. *Neuroscience* 127:845-858. DOI: https://doi.org/10.1016/j.neuroscience.2004.05.050, PMID: 15312897

Sellick GS, Barker KT, Stolte-Dijkstra I, Fleischmann C, Coleman RJ, Garrett C, Gloyn AL, Edghill EL, Hattersley AT, Wellauer PK, Goodwin G, Houlston RS. 2004. Mutations in PTF1A cause pancreatic and cerebellar agenesis. *Nature Genetics* 36:1301-1305. DOI: https://doi.org/10.1038/ng1475, PMID: 15543146

Seto Y, Nakatani T, Masuyama N, Taya S, Kumai M, Minaki Y, Hamaguchi A, Inoue YU, Inoue T, Miyashita S, Fujiyama T, Yamada M, Chapman H, Campbell K, Magnuson MA, Wright CV, Kawaguchi Y, Ikenaka K, Takebayashi H, Ishiwata S, et al. 2014. Temporal identity transition from purkinje cell progenitors to GABAergic interneuron progenitors in the cerebellum. *Nature Communications* 5:3337. DOI: https://doi.org/10.1038/ncomms4337, PMID: 24535035

Shiraishi A, Muguruma K, Sasai Y. 2017. Generation of thalamic neurons from mouse embryonic stem cells. *Development* 144:1211-1220. DOI: https://doi.org/10.1242/dev.144071, PMID: 28219951

Skinner MK, Rawls A, Wilson-Rawls J, Roalson EH. 2010. Basic helix-loop-helix transcription factor gene family phylogenetics and nomenclature. *Differentiation* 80:1-8. DOI: https://doi.org/10.1016/j.diff.2010.02.003, PMID: 20219281

Sommer L, Ma Q, Anderson DJ. 1996. Neurogenins, a novel family of atonal-related bHLH transcription factors, are putative mammalian neuronal determination genes that reveal progenitor cell heterogeneity in the developing CNS and PNS. *Molecular and Cellular Neuroscience* 8:221-241. DOI: https://doi.org/10.1006/mcne.1996.0060, PMID: 9000438

Stevens JD, Roalson EH, Skinner MK. 2008. Phylogenetic and expression analysis of the basic helix-loop-helix transcription factor gene family: genomic approach to cellular differentiation. *Differentiation* 76:1006-1042. DOI: https://doi.org/10.1111/j.1432-0436.2008.00285.x, PMID: 18557763

Storm R, Cholewa-Waclaw J, Reuter K, Bröhl D, Sieber M, Treier M, Müller T, Birchmeier C. 2009. The bHLH transcription factor Olig3 marks the dorsal neuroepithelium of the hindbrain and is essential for the development of brainstem nuclei. *Development* 136:295-305. DOI: https://doi.org/10.1242/dev.027193, PMID: 19088088

Sudarov A, Turnbull RK, Kim EJ, Lebel-Potter M, Guillemot F, Joyner AL. 2011. Ascl1 genetics reveals insights into cerebellum local circuit assembly. *Journal of Neuroscience* 31:11055-11069. DOI: https://doi.org/10.1523/JNEUROSCI.0479-11.2011, PMID: 21795554

Susaki EA, Tainaka K, Perrin D, Yukinaga H, Kuno A, Ueda HR. 2015. Advanced CUBIC protocols for whole-brain and whole-body clearing and imaging. *Nature Protocols* 10:1709-1727. DOI: https://doi.org/10.1038/nprot.2015.085, PMID: 26448360

Takebayashi H, Yoshida S, Sugimori M, Kosako H, Kominami R, Nakafuku M, Nabeshima Y. 2000. Dynamic expression of basic helix-loop-helix olig family members: implication of Olig2 in neuron and oligodendrocyte differentiation and identification of a new member, Olig3. *Mechanisms of Development* 99:143-148. DOI: https://doi.org/10.1016/S0925-4773(00)00466-4, PMID: 11091082

Takebayashi H, Ohtsuki T, Uchida T, Kawamoto S, Okubo K, Ikenaka K, Takeichi M, Chisaka O, Nabeshima Y. 2002. Non-overlapping expression of Olig3 and Olig2 in the embryonic neural tube. *Mechanisms of Development* 113:169-174. DOI: https://doi.org/10.1016/S0925-4773(02)00021-7, PMID: 11960707

Vue TY, Aaker J, Taniguchi A, Kazemzadeh C, Skidmore JM, Martin DM, Martin JF, Treier M, Nakagawa Y. 2007. Characterization of progenitor domains in the developing mouse thalamus. *The Journal of Comparative Neurology* 505:73-91. DOI: https://doi.org/10.1002/cne.21467, PMID: 17729296

Wallace VA. 1999. Purkinje-cell-derived sonic hedgehog regulates granule neuron precursor cell proliferation in the developing mouse cerebellum. *Current Biology* 9:445-448. DOI: https://doi.org/10.1016/S0960-9822(99)80195-X, PMID: 10226030

Wang VY, Rose MF, Zoghbi HY. 2005. Math1 expression redefines the rhombic lip derivatives and reveals novel lineages within the brainstem and cerebellum. *Neuron* 48:31-43. DOI: https://doi.org/10.1016/j.neuron.2005.08.024

Wechsler-Reya RJ, Scott MP. 1999. Control of neuronal precursor proliferation in the cerebellum by sonic hedgehog. *Neuron* 22:103-114. DOI: https://doi.org/10.1016/S0896-6273(00)80682-0, PMID: 10027293

West MJ. 2012. Estimating volume in biological structures. *Cold Spring Harbor Protocols* 2012:1129-1139. DOI: https://doi.org/10.1101/pdb.top071787, PMID: 23118357

Wingate RJ, Hatten ME. 1999. The role of the rhombic lip in avian cerebellum development. *Development* 126:4395-4404.

Yamada M, Seto Y, Taya S, Owa T, Inoue YU, Inoue T, Kawaguchi Y, Nabeshima Y, Hoshino M. 2014. Specification of spatial identities of cerebellar neuron progenitors by ptf1a and atoh1 for proper production of GABAergic and glutamatergic neurons. *The Journal of Neuroscience* 34:4786-4800. DOI: https://doi.org/10.1523/JNEUROSCI.2722-13.2014, PMID: 24695699

Yeung J, Ha TJ, Swanson DJ, Goldowitz D. 2016. A novel and multivalent role of Pax6 in cerebellar development. *Journal of Neuroscience* 36:9057-9069. DOI: https://doi.org/10.1523/JNEUROSCI.4385-15.2016, PMID: 27581449

Zechner D, Mu¨ller T, Wende H, Walther I, Taketo MM, Crenshaw EB, Treier M, Birchmeier W, Birchmeier C. 2007. Bmp and wnt/beta-catenin signals control expression of the transcription factor Olig3 and the specification of spinal cord neurons. *Developmental Biology* 303:181-190. DOI: https://doi.org/10.1016/j.ydbio.2006.10.045, PMID: 17150208

Zervas M, Millet S, Ahn S, Joyner AL. 2004. Cell behaviors and genetic lineages of the mesencephalon and rhombomere 1. *Neuron* 43:345-357. DOI: https://doi.org/10.1016/j.neuron.2004.07.010, PMID: 15294143

8. Complete list of publications including Impact Factors

1. **A critical period of translational control during brain development at codon resolution**

   Dermot Harnett, Mateusz Ambrozkiewicz, Ulrike Zinnall, **Alexandra Rusanova**, Ekaterina Borisova, Rike Dannenberg, Koshi Imami, Agnieszka Münster-Wandowski, Beatrix Fauler, Thorsten Mielke, Matthias Selbach, Markus Landthaler, Christian Spahn, Victor Tarabykin, Uwe Ohler, Amelie Drescher, Marta Couce-Iglesias, Gabriel Villamil, Matthew L. Kraushar
   accepted 19.10.22 in Nature Structural & Molecular Biology
   Impact Factor – 18.361

2. **Olig3 regulates early cerebellar development**

   Elijah D. Lowenstein**, Aleksandra Rusanova**, Jonas Stelzer, Marc Hernaiz-Llorens, Adrian E. Schroer, Ekaterina Epifanova, Francesca Bladt, Eser Göksu Isik, Shiqi Jia, Victor Tara-bykin, Luis R. Hernandez-Miranda
   eLife 2021;10:e64684 doi: 10.7554/eLife.64684
   Published 16.02.2021
   Impact Factor – 8.140

3. **Polarity Acquisition in Cortical Neurons Is Driven by Synergistic Action of Sox9-Regulated Wwp1 and Wwp2 E3 Ubiquitin Ligases and Intronic miR-140.**

   Ambrozkiewicz MC, Schwark M, Kishimoto-Suga M, Borisova E, Hori K, Salazar-Lázaro A, **Rusanova A**, Altas B, Piepkorn L, Bessa P, Schaub T, Zhang X, Rabe T, Ripamonti S, Rosário M, Akiyama H, Jahn O, Kobayashi T, Hoshino M, Tarabykin V, Kawabe H.
   Neuron. 2018 Dec 5;100(5):1097-1115.e15. doi: 10.1016/j.neuron.2018.10.008. Epub 2018 Nov 1.
   Impact Factor – 14.415

4. **Identification of Novel Mutations Controlling Cerebral Cortex Malformations Caused by ENU-Induced Mutagenesis in the Mouse**
   Borisova E.V., Epifanova E.A., Tutukova S.A., Belousova I.I., Zhidkova N.M., **Rusanova A.M.**, Salina V.A., Turovsky E.A., Turovskaya M.V., Tarabykin V.S., Babaev A.A. CTM, 2018, volume 10, issue 3, pages 70-77.

   Impact Factor – no